

Carnegie Supernova Project: Observations of Type II_n Supernovae ^{*}

F. Taddia¹, M. D. Stritzinger², J. Sollerman¹, M. M. Phillips³, J. P. Anderson⁴, L. Boldt⁵, A. Campillay³, S. Castellón³, C. Contreras³, G. Folatelli⁶, M. Hamuy⁴, E. Heinrich-Josties⁷, W. Krzeminski⁸, N. Morrell³, C. R. Burns⁷, W. L. Freedman⁷, B. F. Madore⁷, S. E. Persson⁷, and N. B. Suntzeff^{9,10}

¹ The Oskar Klein Centre, Department of Astronomy, Stockholm University, AlbaNova, 10691 Stockholm, Sweden (e-mail: francesco.taddia@astro.su.se)

² Department of Physics and Astronomy, Aarhus University, Ny Munkegade 120, DK-8000 Aarhus C, Denmark

³ Carnegie Observatories, Las Campanas Observatory, Casilla 601, La Serena, Chile

⁴ Departamento de Astronomía, Universidad de Chile, Casilla 36D, Santiago, Chile

⁵ Argelander Institut für Astronomie, Universität Bonn, Auf dem Hügel 71, D-53111 Bonn, Germany

⁶ Kavli Institute for the Physics and Mathematics of the Universe (IPMU), University of Tokyo, 5-1-5 Kashiwanoha, Kashiwa, Chiba 277-8583, Japan

⁷ Observatories of the Carnegie Institution for Science, 813 Santa Barbara Street, Pasadena, CA, USA

⁸ N. Copernicus Astronomical Center, ul. Bartycka 18, 00-716 Warszawa, Poland

⁹ Department of Physics and Astronomy, Texas A&M University, College Station, TX 77845, USA

¹⁰ The Mitchell Institute for Fundamental Physics and Astronomy, Texas A&M University, College Station, TX 77845, USA

Received 29/01/2013 / Accepted 10/04/2013

Abstract

Aims. The observational diversity displayed by various Type II_n supernovae (SNe II_n) is explored and quantified. In doing so a more coherent picture ascribing the variety of observed SNe II_n types to particular progenitor scenarios is sought.

Methods. *Carnegie Supernova Project* (CSP) optical and near-infrared light curves and visual-wavelength spectroscopy of the Type II_n SNe 2005kj, 2006aa, 2006bo, 2006qq and 2008fq are presented. Combined with previously published observations of the Type II_n SNe 2005ip and 2006jd (Stritzinger et al. 2012), the full CSP sample is used to derive physical parameters which describe the nature of the interaction between the expanding SN ejecta and the circum-stellar material (CSM).

Results. For each SN of our sample we find counterparts, identifying objects similar to SNe 1994W (SN 2006bo), 1998S (SN 2008fq) and 1988Z (SN 2006qq). We present the unprecedented initial *u*-band plateau of SN 2006aa, and its peculiar late-time luminosity and temperature evolution. For each SN, assuming the CSM was formed by steady winds, mass-loss rates of 10^{-4} – $10^{-2} M_{\odot} \text{ yr}^{-1}$ are derived. Typically wind velocities of a few hundreds km s^{-1} are also computed.

Conclusions. The CSP SN II_n sample seems to be divided into sub-categories rather than exhibiting a continuum of observational properties. The wind and mass-loss parameters would favor a Luminous Blue Variable progenitor scenario, however the assumptions made to derive those parameters strongly influence the results, and therefore other progenitor channels behind SNe II_n can not be excluded at this time.

Key words. supernovae: general – supernovae: individual: SN 2005ip, SN 2005kj, SN 2006aa, SN 2006bo, SN 2006jd, SN 2006qq and SN 2008fq

1. Introduction

Schlegel (1990) was the first to introduce the narrow-line Type II_n supernova (SN II_n) sub-class to accommodate objects like SN 1987F (Wegner & Swanson 1996) and SN 1988Z (Stathakis & Sadler 1991; Turatto et al. 1993), which exhibit prevalent narrow-emission features. Today members of this SN sub-class cover a broad range of observational properties; however, they share the commonality of early phase spectra containing narrow Balmer emission features placed over a blue continuum. The most prominent features (e.g. H α) typically exhibit multiple components, consisting of a narrow core (full-width-

at-half-maximum FWHM_n of tenths to hundreds km s^{-1}) that is often situated on top of an intermediate-velocity component ($\text{FWHM}_i \sim 1000 \text{ km s}^{-1}$), as well as a broad base (FWHM_b of a few thousands km s^{-1}).

The multi-component emission features are powered through a combination of SN emission and circum-stellar interaction (CSI) processes. CSI occurs when the SN blast-wave shocks circum-stellar material (CSM) (e.g. Chugai & Danziger 1994; Fransson et al. 2002), which originates from prevalent winds and/or violent eruptions of the progenitors during their pre-SN evolutionary phase (Kudritzki & Puls 2000).

In general one finds that as the outward moving SN blast-wave shocks CSM, a forward shock is generated and propagates through the pre-SN wind, while a reverse shock forms and propagates back through the expanding SN ejecta. At the interface between the forward and reverse shocks, a cold dense shell (CDS) of gas forms and rapidly cools through collisional

* Based on observations collected at the European Organisation for Astronomical Research in the Southern Hemisphere, Chile (ESO Programmes 076.A-0156, 078.D-0048 and 082.A-0526). This paper includes data gathered with the 6.5 m Magellan Telescopes located at Las Campanas Observatory, Chile.

de-excitation processes. Within the shock region high-energy radiation is produced which subsequently ionizes the un-shocked pre-SN wind. As this gas re-combines, narrow emission lines are produced that can span a wide range in ionization potential (e.g. Chevalier & Fransson 1994; Chugai & Danziger 1994; Smith et al. 2009a).

Within this general picture, the broad-line component is typically associated with SN emission, although one can not rule out thermal broadening of the narrow core in the case of an optically thick wind (Chugai 2001), while the intermediate-component originates from gas emitting in the post-shock region. Strong CSI also generates X-ray and radio emission (e.g. Nymark et al. 2006; Dwarkadas & Gruszko 2012; Chandra et al. 2012), and may also have an important influence on producing the necessary conditions to form dust, which has been detected in a handful of SNe II_n (see e.g. Fox et al. 2011).

Over the last two decades observations have led to the realization of a remarkable heterogeneity between the photometric and spectroscopic properties exhibited by various SNe II_n (e.g. Pastorello et al. 2002; Kiewe et al. 2012). Today the SNe II_n class consists of objects that show a large range in peak luminosities. At the very bright end of the distribution are SN 2006gy-like objects (Smith et al. 2007), which can reach peak absolute magnitudes of $M_R \lesssim -21$, while at the faint end, objects like SN 1994aj reach peak values of $M_R \gtrsim -17$ mag (Benetti et al. 1998).

Some SNe II_n are observable in the optical for years past discovery (e.g. SN 1995N, Fransson et al. 2002), while others fade to obscurity within months (e.g. SN 1994W, Sollerman et al. 1998). Moreover, objects discovered soon after explosion indicate rise times ranging from several days to tens of days (see Kiewe et al. 2012). Around peak brightness a handful of SNe II_n show gaussian shaped light curves (e.g. SN 2006gy), whereas others like SN 1994W exhibit a plateau light curve phase reminiscent of Type IIP SNe (Kankare et al. 2012; Mauerhan et al. 2012a). The evolution of SN II_n light curves post maximum also shows a large degree of heterogeneity.

Close examination of SN II_n spectra not only reveals the presence of multi-component emission features, but also a variety of emission line profiles, ranging from symmetric to highly asymmetric. These line profile asymmetries are often observed to grow over time. For example, in the cases of SNe 2006jd (Stritzinger et al. 2012, hereafter S12) and 2010jl (Smith et al. 2012) prevalent attenuation of the red wing of H α was observed to increase over the first six months from discovery. Depending on the nature of the SN-CSM interaction, this behaviour could be linked to increasing absorption due to dust condensation or to the occultation of radiation by a thick photosphere and/or surrounding CSM (e.g. a thick disk).

CSI has also been observed to occur in hydrogen poor core-collapse (CC) SNe that interact with helium-rich CSM. The prototype of such a phenomenon is the Type Ibn SN 2006jc (Pastorello et al. 2008). Furthermore, some thermonuclear explosions may occur in a hydrogen-rich environment producing Type II_n-like SNe Ia. Examples of such events include SNe 2002ic (Hamuy et al. 2003), 2005gj (Aldering et al. 2006; Prieto et al. 2007), 2008J (Taddia et al. 2012) and PTF 11kx (Dilday et al. 2012).

Progenitor stars of SNe II_n must eject enough mass to enable efficient CSI. A Luminous Blue Variable (LBV) star identified in pre-SN explosion images has been linked to the Type II_n SN 2005gl (Gal-Yam & Leonard 2009). More recently, SN 2009ip has also been linked to an LBV (Mauerhan et al. 2012b), which has exhibited episodic re-brightening events three

years prior to core-collapse. However, Pastorello et al. (2012) and Soker & Kashi (2012) have suggested that the last bright event of SN 2009ip is due to other mechanisms rather than by core-collapse. LBVs are known to suffer significant mass loss ($\dot{M} \sim 10^{-2} - 10^{-3} M_{\odot} \text{ yr}^{-1}$) through episodic outbursts that occur on time scales ranging from months to years. Such behavior is well-documented through detailed observations of Eta Carinae and other “SN impostors” (e.g. see Smith et al. 2011).

Nevertheless, the variety of SN II_n properties suggests that their origins may lie with a diversity of progenitor stars. For example, Fransson et al. (2002) and Smith et al. (2009b) have suggested that red supergiant (RSG) stars which experience a pre-SN mass-loss phase driven by a super-wind – as is observed in VY Canis Majoris – could be viable progenitors for a large fraction of observed SNe II_n.

A proper determination of the progenitor mass-loss history is crucial to discern the nature of the progenitor itself. Estimates of mass-loss rates found in the literature are often based on the assumption that the progenitor wind is steady, even though X-ray observations demonstrate this is likely not the case for the majority of objects (Dwarkadas 2011). Ad hoc assumptions on the density profiles of progenitor pre-SN winds can therefore lead to incorrect mass-loss rate estimates. From the theoretical point of view, steady, line-driven winds are the only mass-loss mechanism which is reasonably understood (although see Smith et al. 2011, and reference therein), whereas, by comparison, the physics behind episodic and eruptive mass loss behaviour is still in its infancy (see e.g. Smith & Owocki 2006; Yoon & Cantiello 2010).

In this paper we present and analyze optical and near-infrared (NIR) light curves and visual-wavelength spectroscopy of five SNe II_n observed by the *Carnegie Supernova Project* (CSP, Hamuy et al. 2006). These new objects are SNe 2005kj, 2006aa, 2006bo, 2006qq and 2008fq. Basic information regarding these SNe II_n is provided in Tables 1 and 2. In addition to these five objects, the full CSP SN II_n sample includes detailed observations of SNe 2005ip and 2006jd which are presented by S12.

The organization of this paper is as follows: Sect. 2 contains details concerning data acquisition and reduction; Sect. 3 describes the CSP SN II_n sample; Sect. 4 reports on the broad-band optical and near-infrared photometry; Sect. 5 describes the spectroscopic observations; Sect. 6 presents the discussion and the interpretation of the data; and finally the conclusions are given in Sect. 7.

2. Observations

Optical and NIR photometry of the five SNe II_n presented in this paper were computed from images obtained with the Henrietta Swope 1 m and the Irénée du Pont 2.5 m telescopes located at the Las Campanas Observatory (LCO). The vast majority of optical imaging was taken with the Swope equipped with the direct imaging camera known as “Site3”, and a set of Sloan *ugri* and Johnson *BV* filters. A small amount of optical imaging was also obtained for two objects SNe 2006aa and 2006bo with the du Pont equipped with a direct imaging camera named after its chip Tek-5, which is referred to colloquially as “Tek-cinco”. NIR imaging was performed with both the Swope (+ RetroCam) and du Pont (+ Wide Field IR Camera, WIRC) equipped with a set of *YJH* filters. A small amount of K_s -band imaging was also obtained with the du Pont for SNe 2005kj and 2008fq. The Magellan (Baade) telescope at LCO was also used to get

three epochs of K_s -band imaging for SN 2005kj. Complete details concerning the instruments and passbands used by the CSP can be found in Hamuy et al. (2006), Contreras et al. (2010) and Stritzinger et al. (2011).

A detailed description of CSP observing techniques and data reduction pipelines can be found in Hamuy et al. (2006) and Contreras et al. (2010). In short, each optical image undergoes a series of reduction steps consisting of (i) bias subtraction, (ii) flat-field correction, and (iii) the application of a shutter time and CCD linearity corrections. Given the nature of observing in the NIR, the basic reduction process for these images consists of (i) dark subtraction, (ii) flat-field correction, (iii) sky subtraction, (iv) non-linearity correction, and finally (v) the geometrical alignment and combination of each dithered frame.

Deep template images of each SN host galaxy were obtained using the du Pont telescope under excellent seeing conditions. The templates are used to subtract away the host contamination at the position of the SN from each science image (see Contreras et al. 2010, for details). In Table 6 the UT date of each template observation is reported. In some cases (e.g. SNe 2005kj and 2006qq) we had to wait several years after discovery to obtain useful templates without SN contamination, because of the long-lasting CSI and late-time dust emission. SNe 2005ip and 2006jd are still bright and templates are not available (S12).

PSF photometry of each SN was computed differentially with respect to a local photometric sequence of stars. The calibration of the photometric sequences was done with respect to Smith et al. (2002) (*ugri*), Landolt (1992) (*BV*), and Persson et al. (1998) (*YJHK_s*) standard fields observed over a minimum of three photometric nights. The local sequences for each CSP SN IIIn in the standard photometric systems is provided in Table 3, while final SN optical and NIR photometry *in the natural system* is listed in Table 4 and Table 5, respectively.

Visual-wavelength spectroscopy of the CSP SN IIIn sample was obtained with the Du Pont and Magellan (Baade ad Clay) telescopes at LCO, and the ESO New Technology Telescope (NTT) at the La Silla Observatory. A spectrum of SN 2005kj was obtained with the 60-inches telescope at the Cerro Tololo Inter-American Observatory (CTIO). These data were reduced in a standard manner as described by Hamuy et al. (2006), including: (i) overscan correction, (ii) bias subtraction, (iii) flat-fielding, (iv) 1-D spectrum extraction, (v) wavelength calibration (vi) telluric corrections, (vii) flux calibration, and (viii) combination of multiple exposures. Finally, when necessary the flux of each spectrum was adjusted to match that obtained from the broad-band photometry. The journal of the spectroscopic observations is provided in Table 7.

3. The CSP SN IIIn sample

Table 1 lists properties of the full CSP SN IIIn sample, including the SN coordinates, its host galaxy name, type and distance, as well as estimates of total absorption due to dust extinction [$E(B-V)_{MW} + E(B-V)_{host}$] and the equivalent width (EW) of interstellar Na I D absorption. Finding charts for the five new CSP SNe IIIn are given in Fig. 1. As most of the SNe followed by the CSP were discovered by targeted surveys, it is not surprising that the hosts of the CSP SN IIIn sample are bright, nearby spiral galaxies in the redshift range $0.007 \leq z \leq 0.029$. Quoted distances to each event correspond to the luminosity distances provided by NED, which include corrections for peculiar motion (GA+Shapley+Virgo) and are based on cosmological parameters obtained by WMAP5 (Komatsu et al. 2009). Galactic absorption values were taken from NED (Schlafly & Finkbeiner 2011),

while estimates of $E(B-V)_{host}$ were determined through the combination of EW measurements of interstellar Na I D absorption lines at the host-galaxy redshift combined with the relation: $E(B-V)_{host} = 0.16 \cdot EW(\text{Na I D})_h$ (Turatto et al. 2003). Only two objects display significant Na I D absorption. SN 2006qq exhibits clear Na I D absorption at the host rest-frame in the spectrum taken on January 1st, 2007. We note that the host galaxy of this object is remarkably tilted, exhibiting an inclination between line of sight and polar axis of 85.6 deg. SN 2008fq, that is located close to the center of its host, also shows prominent narrow absorption lines of Na I D in each spectrum, although the individual D1 and D2 components are not resolved. In the case of SN 2008fq we take the mean of the EW measurements as obtained from our series of spectra. We determined $E(B-V)_{host} = 0.12$ and 0.46 mag for SN 2006qq and 2008fq, respectively. We note however that the EW of Na I D from low resolution spectra is a debatable proxy for the extinction of extragalactic sources and it does not work for SNe Ia (Poznanski et al. 2011).

Table 2 indicates that several of the objects were discovered within a few days to weeks past the last non-detection. Specifically, for three SNe IIIn we have early observations and good constraints on their explosion epoch (see column 5 in Table 2). Only SNe 2005kj and 2006bo have poorly constrained explosion dates. As noted in S12, SNe 2005ip and 2006jd are believed to have been discovered soon after explosion. In what follows the discovery date is used to define the temporal phase of each object.

Plotted in Fig. 2 are the optical and NIR light curves of the five new CSP SNe IIIn. Typically each SN was observed for ≈ 100 days with a cadence of several days, however in the case of SN 2005kj observations extend to over 180 days. Due to scheduling constraints the NIR coverage is typically with a lower cadence.

As indicated in Table 7 the number of optical spectra for this sample of five SNe IIIn varies from two (SN 2006bo) to 15 (SN 2005kj) epochs. Spectroscopic follow-up started from at most ≈ 19 days after discovery (i.e. SN 2006aa) down to a minimum of ≈ 2 days after discovery (i.e. SN 2008fq). Depending on the exact instrument used, the wavelength coverage typically ranges from $\approx 3800 \text{ \AA}$ to $\approx 9300 \text{ \AA}$ (see Table 7). The spectroscopic sequences of these five SNe IIIn are presented in Fig. 3 and Fig. 4. Included in each panel as coloured diamonds are photometric broad-band measurements derived from interpolated light curves.

Our dataset is also complemented with data published in the literature. Several of the SNe IIIn in our sample were observed in the mid-infrared (MIR) with the *Spitzer Space Telescope* (Fox et al. 2011). In particular, late-phase Spitzer observations of SN 2006qq (≈ 1050 days past discovery) found this object to be quite bright at $\lambda > 3.6 \mu\text{m}$, while similar imaging of SNe 2006aa and 2006bo showed no MIR emission.

4. Photometry

4.1. Light curves

SN 2005kj was observed only after maximum light and its explosion date is not well constrained by pre-explosion images. Its optical light curves (Fig. 2) show a decline of ≈ 3.5 mag in the first ≈ 100 days in the *u* band, whereas the decline is slower for the redder bands in the same time interval (*i* band becomes only ≈ 0.8 mag fainter). After ≈ 100 days the light curve slope steepens, with the *i* band decaying 1.4 mag in the following ≈ 70 days and the bluer bands showing a higher rate of decline.

The NIR light curves exhibit a somewhat slower evolution at all phases. The SN was detected in Y and J bands even at ≈ 382 days (see Table 5).

SN 2006aa was discovered relatively young and has an uncertainty of ± 8 days on the explosion date. Its light curves are characterized by a “gaussian” shape, with an initial rise that culminates at maximum light ≈ 50 days after discovery for all the filters. Interestingly, also the super-luminous SNe II (Gal-Yam 2012) and the peculiar SN Ib/c 2005bf (Folatelli et al. 2006) peak at ≈ 50 -60 days. However, in the case of SN 2005bf no sign of interaction was seen and its long rise time can be attributed to the delay in the diffusion of photons through the ejecta. The rise in the u band follows an initial ≈ 10 days “plateau”. This feature is observed for the first time in the SN II In class, for which a small number of early time observations in the near ultra-violet exists. We note that the SN II In 2011ht did not present this “plateau” although discovered soon after explosion (Roming et al. 2012). After maximum, the decline is steeper in the bluer bands as in the case of SN 2005kj, with B and i bands fading by ≈ 2 mag and ≈ 1 mag respectively in ≈ 80 days.

SN 2006bo was discovered after maximum (its explosion date is not well constrained from pre-SN images), and its optical light curves are characterized by an initial linear decline (in mag), more pronounced in the bluer bands. In the first ≈ 40 days the u band faded by ≈ 2 mag, whereas the i band faded by only ≈ 0.5 mag. The last optical observation, that was obtained ≈ 150 days after discovery and ≈ 3 months subsequent to the previous optical observation, reveals that at some point after ≈ 60 days an increase in decline rate occurred. The NIR light curves cover only the first tens of days after discovery and are nearly flat, showing only a marginal decline in brightness.

SN 2006qq was observed after maximum in the optical bands and before maximum in the NIR. Each optical band is characterized by a decline which becomes progressively less steep with time and wavelength. The NIR light curves show maximum emission at ≈ 20 –30 days after discovery. The SN was detected in H band even later than 700 days after discovery (see Table 5).

SN 2008fq was discovered no later than 9 days after explosion. It has a light curve that exhibits a fast rise culminating in an early maximum (at ≈ 10 days in B band, ≈ 20 days in i band, and a few days later in the NIR). Then a steep decline lasting ≈ 2 weeks is followed by a slow, linear decline until the end of the observations on day ≈ 70 .

We determined the slopes of the optical light curves by dividing the difference in magnitude of contiguous photometric epochs by their temporal difference, and then fitting the obtained slopes with low-order polynomials. The slope evolutions confirm that, after maximum light, bluer bands tend to decline faster than redder bands (this is not true for the long-lasting SNe 2005ip, 2006jd and also not for SN 2006qq). The decline after maximum is not linear at least for those objects which were observed for less than ≈ 100 days, whereas after ≈ 100 days SN 2006qq shows an almost linear decline in each band. For SNe 2005kj and 2006aa the decline rate increases with time, whereas for SNe 2005ip, 2006jd and also for SN 2006bo the decline rate decreases. When we compare the decay rate of ^{56}Co ($0.0098 \text{ mag day}^{-1}$) with that of the V band for the five SNe observed after 100 days since discovery, we find that only SN 2006qq (and marginally SN 2005ip) has a slope compatible with radioactive decay. SN 2006bo might also be characterized by a late-time decline rate compatible with radioactive decay, but unfortunately the data do not allow this to be confirmed. Decline rates at 100 days are summarized in Table 8.

4.2. Absolute magnitudes and colors

Armed with the distances and $E(B - V)_{tot}$ color excess values listed in Table 1, absolute magnitude light curves were computed for the entire CSP SN II In sample and are plotted in Fig. 5 (top panels). In doing so a standard reddening law characterized by an $R_V = 3.1$ (Cardelli et al. 1989) was used to convert $E(B - V)_{tot}$ to absorption in each photometric bandpass. We assume the host reddening is zero for the SNe with no detectable Na I D.

SN 2008fq turns out to be the intrinsically brightest object in the sample, being ≈ 1 mag more luminous than SNe 2005kj, 2006aa and 2006qq. We note that SN 2008fq was corrected for a substantial amount of extinction ($A_V = 1.6$ mag), derived from Na I D absorption, which is known to provide poor constraints on reddening (Blondin et al. 2009; Folatelli et al. 2010; Poznanski et al. 2011). Nevertheless when adopting the Na I D-based color excess, the r -band light curve of SN 2008fq reaches a maximum value only ≈ 0.2 mag brighter than SN 1998S (Liu et al. 2000), which exhibits similar light curve shape and spectral properties (see bottom panel of Fig. 5 and Sect. 5.6). With this color excess the intrinsic broad-band colors of SN 2008fq also appear consistent to those of SN 1998S, as revealed in the top panel of Fig. 6. Peaking at $V = -19.3$ mag, SN 2008fq belongs to the bright-end of the “normal” SN II In category, whereas the super-luminous SNe II In exhibit absolute magnitudes brighter than -21 (Gal-Yam 2012).

SN 2006bo is the faintest object within the full CSP SN II In sample; being ≈ 2 mag less luminous than SN 2008fq at peak and never brighter than $V \approx -17$ mag. The r -band light curve evolves along a plateau phase over the first two months of monitoring and, as revealed in Fig. 5, is similar in overall shape to the 1994W-like SN 2011ht (Mauerhan et al. 2012a), but with a somewhat fainter luminosity along the plateau. As the explosion epoch of SN 2006bo is poorly constrained, it may have been discovered weeks after explosion. This possibility would then imply a higher tail luminosity as compared to that of SN 2011ht.

SNe 2005kj, 2006aa and 2006qq have peak V - and r -band absolute magnitudes between ≈ -17.7 and -18.5 mag. Among them, SN 2006qq decays slower, similarly to the long-lasting SNe 2005ip and 2006jd (S12), although it is brighter than those objects (see Fig. 5). In addition, SN 2005kj exhibits a relatively high luminosity for more than 180 days, but its decline rate beyond ≈ 100 days is larger than that of SN 2006qq. The evolution and brightness of the r -band light curve of SN 2006aa closely resembles that of SN 2005db (Kiewe et al. 2012). However, the rise time for SN 2006aa is particularly long (≈ 50 days). SN 2006aa also displays faint emission in the NIR, being ≈ 1 mag fainter than the bright SN 2008fq.

Estimates of the peak absolute magnitudes, derived from the individual light curves of each SN, are given in Table 9. These values have been determined by fitting the light curves with low-order polynomials. For completeness the peak absolute magnitudes of SNe 2005ip and 2006jd are also included in Table 9 (S12).

Figure 6 contains the comparison of intrinsic $(B - V)$, $(V - i)$ and $(J - H)$ colors of the full CSP SN II In sample. For comparison the panel containing the $(B - V)$ color curve evolution also includes several well-observed objects taken from the literature. Both the $(B - V)$ and $(V - i)$ color curves indicate an overall trend that SNe II In evolve to the red over time, and in this sample SNe 2008fq and 2006bo show the largest $(B - V)$ color evolution ranging from ≈ 0.2 mag to ≈ 1.0 mag over a period of ≈ 50 days. SN 2006bo appears to be much redder than the 1994W-like SN 2011ht, even though the light curve shapes are similar.

SNe 2005kj and 2006qq experience a slow cooling, comparable to that of the long-lasting SNe II in 2005ip and 2006jd. In particular SN 2005kj takes ≈ 120 days to reach a $(B - V) = 1.0$ mag. Interestingly, SN 2006aa first evolves to the blue, then reaches a minimum value in the optical colors at the time of maximum light and then over time evolves to the red.

The NIR ($J - H$) color curves follow more flat trajectories compared to the optical color curves. However, in the case of SNe 2005ip and 2006jd, the ($J - H$) color curve clearly exhibits values that increase over time, and this evolution is likely driven by emission related to newly formed dust (Fox et al. 2011, S12).

4.3. Bolometric properties

The photometric dataset of our CSP SN II in sample is well-suited to construct quasi-bolometric light curves. To do so requires the interpolation (when necessary extrapolation) of NIR magnitudes at epochs that coincide with the optical observations. Next broad-band magnitudes were converted to fluxes at the effective wavelength of each bandpass. After correcting each flux point for reddening, a spectral energy distribution (SED) at each observed epoch was fit with a spline resulting in a nearly complete UV-optical-NIR (UVOIR) SED. The SEDs were then integrated over wavelength space spanning from u to H band, and then the final UVOIR luminosity was computed by multiplying the UVOIR flux with $4\pi D_L^2$ (where D_L is the luminosity distance). A 1σ error on L was obtained through simulating hundreds of SEDs (according to the uncertainties on the specific fluxes) and taking the standard deviation of their integrals.

The final UVOIR light curves for the full CSP SN II in sample are plotted in the top panel of Fig. 7. As observed in the r -band absolute magnitude light curves, SN 2008fq and SN 2006bo are the brightest and faintest objects within the CSP SN II in sample, respectively, while SN 2006aa and SN 2008fq appear to have been discovered before reaching maximum. The peak bolometric luminosities range from those of normal CC SNe IIP, up to values 10 times higher, comparable to luminous SNe II (Inserra et al. 2012).

Inspection of the late phase portion of the UVOIR light curves reveals that the sample exhibits a diversity of decline rates, ranging from values both above and below the decline rate expected from the full trapping of energy produced by the radioactive decay chain $^{56}\text{Co} \rightarrow ^{56}\text{Fe}$. SNe 2005kj and 2006aa exhibit slopes steeper than that expected for full trapping of gamma-rays produced from the ^{56}Co decay, while the slopes of SNe 2005ip, 2006jd and 2006qq are more shallow. UVOIR light curve decline rates at 100 days after discovery are reported in Table 8. The inconsistency between observed and ^{56}Co decline rates suggests radioactivity is not the prevalent energy source for these objects.

The SEDs were also used to estimate temperature (T) and radius (R) of the emitting region assuming black-body (BB) fits. When performing the BB fits, u - and B -band flux points were excluded as they sample portions of the optical spectrum that suffer a significant reduction in continuum flux due to line blocking effects, particularly at late epochs. In addition, the r band was also excluded from the BB fits given the presence of prevalent $H\alpha$ emission.

The time-evolution of T and R for the full CSP SN II in sample is plotted in the bottom portion of Fig. 7. During early epochs, T monotonically drops over time in all cases but SN 2006aa, which shows a peak at ≈ 9000 K at the time of maximum light. At epochs past 50 days after discovery all objects decrease in T except SNe 2005ip and 2006jd, as they both show

enhanced thermal emission related to dust condensation (S12). The maximum T values range from ≈ 7000 to $11,500$ K and decline over time to values no less than 5500 K by day ≈ 60 . These values are consistent with SNe II in presented in the literature (see e.g. Smith et al. 2009a).

Figure 7 also reveals that R slowly increases over time for all the SNe with a SED that is well fit by a single BB component (i.e. all objects except SNe 2005ip and 2006jd), reaching an almost constant value at late times. Typical radii extend to $\approx 10^{15}$ cm, which is also typical for many SNe II in the literature (e.g. SN 1998S, Fassia et al. 2001). In a SN II in, most of the continuum emission is likely to come from an expanding thin cold dense shell. This shell continually expands to larger radii, but the black-body (BB) radius appears to stall or in some cases even to shrink because the shell covering factor decreases as the optical depth drops. This was discussed by Smith et al. (2008) where they present SN 2006tf.

5. Spectroscopy

In this section the visual-wavelength spectra of the five new CSP SNe II in are analysed and compared to other objects in the literature. A special emphasis is placed on constraining the evolution of both luminosity and line profile shape for the $H\alpha$ and $H\beta$ emission features. We note that the resolution of our spectra (see Table 7) allow us to resolve $H\alpha$ FWHM velocities down to only 320 km s^{-1} for SNe 2008fq, while for the other objects $H\alpha$ FWHM velocities are resolved down to 180 km s^{-1} .

5.1. SN 2005kj

The spectral sequence of SN 2005kj (Fig. 3, top panel) covers ≈ 150 days of evolution. Each spectrum exhibits prevalent, symmetric Balmer emission lines. The left panel of Fig. 8 displays the $H\alpha$ and $H\beta$ emission features, each fit with multiple Lorentzian components, while the right panel contains the flux and velocity evolution of both features. Flux and velocity measurements are also reported in Tables 10 and 11.

During the first 70 days of evolution, $H\alpha$ and $H\beta$ are characterized by a narrow $\text{FWHM}_n \approx 1000 \text{ km s}^{-1}$ and a broad $\text{FWHM}_b \approx 2500 \text{ km s}^{-1}$ component. Around ≈ 70 days the broad component becomes difficult to detect, while $H\beta$ begins to form a P-Cygni profile with an absorption minimum of $v_{min} \approx -600\text{--}800 \text{ km s}^{-1}$.

$H\beta$ is initially very bright, almost comparable to $H\alpha$ in luminosity. However, the Balmer decrement increases over time and $H\beta$ is found to be much fainter at late epochs. The total flux of both $H\alpha$ and $H\beta$ drops over time.

$H\gamma$ and $H\delta$ lines are also detected, both exhibiting a P-Cygni profile with a minimum absorption with similar velocity as shown by $H\beta$, but after ≈ 35 days they are barely discernible from the noise.

$\text{He I } \lambda 5876$ is visible until ≈ 20 days, showing narrow and broad components in emission. Concerning the narrow absorption lines, Na I D is not detected during early epochs, however the presence of $\text{Ca II H\&K } \lambda\lambda 3933, 3968$ is clear. Numerous Fe II and Ti II P-Cygni profiles are visible in the blue portion of the spectra of SN 2005kj from day $+32.8$. At epochs $\gtrsim 70$ days, the Ca II triplet and $\text{O I } \lambda 8447$ emerge and at later times ($\gtrsim 100$ days) a P-Cygni profile identified with Na I D is also visible.

The continuum flux, initially dominated by UV and blue photons, progressively becomes red, as expected from the decreasing temperature (see Fig. 7, middle panel).

5.2. SN 2006aa

The seven spectra that we obtained for SN 2006aa (Fig. 3, bottom panel) are typical SN II In spectra, mainly characterized by Balmer emission lines, in particular $H\alpha$ and $H\beta$, but also $H\gamma$ and $H\delta$. As shown in Fig. 9, their continuum-subtracted, extinction-corrected profiles are well fit by the sum of a broad ($\text{FWHM}_b \sim 2000 \text{ km s}^{-1}$) and a narrow ($\text{FWHM}_n \lesssim 700 \text{ km s}^{-1}$) Lorentzian in emission. In addition, in order to reproduce the narrow absorption feature, a narrow Lorentzian in absorption is fit at $\approx -800 \text{ km s}^{-1}$ from the central wavelength. The $H\alpha$ and $H\beta$ broad-component fluxes reach maximum values when the SN is at maximum light, whereas the narrow component exhibits nearly constant emission over time. Fluxes and velocities of the most important hydrogen lines are reported in Tables 12 and 13.

Fe II features are observed in all the spectra (between ≈ 20 and ≈ 80 days). As in the case of SN 2005kj, narrow lines of Na I D in absorption are not detected at the host galaxy rest frame, whereas narrow Ca II H&K absorption lines are observed. The spectral continuum is well fit by a BB function with temperature $T_{BB} \approx 8000\text{-}10000 \text{ K}$.

5.3. SN 2006bo

Only two early-time spectra were collected for SN 2006bo (Fig. 4, top panel). However, these reveal an interesting $H\alpha$ profile (see Fig. 10) characterized by a prevalent narrow emission ($\text{FWHM}_n \sim 1000 \text{ km s}^{-1}$) feature, and an absorption component at $\approx -600 \text{ km s}^{-1}$. Identical features are present in $H\beta$ and in the faint $H\gamma$ line, where the absorption is even more pronounced. This is a case of a SN II In that shows no clear signatures of a broad component. $H\alpha$ and $H\beta$ fluxes and velocities are given in Tables 14 and 15.

No Na I D absorption features are found in the spectra at the redshift of SN 2006bo, however features attributed to Ca II H&K are discernible. Fe II and Ti II P-Cygni profiles are also observed, while weak traces of the Ca II NIR triplet characterize the red end of the spectrum. The spectral continuum is well reproduced by a BB function with temperature $T_{BB} \approx 7000\text{-}8000 \text{ K}$.

5.4. SN 2006qq

The spectral sequence of SN 2006qq covers the first ≈ 70 days (Fig. 4, middle panel). $H\alpha$ is the most conspicuous feature in emission. At 30 days, besides its narrow, unresolved component ($\text{FWHM}_n \lesssim 200 \text{ km s}^{-1}$), a broad, strongly blue-shifted component emerges, reaching maximum flux at ≈ 60 days. At this epoch, both $H\alpha$ and $H\beta$ have an almost parabolic shape (see Fig. 11). The blue and red velocities at zero intensity (BVZI and RVZI) of the asymmetric $H\alpha$ profile are $\approx 10,000 \text{ km s}^{-1}$ and $\approx 3000 \text{ km s}^{-1}$. We note that the narrow Balmer lines are likely contaminated by the emission of an underlying H II region. In the last two spectra the broad Balmer emission significantly drops, indicating that after ≈ 70 days the ejecta-CSM interaction is weaker. This is consistent with the r -band “jump” at similar epochs (see Fig. 2). All the Balmer line fluxes and velocities are given in Tables 16 and 17.

Beside the Balmer lines, the spectra are characterized by broad features in the blue, especially in the first two spectra. $H\beta$ falls inbetween two of these broad features, which we identify as Fe II (similar broad features were identified in SN 1996L by Benetti et al. 1999). At late times the spectrum is flatter and only Balmer lines are clearly identifiable on a continuum that

is well represented by a 6000 K BB function. In the spectrum taken on 1st January 2007, narrow Na I D absorption is present ($\text{EW} = 0.76 \pm 0.21 \text{ \AA}$), as well as traces of Ca II H&K. Narrow emission of [N II] $\lambda 5755$ are clearly observed until ≈ 70 days. In the first spectrum narrow emission lines of He I $\lambda 5876$ and $\lambda 7065$ are also present.

5.5. SN 2008fq

The spectral sequence of SN 2008fq (Fig. 4, bottom panel) shows strong evolution within the first month of followup, including the appearance of a broad $H\alpha$ emission line that dominates the last spectra. The analysis of the Balmer lines is presented in Fig. 12, where $H\alpha$ and $H\beta$ are shown after low-order polynomial continuum-subtraction and extinction correction. $H\alpha$ lines have also been fit by the sum of several Lorentzian functions in order to measure fluxes and typical velocities (see also Tables 18 and 19). The first three spectra exhibit a narrow $H\alpha$ P-Cygni profile, characterized by unresolved emission ($\text{FWHM}_n < 200\text{-}400 \text{ km s}^{-1}$) and blue-shifted absorption with velocity $v_{min} \approx -400\text{-}500 \text{ km s}^{-1}$. $H\beta$ presents a similar shape. A narrow [N II] emission is also present, providing indication that the narrow Balmer lines are contaminated by the flux of an underlying H II region. A faint and broad $H\alpha$ P-Cygni profile is also observable in the first two spectra, with $\text{FWHM}_b \sim 4000 \text{ km s}^{-1}$ in emission and absorption minimum at $v_{min} \approx -7000\text{-}8000 \text{ km s}^{-1}$. $H\beta$ shows broad features as well, but the presence of nearby, broad Fe II lines makes it difficult to fit these components. In the first two spectra narrow emission lines of He I $\lambda 5876$ are also observed. This line is located close to the narrow Na I D absorption line, which is present in all the five spectra. Ca II H&K is also detected in all the spectra. In the first spectrum, the emission feature at $\approx 4640\text{-}4690 \text{ \AA}$ is likely due to C III $\lambda 4648$, N III $\lambda 4640$ and He II $\lambda 4686$. Given the strong similarity between SN 2008fq and SN 1998S (see Sect. 5.6), we follow the line identification of the latter published by Fassia et al. (2001). We note that high-ionization lines of carbon and nitrogen are common in the spectra of Wolf-Rayet stars. At V_{max} (≈ 14 days after discovery), the broad $H\alpha$ emission increases in brightness, while the faint, broad absorption continues to be present. Contemporaneously, the continuum in the blue portion of the spectrum exhibits some P-Cygni features, that we attribute to Fe II, Sc II and Na I D lines, while in the red portion of the SED broad Ca II triplet features emerge. After ≈ 30 days, $H\alpha$ shows a prevalent, broad emission ($\text{FWHM}_b \sim 7000 \text{ km s}^{-1}$). The faint and broad blue absorption is characterized by $v_{min} \approx -7000 \text{ km s}^{-1}$. The narrow Balmer P-Cygni absorption is difficult to identify, whereas the narrow Balmer emission ($\text{FWHM}_n \sim 200 \text{ km s}^{-1}$) is still present.

The spectral continuum is affected by a significant amount of extinction (through the EW of Na I D we estimate $E(B - V)_{host} = 0.46 \pm 0.03 \text{ mag}$), which makes the blue portion of the spectrum very faint.

5.6. Spectral comparison

Each of our five objects discussed in the previous sections has prevalent $H\alpha$ and $H\beta$ features, which serve as the basis for their classification as bonafide SNe II In. In three of them (SNe 2005kj, 2006aa, 2006bo), the narrow Balmer lines show P-Cygni profiles sitting on top of broad and symmetric bases. In the three panels of Fig. 13 the Balmer lines of these three objects are compared, after continuum-subtraction, extinction correction and peak nor-

malization. It turns out that the shorter the wavelength the deeper the narrow absorption.

The broad component is likely produced by fast moving material associated with the underlying SN ejecta, but it might also be due to the electron scattering of the narrow line photons.

Concerning the narrow Balmer lines, their narrow P-Cygni profiles suggest they arise from the recombination of a slow CSM surrounding the SN rather than from an underlying H II region. Only for SN 2006qq the narrow Balmer absorption is not detected, and in the spectra of this event we also observe narrow emission from [N II], typical of H II regions. However, the absence of strong oxygen and sulphur emission lines suggests that the narrow emission in SN 2006qq is not only due to contamination, but also to ionization of the CSM.

Plotted in the left panel of Fig. 14 are the $H\alpha$ EW values for the full CSP SN II_n sample, along with those of several objects from the literature. For some objects this parameter tends to increase over time, suggesting that the bulk of the radiation at early phases is related to continuum flux, whereas line emission dominates at later epochs. In particular, SNe 1998S and 2008fq stand out, both showing a strong $H\alpha$ EW enhancement of $\approx 10 \text{ \AA}$ to $\approx 250 \text{ \AA}$ within the first 70 days of evolution. Other events like SNe 2005kj and 2006aa exhibit an almost constant $H\alpha$ EW. In Table 20 we report the EW values of our five objects.

We also examine the total $H\alpha$ luminosity, as is shown in the right panel of Fig. 14. $L(H\alpha)$ values were computed by multiplying the de-reddened fluxes presented in Figs. 8–12 by $4\pi D_L^2$, where D_L is the luminosity distance listed in Table 1. $H\alpha$ luminosities of our objects are comparable with the typical values found for SNe II_n in the literature.

Concerning other lines, it is known that SNe II_n can exhibit Fe II and Ti II P-Cygni profiles. Following the line identification presented by Kankare et al. (2012), in Fig. 15 (left panel) these features are identified in moderately young spectra of SNe 2005kj, 2006aa and 2006bo. In SNe 2006qq and 2008fq, Fe II features are present as well, although they appear heavily blended.

As shown in the right panel of Fig. 15, the Ca II NIR triplet is not observed in SNe 2006aa or 2006qq, is barely detected in SNe 2005kj and 2006bo, and is clearly observed in SN 2008fq, where broad P-Cygni profiles characterize the red portion of the spectrum.

All of our objects are found to be spectroscopically similar to other events previously reported in literature. In Fig. 16 we present a spectral comparison of SNe 2005kj and 2006aa to SNe 2005db (Kiewe et al. 2012) and 1995G (Pastorello et al. 2002). Each spectrum is corrected for reddening and presented in its rest frame. The spectra are mainly characterized by a combination of narrow and broad Balmer features. Fe II lines are also present, modifying the bright blue continuum. The red continuum is almost featureless. Basically the spectra of SNe 2005kj and 2006aa follow the definition of SN II_n provided by Schlegel (1990) and are similar to those of many other SNe II_n in the literature (e.g. SNe 1999eb and 1999el; see Fig. 8 of Pastorello et al. 2002).

SN 2006bo appears to fit well within the recently suggested Type II_n-P sub-class (see Mauerhan et al. 2012a). The light curves presented in Sect. 4 show a luminosity drop after a plateau phase, exactly as was observed in SNe 1994W (Sollerman et al. 1998), 2009kn (Kankare et al. 2012) and 2011ht (Mauerhan et al. 2012a). The spectral comparison to SN 2009kn confirms that SN 2006bo is a similar object, as shown in Fig. 17. SN 2006bo spectra clearly resemble those of SN 2009kn ≈ 2 months after explosion (during the plateau

phase). The common features are the narrow Balmer emission lines along with the narrow Balmer absorption lines, and the Fe II P-Cygni profiles.

SN 2006qq is a peculiar object, with very broad emission features and a strong asymmetry in the $H\alpha$ profile. In Fig. 18 its $H\alpha$ profile is compared to those of SNe 1988Z (Turatto et al. 1993) and 2006jd (S12). Even though SN 2006qq clearly exhibits slower velocities in the broad component than those of SNe 1988Z and 2006jd, the profile is similarly characterized by a strong suppression of the red-wing. The fact that the broad $H\alpha$ component significantly strengthens weeks after explosion is similar to what was observed in SN 2006jd, but on different time scales (for SN 2006jd $H\alpha$ became remarkably brighter ≈ 400 days after explosion).

SN 2008fq can be defined as a SN 1998S-like event. SN 1998S is among the best studied interacting SNe. A comparison of the spectral evolution of SNe 1998S and 2008fq is presented in Fig. 19. Here the spectra were de-reddened and the listed epochs are relative to the time of V -band maximum. The similarity between the two objects is remarkable at all epochs. We note that the light curves are also very similar, as demonstrated in Sect. 4. The first example of SNe like 1998S and 2008fq is actually SN 1983K (Niemela et al. 1985; Phillips et al. 1990), but for this object a less extensive set of spectral and photometric observations exists. SN 2005gl also shows a spectral evolution that resemble that of SN 1998S (Gal-Yam et al. 2007; Gal-Yam & Leonard 2009). Another object sharing similar properties to SNe 1998S and 2008fq is SN 2007pk, which has recently been presented by Inserra et al. (2012). We note that SNe 2007pk and 2008fq show traces of C III and N III emission that were strong at early epochs in both SNe 1983K and 1998S. Finally, the late-time spectra (≥ 232 days) of SN 2007od (Andrews et al. 2010) are similar to those of SN 1998S. Interestingly, the absolute magnitudes of the above-mentioned events are also similar, ranging between $V_{\max} \sim -18.5$ mag (SN 2007pk) and $V_{\max} \sim -19.3$ mag (SN 2008fq). These values are affected by large uncertainties on the extinction.

6. Discussion

In the following we discuss the data for each of the five new CSP SNe II_n with the intent to determine the likely scenario underlying each object. Consistently with the interpretation of other SNe II_n, we assume that the ejecta of the exploding progenitor stars are experiencing strong interaction with surrounding CSM. In the following, constraints are placed on the mass-loss rate, the density and the extent of the CSM for each SN. Estimates derived in the following section are summarized in Table 21, which also includes the corresponding values derived from observations of SNe 2005ip and 2006jd. We stress that the mass-loss rate estimates are based on the uncertain assumption that the progenitor wind was steady. Therefore in Table 21 the more robust density wind parameter $w = \dot{M} v_w^{-1}$ is also reported.

6.1. SN 2005kj

The explosion date of SN 2005kj is not well constrained by pre-explosion images (see Table 2). However, its light curves were probably observed only a few days after maximum, as can be inferred from their flattening at early epochs. The high ($\approx 10,000$ K) early-time temperatures determined by BB fits and presented in Fig. 7 (middle panel) also suggest that the obser-

vations began soon after explosion. Based on the temperature comparison between SN 2005kj to SN 2008fq, we here assume that the explosion of SN 2005kj occurred 8 days prior to its discovery.

The high-energy radiation produced via shock interaction ionizes the slow moving CSM and gives rise to observed narrow ($\text{FWHM}_n \approx 1000 \text{ km s}^{-1}$) Balmer emission lines through recombination. The narrow Balmer absorption feature appearing a couple of months after discovery (well visible in $\text{H}\beta$) is also likely produced within the slow moving CSM ($v_{\min} \approx 600 \text{ km s}^{-1}$).

SN 2005kj presents iron and hydrogen P-Cygni profiles that are rounded and symmetric. The same properties were observed in the spectra of SN 1994W (Sollerman et al. 1998) and SN 1995G (Pastorello et al. 2002). Because of that, line optical depths of $\tau > 1$ were inferred for both objects, allowing the use of the expression $n_{\text{H}} > 3 \times 10^8 v_3 r_{15}^{-1} \text{ cm}^{-3}$ (Mihalas 1978) to estimate the electron density of the CSM. Here r_{15} is the CSM shell radius, which is close to the photospheric radius (expressed in units of 10^{15} cm , from BB fits to the SED); v_3 is the CSM shell velocity measured from the narrow P-Cygni absorption minimum and given in units of 10^3 km s^{-1} . We use the same expression for SN 2005kj ($v_3 \approx 0.6$ and $r_{15} \approx 1$), obtaining a lower limit for the CSM electron density: $n_{\text{H}} > 1.8 \times 10^8 \text{ cm}^{-3}$.

Clear signs of CSI are observed from the epoch of the first spectrum to the epoch of the last one (≈ 170 days since explosion). That means the ejecta did not overtake the outer radius of the CSM in 170 days. If the fastest ejecta were moving at $v_{\text{ejecta}}^{\max} \approx 3000 \text{ km s}^{-1}$ (BVZI of the broad component of $\text{H}\alpha$), this would then suggest that the outer radius of the CSM is $R_{\text{CSM}}^{\text{out}} \gtrsim 4.4 \times 10^{15} \text{ cm}$. Given that the interaction is already present at ≈ 15 days after explosion, the inner radius of the CSM is $R_{\text{CSM}}^{\text{in}} < 0.4 \times 10^{15} \text{ cm}$.

Following Salamanca et al. (1998), a rough estimate of the mass-loss rate (\dot{M}) can be computed via: $L(\text{H}\alpha_{\text{broad}}) \approx 0.25 \epsilon_{\text{H}\alpha} \dot{M} v_s^3 v_w^{-1}$, which is based on the assumption that the wind forming the CSM is steady. Here we adopted the shock velocity $v_s \approx 3000 \text{ km s}^{-1}$, derived from the FWHM of the broad component, and the wind velocity of $v_w \approx 600 \text{ km s}^{-1}$, which is obtained from the minimum of the narrow P-Cygni absorption. The efficiency factor is assumed to be $\epsilon_{\text{H}\alpha} = 0.1$, as in the literature (see e.g. Kiewe et al. 2012). The broad $\text{H}\alpha$ luminosity is measured to be $L(\text{H}\alpha_{\text{broad}}) \approx 1.0 - 3.4 \times 10^{40} \text{ erg s}^{-1}$. From these values we obtain $\dot{M} \approx 1.4 - 4.8 \times 10^{-3} M_{\odot} \text{ yr}^{-1}$.

6.2. SN 2006aa

SN 2006aa was discovered before maximum and its explosion date is well constrained (uncertainty of ± 8 days) thanks to pre-explosion images. We therefore assume the core-collapse occurred ≈ 8 days before discovery (see Table 2).

The spectra and the bolometric light curve suggest that the main source of energy is CSI, rather than the radioactive decay of ^{56}Ni and ^{56}Co . If we naively assume that the peak luminosity is powered solely due to radioactive decay, combining the epoch of the peak and the peak bolometric luminosity with Arnett's rule (Arnett 1982; Arnett et al. 1985; Branch 1992) gives a ^{56}Ni mass = $0.3 M_{\odot}$. This value is large compared to the typical ^{56}Ni masses measured for SNe II (see Figure 9 in Smartt et al. 2009).

BB fits of the SEDs reveals that the peak temperature was reached close to maximum light i.e. around ≈ 60 days after explosion. This late-time peak and the initial rise of the temperature can be explained by a strengthened interaction due to the

presence of a dense shell of CSM. Given that the maximum ejecta velocity is $v_{\text{ejecta}}^{\max} \approx 2500 \text{ km s}^{-1}$ (BVZI of $\text{H}\alpha$), and $t_{\text{max}} \approx 60$ days, the densest part of the CSM is likely located at $R_{\text{CSM}}^{\text{sh}} \approx 1.3 \times 10^{15} \text{ cm}$. Since the wind velocity derived from the narrow P-Cygni absorption minimum is $\approx 600 \text{ km s}^{-1}$, the mass-loss episode that produced this dense shell likely occurred ≈ 8 months prior to core-collapse.

As the spectra of SN 2006aa are quite similar to those of SN 2005kj, similar techniques can be adopted to estimate the electron density of the wind, the physical extension in radius from the progenitor of the CSM, and the progenitor's mass-loss rate. We obtain $n_{\text{H}} > 7.6 \times 10^8 \text{ cm}^{-3}$, by assuming $v_3 \approx 0.6$ and $r_{15} \approx 0.8$. The inner CSM radius is $R_{\text{CSM}}^{\text{in}} < 0.5 \times 10^{15} \text{ cm}$ and the outer one is $R_{\text{CSM}}^{\text{out}} \gtrsim 1.8 \times 10^{15} \text{ cm}$, assuming the above mentioned v_{ejecta}^{\max} and the beginning and the end of the interaction occurring on 24 and 85 days after explosion.

The mass-loss rate is $\dot{M} \approx 5.4 - 16.2 \times 10^{-3} M_{\odot} \text{ yr}^{-1}$, where a wind velocity $v_w \approx 600 \text{ km s}^{-1}$ and a shock velocity $\approx 2000 \text{ km s}^{-1}$ (FWHM_b) were used. The efficiency factor is again assumed to be $\epsilon_{\text{H}\alpha} = 0.1$. The broad $\text{H}\alpha$ luminosity is found to be $L(\text{H}\alpha_{\text{broad}}) \approx 1.1 - 3.4 \times 10^{40} \text{ erg s}^{-1}$.

6.3. SN 2006bo

The explosion date of SN 2006bo is not well constrained by pre-explosion images. Since a plateau in the light curve having a duration of ≈ 70 days and then a sudden drop in luminosity was observed, we classify SN 2006bo as being a SN 1994W-like event. These transients are characterized by a ≈ 100 days plateau, therefore it is possible that SN 2006bo was discovered even a month after explosion. The fact that we did not observe the SN between 70 and 145 days after discovery makes it impossible to know whether the drop in luminosity occurred immediately after 70 days or later, and therefore a proper comparison of the plateau's length is difficult. On the other hand, the spectral comparison to SN 2009kn shown in Fig. 17 suggests that the SN could have been discovered at least ≈ 40 days after explosion. The large uncertainty on the explosion date determines the uncertainty on the amount of ^{56}Ni that is likely to power the light curve tail, as was the case in SN 2009kn (Kankare et al. 2012). Assuming that the explosion occurred on the day of discovery, then the bolometric light curve tail yields a ^{56}Ni mass of $M_{^{56}\text{Ni}} = 0.007 M_{\odot}$. If the explosion occurred 40 days before, then a $M_{^{56}\text{Ni}} = 0.011 M_{\odot}$ is obtained. In any case that would be lower than the upper limit estimated for SN 2009kn of $0.023 M_{\odot}$ (Kankare et al. 2012), and comparable to the value $0.01 M_{\odot}$, inferred for SN 2011ht (Mauerhan et al. 2012a). Unfortunately, as only a single photometric epoch was obtained at late epochs, it is not possible to determine if the slope of the SN tail is consistent with the ^{56}Co decay.

The Balmer lines appearing in the two spectra of SN 2006bo seem to be well reproduced by a single Lorentzian function, with typical $\text{FWHM} \approx 1000 \text{ km s}^{-1}$, plus an absorption component peaking at -600 km s^{-1} . We believe that both components are generated in the CSM, with wind velocity $v_w \approx 600 \text{ km s}^{-1}$. The fact that the narrow emission component has slightly higher velocities than the narrow absorption might be due to electron scattering broadening of the narrow emission in the wind. The likely absence of a broad component might mean that ionized ejecta are not visible because of a CDS (cold-dense-shell). Given that we do not observe the broad component, we assume the shock velocity to have a lower limit equal to the FWHM of the narrow component, i.e. $v_s \gtrsim 1000 \text{ km s}^{-1}$.

The duration of the plateau is $\approx 70\text{--}110$ days; that means the outer radius of the CSM surrounding SN 2006bo is $R_{\text{CSM}}^{\text{out}} \approx 1.5\text{--}2.4 \times 10^{15}$ cm. Here we assume that the emission after the plateau phase is mainly due to radioactive decay rather than to CSI and a maximum ejecta velocity of $v_{\text{ejecta}}^{\text{max}} \approx 2500$ km s $^{-1}$ (BVZI of H α). The limit on the inner CSM radius is computed from the epoch of the first spectrum (11–41 days depending on the explosion date). We obtain $R_{\text{CSM}}^{\text{in}} \approx 0.2\text{--}0.9 \times 10^{15}$ cm.

The mass-loss rate estimate gives $\dot{M} \lesssim 2.28\text{--}3.42 \times 10^{-2} M_{\odot} \text{ yr}^{-1}$. Here we assume the total H α luminosity as the upper limit value for the broad H α luminosity, $L(\text{H}\alpha_{\text{broad}}) \lesssim 0.6\text{--}0.9 \times 10^{40}$ erg s $^{-1}$, using the above mentioned $\epsilon_{\text{H}\alpha}$, v_s and v_w . For a photospheric radius of 7.9×10^{14} cm (see Fig. 7, bottom panel), the electron density is $n_{\text{H}} > 3.8 \times 10^8$ cm $^{-3}$.

6.4. SN 2006qq

SN 2006qq was discovered relatively soon after explosion. Given the constraint from the pre-explosion images, we assume the explosion occurred ≈ 16 days before discovery (see Table 2). This appears consistent with the temperature comparison to SN 2008fq (see Fig. 7, middle panel), whose explosion date is better constrained, although the temperature evolution is hard to standardize.

Given the bright emission lines, it is likely that CSI powers the emission of SN 2006qq, although the bolometric light curve seems to follow the ^{56}Co radioactive decay at late times. If radioactive decay was the main powering source at late times, a ^{56}Ni mass of $M_{^{56}\text{Ni}} = 0.4 M_{\odot}$ is derived.

As discussed in Sect. 5, the spectra reveal strong, broad H α and H β emission from the ionized ejecta, whose luminosity reaches maximum at ≈ 76 days after explosion. The broad emission from the ejecta is strongly asymmetric, with H α BVZI $\approx 10^4$ km s $^{-1}$ and RVZI $\approx 3 \times 10^3$ km s $^{-1}$. The asymmetry can be explained in terms of dust obscuration of the radiation coming from the back of the ejecta. Indeed Fox et al. (2011) detected $0.5\text{--}1.7 \times 10^{-2} M_{\odot}$ of (graphite) dust emitting in the MIR for this SN. The strong asymmetric H α profile can also be produced through the occultation of the radiation coming from the receding ejecta by an opaque photosphere. The ratio between the photospheric radius and the maximum ejecta radius (R_p/R_{max}) can be determined from H α BVZI and RVZI for each spectral epoch (see S12). In this case we obtain $R_p/R_{\text{max}} \approx 0.87$ and 0.95 at ≈ 28 and at ≈ 76 days after explosion, respectively.

The epoch of the maximum broad emission and the maximum ejecta velocity ($v_{\text{ejecta}}^{\text{max}}$, from the H α BVZI) set the distance ($R_{\text{CSM}}^{\text{sh}}$) to the densest part of the CSM to be $R_{\text{CSM}}^{\text{sh}} \approx 6.6 \times 10^{15}$ cm. This dense shell was ejected during the end of the life of the progenitor star. If the wind velocity is $v_w \lesssim 200$ km s $^{-1}$, as measured from the FWHM of the narrow emission lines, then the mass-loss episodes that produced the dense shell occurred at least 10 years before core-collapse.

The broad H α luminosity along with the assumed v_w and $v_s \approx 6000$ km s $^{-1}$ (from the broad H α FWHM neglecting the occultation effect) gives a mass-loss rate of $\dot{M} \lesssim 0.3\text{--}0.7 \times 10^{-3} M_{\odot} \text{ yr}^{-1}$.

We derive an electron density lower limit of $n_{\text{H}} > 1.1 \times 10^9$ cm $^{-3}$, from a photospheric radius of 1.6×10^{15} cm.

The inner and the outer CSM radius that we can probe correspond to the phase of the first and the last spectral epoch (≈ 29 and 91 days since explosion respectively) multiplied by $v_{\text{ejecta}}^{\text{max}}$. We obtain $R_{\text{CSM}}^{\text{in}} \lesssim 2.5 \times 10^{15}$ cm and $R_{\text{CSM}}^{\text{out}} \gtrsim 7.9 \times 10^{15}$ cm.

6.5. SN 2008fq

The explosion date of SN 2008fq is well constrained by pre-explosion images (± 4.5 days uncertainty). The light curve comparison with SN 1998S (see bottom panel of Fig. 5) suggests that the explosion occurred soon after the last non-detection, ≈ 8 days before discovery. The presence of broad H α P-Cygni features in the early time spectra allows us to estimate the ejecta velocity; we obtain $v_{\text{min}} \sim 7000\text{--}8000$ km s $^{-1}$. Given that the first spectrum was observed 1.7 days after discovery, and that the photospheric radius at that epoch was $\approx 10^{15}$ cm, by assuming free expansion we confirm that the core-collapse occurred soon after the last non-detection.

The lack of a very early time spectrum prevents us from determining if SN 2008fq displayed strong CSI soon after core collapse, as was observed in SN 1998S (Leonard et al. 2000; Fassia et al. 2001, and see strong emission lines in the spectrum of SN 1998S at -15 days since maximum in Fig. 19).

The presence of a wind moving at $v_w \approx 500$ km s $^{-1}$ (from the narrow absorption minimum) is observed in SN 2008fq, as was also detected for SN 1998S at similar phases (Leonard et al. 2000; Fassia et al. 2001). We note, however, that the wind velocity of SN 1998S was lower (≈ 150 km s $^{-1}$). From the extreme blue edge of the broad H α absorption, we determine a maximum ejecta velocity $v_{\text{ejecta}}^{\text{max}} \approx 9000$ km s $^{-1}$. If we assume that SN 2008fq had an inner CSM (ICSM) like in the case of SN 1998S (Leonard et al. 2000; Fassia et al. 2001), given that the first spectrum is observed ≈ 10 days after explosion and the above mentioned $v_{\text{ejecta}}^{\text{max}}$, the ICSM could not be more extended than $R_{\text{CSM}}^{\text{in}} \approx 7.8 \times 10^{14}$ cm.

As shown in Sect. 5, about 20 days after maximum (≈ 45 days after explosion) a broad, prevalent Balmer emission component emerges. Following the interpretation of Leonard et al. (2000); Fassia et al. (2001) for SN 1998S, this is likely due to the interaction with an outer, denser CSM (OCSM). Given the assumed $v_{\text{ejecta}}^{\text{max}}$, the inner part of the OCSM is placed at $R_{\text{CSM}}^{\text{sh}} \approx 3.5 \times 10^{15}$ cm. A similar inner radius was found for the OCSM of SN 1998S (Fassia et al. 2001). The outer radius of the OCSM corresponds to the last spectral epoch (≈ 78 days after explosion); we obtain $R_{\text{CSM}}^{\text{out}} \gtrsim 6.1 \times 10^{15}$ cm. Given these radii and the assumed wind velocity, the OCSM was ejected during an episodic mass loss that started at least ≈ 3.9 years before core-collapse and ended ≈ 2.2 years prior to core collapse. Assuming the same wind velocity, the ICSM was formed during a mass-loss that started less than 6 months before core collapse.

The most likely scenario is that the observed spectra up to 6 days after maximum are mainly powered by the ejecta interaction with a low-density, mid-CSM (MCSM). As suggested by Fassia et al. (2001) for SN 1998S, this would explain the low contrast of the P-Cygni profiles (formed in the ejecta) on the blue continuum of the spectra (produced in a cold dense shell at the ejecta/MCSM interface). Only 20 days after maximum the ejecta reach the OCSM, giving rise to a stronger interaction.

The mass-loss history of SN 2008fq is likely characterized by episodic outbursts that gave rise to a complex CSM. Therefore an estimate of the mass-loss rate is difficult to obtain as the steady wind hypothesis is likely wrong. However, if we assume the shock velocity to be similar to the ejecta velocity v_{min} (consistently with the FWHM of the broad H α component in the last spectra), for the above-mentioned v_w and $L(\text{H}\alpha)_{\text{broad}} \approx 1.5 \times 10^{41}$ erg s $^{-1}$ we obtain $\dot{M} \approx 1.1 \times 10^{-3} M_{\odot} \text{ yr}^{-1}$. We also obtain $n_{\text{H}} > 9.0 \times 10^8$ cm $^{-3}$ (for a typical photospheric radius $R_{\text{ph}} \approx 2.5 \times 10^{15}$ cm).

6.6. SN II_n sub-types and progenitor scenarios

The seven CSP SNe II_n confirm the diversity of observational properties from this sub-class of CC explosions, while the case of SN 2006aa displays previously unobserved properties. Under close examination these objects show how SNe II_n can be separated out into rather different categories.

SN 2006bo belongs to the rare SN 1994W-like class (Mauerhan et al. 2012a). Beside SN 1994W (Sollerman et al. 1998), only two additional objects are known to belong to this group, namely SNe 2009kn (Kankare et al. 2012) and 2011ht (Mauerhan et al. 2012a). These objects all have Type II_n spectral features but a characteristic light curve plateau phase like that observed in SNe IIP.

SN 2008fq forms with a few other objects (e.g. SNe 2007pk and 1983K) the SN 1998S-like category, that presents optical light curves peaking within $\approx 10\text{--}20$ days at $-18.5 \lesssim V_{\max} \approx -19.3$ mag, and displays characteristic spectral evolution with broad emission components arising after maximum light.

SN 2006qq, together with SNe 2005ip and 2006jd (S12), resemble the Type II_n SNe 1988Z and 1995N (Turatto et al. 1993; Fransson et al. 2002). Evidently a common property amongst these objects is an asymmetric H α profile, and long-lasting dust emission that peaks at MIR wavelengths.

SNe 2005kj is similar to more common SNe II_n, like those presented in Kiewe et al. (2012) (e.g. SN 2005cp) that represent the majority of the Type II_n population. SN 2006aa shows an interesting and unprecedented initial plateau in the u band and an uncommon late time increase of the photospheric temperature. However, like in the case of SN 2005kj, its spectral features are similar to those of typical SNe II_n (Kiewe et al. 2012).

We note that the initial class of Type II_n SNe (Schlegel 1990) likely included a variety of phenomena, with the common characteristics of CSI giving rise to narrow Balmer lines. Some sub-types have already been identified and singled out in the past, and we note that some of these rare interacting, core-collapse SN types are not represented in the CSP sample, like superluminous SNe-II (Gal-Yam 2012) and SNe Ibn (Pastorello et al. 2008). A couple of SN 2002ic-like objects (Hamuy et al. 2003) were observed by the CSP and presented in Prieto et al. (2007) and Taddia et al. (2012). These events show spectra resembling those of SNe Ia, although diluted by a blue continuum with the addition of Balmer emission lines. These properties can be interpreted as the result of the interaction between a thermonuclear SN and its dense CSM. Following this interpretation, we believe these transients do not belong to the family of core-collapse SNe II_n, and therefore we do not include them in our sample. However, we note that alternative explanations support the idea that SN 2002ic-like objects might actually be core-collapse events (Benetti et al. 2006).

Smith et al. (2011) found that the SNe II_n sub-class constitutes ≈ 9 percent of all CC SNe. Although the CSP was not an unbiased survey, the number of SNe II_n (7) among the total number of CC SNe (116) is consistent with the fraction found by Smith et al. (2011). As noted by Kiewe et al. (2012), – who added 4 more SNe II_n – the current number of well studied SNe II_n is still very low, and often publications are driven by more peculiar objects. The CSP sample presented here therefore contributes significantly to the current Type II_n sample.

Although our sample is still too small to allow further sub-classifications, we have noted that even if there is large diversity in the properties of SNe II_n, the objects we have found all do match up with similar objects in the literature. It thus seems that the population of narrow-line CC SNe separate out into discrete

sub-categories. This is based on only a handful of objects, and further observations are clearly needed to map out the diversity of SNe II_n.

What determines the appearance of these objects is foremost the mass-loss history, since this shapes the CSM the SN interacts with. For line-driven stellar winds the main factors affecting the mass-loss are the progenitor mass and the metallicity. If that was the main mass-loss mechanism, then we could expect a continuum of observational properties reflecting the continuous variation of progenitor mass and metallicity. However, SN 1994W-like, SN 1998S-like and long-lasting SNe II_n look distinctively different, and we have not yet found any transitional or intermediate object connecting these different subtypes. This could imply that the final fate of these stars can only follow certain specific paths.

One overall aim of continued studies of SNe II_n is to identify the progenitor stars that end their lives following these paths. This is often done by comparing the derived mass-loss properties with those of massive stars. In this regard we note some caveats.

The mass-loss rate estimates that we have presented assume steady winds. This makes them easy to calculate from the observables, and easy to compare to many similar estimates in the literature. It should be emphasized, however, that this is likely a much too simplistic assumption (e.g. Dwarkadas 2011). In fact, much of the observations of SNe II_n seem to favour mass-loss histories of more complicated kinds, including clumped winds and ejected shells. The wind density parameters presented in Table 21 are more closely tied up to the observations, being independent from wind velocities.

We also remind the reader that the mass-loss period probed by observations of SNe II_n is only a very tiny fraction of the life time of the progenitor stars. What we actually know observationally about the mass-loss properties of RSG or LBV stars is of course derived from stars that are not that close ($\lesssim 1000$ years) to their final explosion.

If the mass-loss history in SNe II_n was dominated by other mechanisms like pulsations (Yoon & Cantiello 2010), which drive episodic outbursts occurring only under specific conditions, we could more easily explain the existence of such different sub-types. Our sample does imply that for some SNe (2006aa, 2006jd, 2006qq, and 2008fq) dense shells have likely been ejected soon before explosion by episodic outbursts.

The values derived for the mass-loss rates in this work ($10^{-4}\text{--}10^{-2} M_{\odot} \text{ yr}^{-1}$) are similar to those found by Kiewe et al. (2012) for other SNe II_n. Such high numbers may imply that LBVs are the most likely progenitor channel, but it is unclear if RSG may not also be able to produce some of the events if the steady wind assumption is not enforced. The wind density parameter of three SNe in our sample is higher than $10^{16} \text{ g cm}^{-1}$, the other objects exhibit $w \sim 10^{15} \text{ g cm}^{-1}$. These values are consistent with those found for other events in the literature (e.g. Chugai & Danziger 1994; Smith et al. 2009a)

Certainly there are objects with identified LBV progenitors, like SN 2005gl (Gal-Yam & Leonard 2009) and SN 2009ip (Mauerhan et al. 2012b; Pastorello et al. 2012); in these cases the progenitor was directly detected before core collapse. However, we caution that other channels (like RSGs) can not be excluded on the basis of rough mass-loss rate estimates. Interestingly, Anderson et al. (2012) show that SNe II_n are located in environments similar to those of SNe IIP (whose progenitors are RSGs), indicating that the majority of events may not arise from very massive stars like LBVs.

The estimates of wind velocities from the narrow P-Cygni absorption features (for our sample we find typical values of \approx

500–600 km s⁻¹) are also consistent with LBV wind velocities. However, slower winds might have been accelerated at the shock breakout by the radiation pressure. In that case, we would detect velocities of hundreds of km s⁻¹ even though the wind had an original velocity of tenths of km s⁻¹ (like those measured for RSGs).

7. Conclusions

In this paper we have presented the data for five of the seven CSP SNe II_n, including extensive optical and NIR photometry and visual-wavelength spectroscopy. We confirm the diversity of this class of SNe, although a comparison to objects in the literature provides counterparts for each object. This implies that several sub-categories are present within the SNe II_n class, including SN 1994W-like (SN 2006bo), SN 1998S-like (SN 2008fq) and SN 1988Z-like (SN 2006qq) events. These sub-categories appear significantly different from each other, suggesting that SNe II_n might be the result of different conditions in the progenitor mass/metallicity phases space. With a late-time maximum and an initial *u*-band plateau, the peculiar SN 2006aa was also studied. Estimates for CSM parameters have been derived and compared to objects in the literature. Mass-loss rates and wind velocities derived from this sample are compatible with LBV progenitors, although caveats of such a connection are discussed.

Acknowledgements. We thank the referee, Nathan Smith, for providing comments that helped to improve the paper. We are grateful to Eric Hsiao, David Osip and Yuri Beletsky for taking the *K*-band template of SN 2005kj. We also thank Erkki Kankare for sharing the spectra of SN 2009kn, Seppo Mattila for his inputs, Keiichi Maeda and Takashi J. Moriya for helpful discussions, and Miguel Roth for his important contribution to the CSP.

F. Taddia acknowledges the Instrument Centre for Danish Astrophysics (IDA) for funding his visit to Aarhus University. This material is also based upon work supported by NSF under grants AST-0306969, AST-0607438 and AST-1008343. M. Stritzinger acknowledges generous support provided by the Danish Agency for Science and Technology and Innovation realized through a Sapere Aude Level 2 grant. The Oskar Klein Centre is funded by the Swedish Research Council. J. P. Anderson and M. Hamuy acknowledge support by CONICYT through FONDECYT grant 3110142, and by the Millennium Center for Supernova Science (P10-064-F), with input from ‘Fondo de Innovación para la Competitividad, del Ministerio de Economía, Fomento y Turismo de Chile’. This research has made use of the NASA/IPAC Extragalactic Database (NED) which is operated by the Jet Propulsion Laboratory, California Institute of Technology, under contract with the National Aeronautics and Space Administration.

References

- Aldering, G., Antilogus, P., Bailey, S., et al. 2006, *ApJ*, 650, 510
 Anderson, J. P., Habergham, S. M., James, P. A., & Hamuy, M. 2012, *MNRAS*, 424, 1372
 Andrews, J. E., Gallagher, J. S., Clayton, G. C., et al. 2010, *ApJ*, 715, 541
 Arnett, W. D. 1982, *ApJ*, 253, 785
 Arnett, W. D., Branch, D., & Wheeler, J. C. 1985, *Nature*, 314, 337
 Benetti, S., Turatto, M., Cappellaro, E., Danziger, I. J., & Mazzali, P. A. 1999, *MNRAS*, 305, 811
 Benetti, S., Cappellaro, E., Danziger, I. J., et al. 1998, *MNRAS*, 294, 448
 Benetti, S., Cappellaro, E., Turatto, M., et al. 2006, *ApJ*, 653, L129
 Blanc, N., Copin, Y., Gangler, E., et al. 2006, *The Astronomer’s Telegram*, 732, 1
 Blondin, S., Modjaz, M., Kirshner, R., Challis, P., & Hernandez, J. 2006, *Central Bureau Electronic Telegrams*, 481, 1
 Blondin, S., Modjaz, M., Kirshner, R., et al. 2006, *Central Bureau Electronic Telegrams*, 679, 1
 Blondin, S., Prieto, J. L., Pata, F., et al. 2009, *ApJ*, 693, 207
 Boles, T., Nakano, S., & Itagaki, K. 2005, *Central Bureau Electronic Telegrams*, 275, 1
 Boles, T., & Monard, L. A. G. 2006, *Central Bureau Electronic Telegrams*, 468, 1
 Bonnaud, C., Pecontal, E., Blanc, N., et al. 2005, *Central Bureau Electronic Telegrams*, 296, 1
 Branch, D. 1992, *ApJ*, 392, 35
 Cardelli, J. A., Clayton, G. C., & Mathis, J. S. 1989, *ApJ*, 345, 245
 Chandra, P., Chevalier, R. A., Chugai, N., et al. 2012, *ApJ*, 755, 110
 Chevalier, R. A., & Fransson, C. 1994, *ApJ*, 420, 268
 Chugai, N. N., Blinnikov, S. I., Cumming, R. J., et al. 2004, *MNRAS*, 352, 1213
 Chugai, N. N. 2001, *MNRAS*, 326, 1448
 Chugai, N. N., & Danziger, I. J. 1994, *MNRAS*, 268, 173
 Contreras C., Hamuy, M., Phillips, M. M., et al. 2010, *AJ*, 139, 519
 Dilday, B., Howell, D. A., Cenko, S. B., et al. 2012, *Science*, 337, 942
 Leonard, D. C., Filippenko, A. V., Barth, A. J., & Matheson, T. 2000, *ApJ*, 536, 239
 Dwarkadas, V. V., & Gruszko, J. 2012, *MNRAS*, 419, 1515
 Dwarkadas, V. V. 2011, *MNRAS*, 412, 1639
 Fassia, A., Meikle, W. P. S., Chugai, N., et al. 2001, *MNRAS*, 325, 907
 Folatelli, G., Contreras, C., Phillips, M. M., et al. 2006, *ApJ*, 641, 1039
 Folatelli, G., Phillips, M. M., Burns, C. R. et al. 2010, *AJ*, 139, 120
 Fransson, C., Chevalier, R. A., Filippenko, A. V., et al. 2002, *ApJ*, 572, 350
 Fox, O. D., Chevalier, R. A., Skrutskie, M. F., et al. 2011, *ApJ*, 741, 7
 Fransson, C., Chevalier, R. A., Filippenko, A. V., et al. 2002, *ApJ*, 572, 350
 Gal-Yam, A., Leonard, D. C., Fox, D. B., et al. 2007, *ApJ*, 656, 372
 Gal-Yam, A., & Leonard, D. C. 2009, *Nature*, 458, 865
 Gal-Yam, A. 2012, *Science*, 337, 927
 Hamuy, M., Folatelli, G., Morrell, N., & Phillips, M. M. 2006, *PASP*, 118, 2
 Hamuy, M., Phillips, M. M., Suntzeff, N. B., et al. 2003, *Nature*, 424, 651
 Inserra, C., Pastorello, A., Turatto, M., et al. 2012, *arXiv:1210.1411*
 Kankare, E., Ergon, M., Bufano, F., et al. 2012, *MNRAS*, 424, 855
 Kiewe, M., Gal-Yam, A., Arcavi, I., et al. 2012, *ApJ*, 744, 10
 Komatsu, E., Dunkley, J., Nolte, M. R., et al. 2009, *ApJS*, 180, 330
 Kudritzki, R.-P., & Puls, J. 2000, *ARA&A*, 38, 613
 Landolt, A. U. 1992, *AJ*, 104, 340
 Lee, E., & Li, W. 2006, *Central Bureau Electronic Telegrams*, 395, 1
 Leonard, D. C., Filippenko, A. V., Barth, A. J., & Matheson, T. 2000, *ApJ*, 536, 239
 Liu, Q.-Z., Hu, J.-Y., Hang, H.-R., et al. 2000, *A&AS*, 144, 219
 Mauerhan, J. C., Smith, N., Silverman, J. M., et al. 2012, *arXiv:1209.0821*
 Mauerhan, J. C., Smith, N., Filippenko, A., et al. 2012, *arXiv:1209.6320*
 Mihalas, D. 1978, *San Francisco, W. H. Freeman and Co.*, 1978. 650 p.,
 Modjaz, M., Kirshner, R., Challis, P., & Calkins, M. 2005, *Central Bureau Electronic Telegrams*, 276, 1
 Niemela, V. S., Ruiz, M. T., & Phillips, M. M. 1985, *ApJ*, 289, 52
 Nymark, T. K., Fransson, C., & Kozma, C. 2006, *A&A*, 449, 171
 Pastorello, A., Aretxaga, I., Zampieri, L., et al. 2005, *ASPC*, 342, 285
 Pastorello, A., Turatto, M., Benetti, S., et al. 2002, *MNRAS*, 333, 27
 Pastorello, A., Mattila, S., Zampieri, L., et al. 2008, *MNRAS*, 389, 113
 Pastorello, A., Cappellaro, E., Inserra, C., et al. 2012, *arXiv:1210.3568*
 Phillips, M. M., Hamuy, M., Maza, J., et al. 1990, *PASP*, 102, 299
 Poznanski, D., Ganeshalingam, M., Silverman, J. M., Filippenko, A. V. 2011, *MNRAS*, 415, L81
 Persson, S. E., Murphy, D. C., Krzeminski, W., Roth, M., & Rieke, M. J. 1998, *AJ*, 116, 2475
 Poznanski, D., Ganeshalingam, M., Silverman, J. M., & Filippenko, A. V. 2011, *MNRAS*, 415, L81
 Prasad, R. R., & Li, W. 2006, *Central Bureau Electronic Telegrams*, 673, 1
 Prieto, J. L., Garnavich, P. M., Phillips, M. M., et al. 2007, *arXiv:0706.4088*
 Quinn, J., Baade, D., Clocchiatti, A., et al. 2008, *Central Bureau Electronic Telegrams*, 1510, 1
 Roming, P. W. A., Pritchard, T. A., Prieto, J. L., et al. 2012, *ApJ*, 751, 92
 Salamanca, I., Cid-Fernandes, R., Tenorio-Tagle, G., et al. 1998, *MNRAS*, 300, L17
 Schlafly, E. F., & Finkbeiner, D. P. 2011, *ApJ*, 737, 103
 Schlegel, E. M. 1990, *MNRAS*, 244, 269
 Silverman, J. M., Wong, D., Filippenko, A. V., & Chornock, R. 2006, *Central Bureau Electronic Telegrams*, 766, 2
 Smartt, S. J., Eldridge, J. J., Crockett, R. M., & Maund, J. R. 2009, *MNRAS*, 395, 1409
 Smith, N., Silverman, J. M., Filippenko, A. V., et al. 2012, *AJ*, 143, 17
 Smith, N., Li, W., Filippenko, A. V., & Chornock, R. 2011, *MNRAS*, 412, 1522
 Smith, N., Li, W., Silverman, J. M., Ganeshalingam, M., & Filippenko, A. V. 2011, *MNRAS*, 415, 773
 Smith, N., Hinkle, K. H., & Ryde, N. 2009, *AJ*, 137, 3558
 Smith, N., Silverman, J. M., Chornock, R., et al. 2009, *ApJ*, 695, 1334
 Smith, N., Chornock, R., Li, W., et al. 2008, *ApJ*, 686, 467
 Smith, N., Li, W., Foley, R. J., et al. 2007, *ApJ*, 666, 1116
 Smith, N., & Owocki, S. P. 2006, *ApJ*, 645, L45
 Smith, J. A., Tucker, D. L., Kent, S., et al. 2002, *AJ*, 123, 2121
 Soker, N., & Kashi, A. 2012, *arXiv:1211.5388*
 Sollerman, J., Cumming, R. J., & Lundqvist, P. 1998, *ApJ*, 493, 933
 Stathakis, R. A., & Sadler, E. M. 1991, *MNRAS*, 250, 786

- Stritzinger, M., Taddia, F., Fransson, C., et al. 2012, *ApJ*, 756, 173
Stritzinger, M. D., Phillips, M. M., Boldt, L. N., et al. 2011, *AJ*, 142, 156
Taddia, F., Stritzinger, M. D., Phillips, M. M., et al. 2012, *A&A*, 545, L7
Thrasher, P., Li, W., & Filippenko, A. V. 2008, *Central Bureau Electronic Telegrams*, 1507, 1
Turatto, M., Benetti, S., & Cappellaro, E. 2003, *From Twilight to Highlight: The Physics of Supernovae*, ed. W. Hillebrandt & B. Leibundgut (Berlin: Springer), 200
Turatto, M., Cappellaro, E., Danziger, I. J., et al. 1993, *MNRAS*, 262, 128
Wegner, G., & Swanson, S. R. 1996, *MNRAS*, 278, 22
Yoon, S.-C., & Cantiello, M. 2010, *ApJ*, 717, L62

Table 1. Full CSP sample of SNe II_n.

SN	RA	DEC	Galaxy	Galaxy Type	Redshift	Distance (Mpc)	$E(B - V)_{MW}$ (mag)	$E(B - V)_{host}$ (mag)	$EW(\text{Na I D})_h$ (Å)
2005ip	09:32:06.42	+08:26:44.4	NGC 2906	Scd	0.0071	34.9±0.6	0.042
2005kj	08:40:09.18	-05:36:02.2	A084009-0536	...	0.0170	77.3±1.5	0.025
2006aa	11:53:19.89	+20:45:18.2	NGC 3947	SBb	0.0207	97.5±1.8	0.036
2006bo	20:30:41.90	+09:11:40.8	UGC 11578	Sdm	0.0153	70.0±1.3	0.091
2006jd	08:02:07.43	+00:48:31.5	UGC 4179	SBb	0.0186	83.8±1.5	0.048
2006qq	05:19:50.43	-20:58:06.4	E553-G36	Sb	0.0290	125.0±2.3	0.034	0.12±0.03	0.76±0.21
2008fq	20:25:06.20	-24:48:28.00	NGC 6907	SB(s)bc	0.0106	49.6±0.9	0.056	0.46±0.03	2.90±0.20

Table 2. Discovery Telegrams.

SN	Discovery ^a telegram	Classification ^a telegram	Last non detection JD-2453000	Discovery JD-2453000	Explosion date JD-2453000
2005ip	CBET 275	CBET 276	391.50	679.66	535.58±144.08
2005kj	CBET 296	CBET 296	...	692.00	...
2006aa	CBET 395	ATel 732	758.99	774.98	766.99±8.00
2006bo	CBET 468	CBET 481	702.5 0	830.65	766.58±64.07
2006jd	CBET 673	CBET 679	846.7	1021.04	933.87± 87.17
2006qq	CBET 766	CBET 766	1035.90	1069.87	1052.89±16.98
2008fq	CBET 1507	CBET 1510	1715.80	1724.79	1720.29±4.49

^aReferences: CBET 275: Boles et al. (2005); CBET 276: Modjaz et al. (2005); CBET 296: Bonnaud et al. (2005); CBET 395: Lee & Li (2006); Atel 732: Blanc et al. (2006); CBET 468: Boles & Monard (2006); CBET 481: Blondin et al. (2006); CBET 673: Prasad & Li (2006); CBET 679: Blondin et al. (2006); CBET 766: Silverman et al. (2006); CBET 1507: Thrasher et al. (2008); CBET 1510: Quinn et al. (2008).

Table 8. Decay Rate at 100 Days Since Discovery for five CSP SNe II_n.

SN	B (mag/10 days)	g (mag/10 days)	V (mag/10 days)	r (mag/10 days)	i (mag/10 days)	UVOIR (mag/10 days)
2005ip	0.28	0.27	0.32	0.29	0.29	0.11
2005kj	0.28	0.24	0.20	0.18	0.15	0.16
2006aa	0.4	0.33	0.27	0.20	0.20	0.23
2006jd	0.07	0.06	0.06	0.07	0.08	0.03
2006qq	0.06	0.10	0.08	0.05	0.12	0.09

Table 9. Peak Absolute Magnitudes for the Full CSP SN II_n Sample.

SN	u (mag)	B (mag)	g (mag)	V (mag)	r (mag)	i (mag)	Y (mag)	J (mag)	H (mag)
2005ip	< -16.99	< -17.28	< -17.50	< -17.63	< -17.78	< -17.77	< -18.18	< -18.34	< -18.56
2005kj	< -18.40	< -18.38	< -18.49	< -18.48	< -18.47	< -18.33	< -18.60	< -18.70	< -18.91
2006aa	-17.41	-17.49	-17.63	-17.60	-17.67	-17.58	-17.94	-18.03	-18.14
2006bo	< -15.97	< -16.54	< -16.75	< -16.84	< -16.95	< -17.00	< -17.26	< -17.48	< -17.67
2006jd	< -16.26	< -16.69	< -16.92	< -17.03	< -17.29	< -17.17	< -17.96	-18.14	-19.16
2006qq	< -17.84	< -18.10	< -18.25	< -18.32	< -18.36	< -18.33	< -18.75	< -18.96	< -19.21
2008fq	< -18.73	-19.09	-19.26	-19.33	-19.31	-19.19	-19.43	-19.43	-19.58

Note. — Typical uncertainties are 0.1 mag, and are dominated by the errors on distance and extinction. Upper limits are given when the SN was observed after maximum.

Table 21. CSI Parameters for the full CSP SN II_n Sample.

SN	$L(H\alpha_{\text{broad}})$ (10^{40} erg s $^{-1}$)	v_s (10^3 km s $^{-1}$)	v_w (10^2 km s $^{-1}$)	$v_{\text{ejecta}}^{\text{max}}$ (10^3 km s $^{-1}$)	\dot{M} (10^{-3} M $_{\odot}$ yr $^{-1}$)	w (10^{15} g cm $^{-1}$)	n_{H} (10^8 cm $^{-3}$)	$R_{\text{CSM}}^{\text{in}}$ (10^{15} cm)	$R_{\text{CSM}}^{\text{out}}$ (10^{15} cm)	$R_{\text{CSM}}^{\text{sh}}$ (10^{15} cm)	t_{sh} (yr before core collapse)
05ip	4	1.0	1.2	16.0	0.2–0.4	1.0–2.0	$>3 \times 10^{-3}$	<0.1	>325.1	–	–
05kj	1.0–3.4	3.0	6.0	3.0	1.4–4.8	1.5–5.0	>1.8	<0.4	>4.4	–	–
06aa	1.1–3.4	2.0	6.0	2.5	5.0–16.0	5.7–17.1	>7.6	<0.5	>1.8	1.3	0.7
06bo	<0.6 –0.9	>1.0	6.0	2.5	<23.0 –34.0	<24.0 –36.0	>3.8	<0.2 –0.9	>1.5 –2.4	–	–
06jd	3.0–13.0	1.6	<1.6	16.0	<7.0 –32.0	29.3–126.9	$>10^{-2}$	<3.0	>213.1	55.3	>110
06qq	5.6–12.1	6.0	<2.0	10.0	<0.3 –0.7	1.0–2.2	>11.4	<2.5	>7.9	6.6	>10
08fq	15.0	7.5	5.0	9.0	1.1	1.4	>9.0	<0.8	>6.1	3.5	0.5–0.0 / >3.9 –2.2

Note. — Luminosity values for H α of SNe 2005ip and 2006jd are from S12 (here we use the intermediate component, which is associated with post-shock gas). v_s , v_w , $v_{\text{ejecta}}^{\text{max}}$ and n_{H} for SNe 2005ip and 2006jd are from Smith et al. (2009a) and S12, respectively. The mass-loss rate and the wind density (w) of SN 2005ip are from Smith et al. (2009a). The limits for $R_{\text{CSM}}^{\text{in}}$ and $R_{\text{CSM}}^{\text{out}}$ of SNe 2005ip and 2006jd are obtained from the first and the last spectral epochs (Smith et al. 2009a, , S12), and from the assumed $v_{\text{ejecta}}^{\text{max}}$. The CSM of SN 2006jd is characterized by the presence of a dense structure, as indicated by the re-brightening of the r -band light curve ≈ 400 days after explosion. Its radius ($R_{\text{CSM}}^{\text{sh}}$) and epoch of the outburst are computed from the epoch of the r -band maximum and from the assumed $v_{\text{ejecta}}^{\text{max}}$ and v_w . In the case of SN 2008fq, we present the epochs of two outbursts that formed the inner and the outer CSM, as described in Section 6. Here $R_{\text{CSM}}^{\text{in}}$ is the extent of the inner CSM, $R_{\text{CSM}}^{\text{sh}}$ the inner radius of the outer CSM and $R_{\text{CSM}}^{\text{out}}$ the outer radius of the outer CSM.

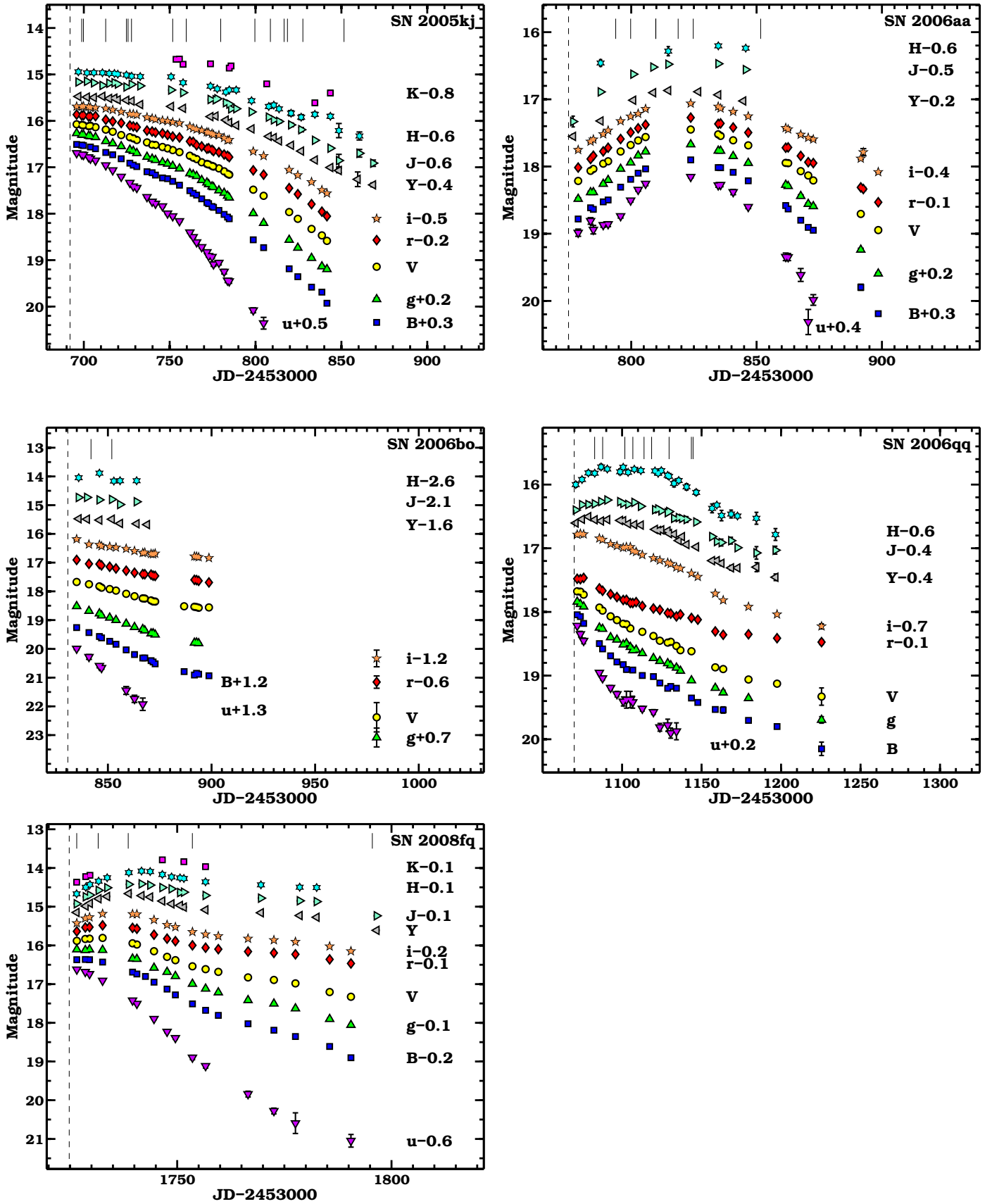


Figure 2: Optical and NIR light curves of 5 CSP SNe IIc. For presentation the light curves have been offset by arbitrary values. Epochs coinciding with spectral observations are indicated with vertical lines at the top of each panel. The discovery epoch is indicated by a vertical dashed line.

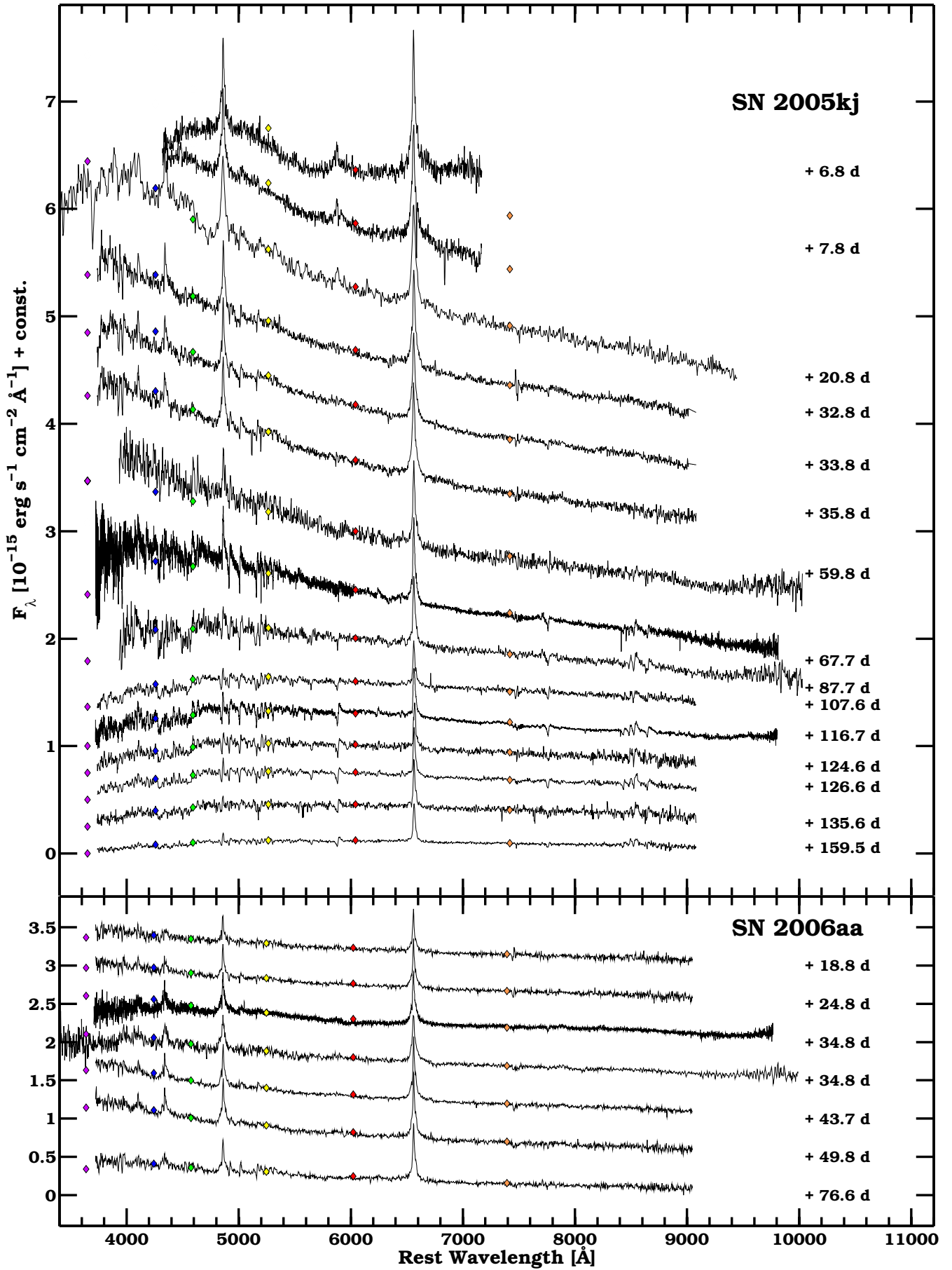


Figure 3: Spectroscopic sequences of SNe 2005kj and 2006aa. Days relative to the discovery epoch are reported next to each spectrum. Fluxes obtained from interpolated magnitudes at the epoch of each spectrum in each optical filter are marked by diamonds.

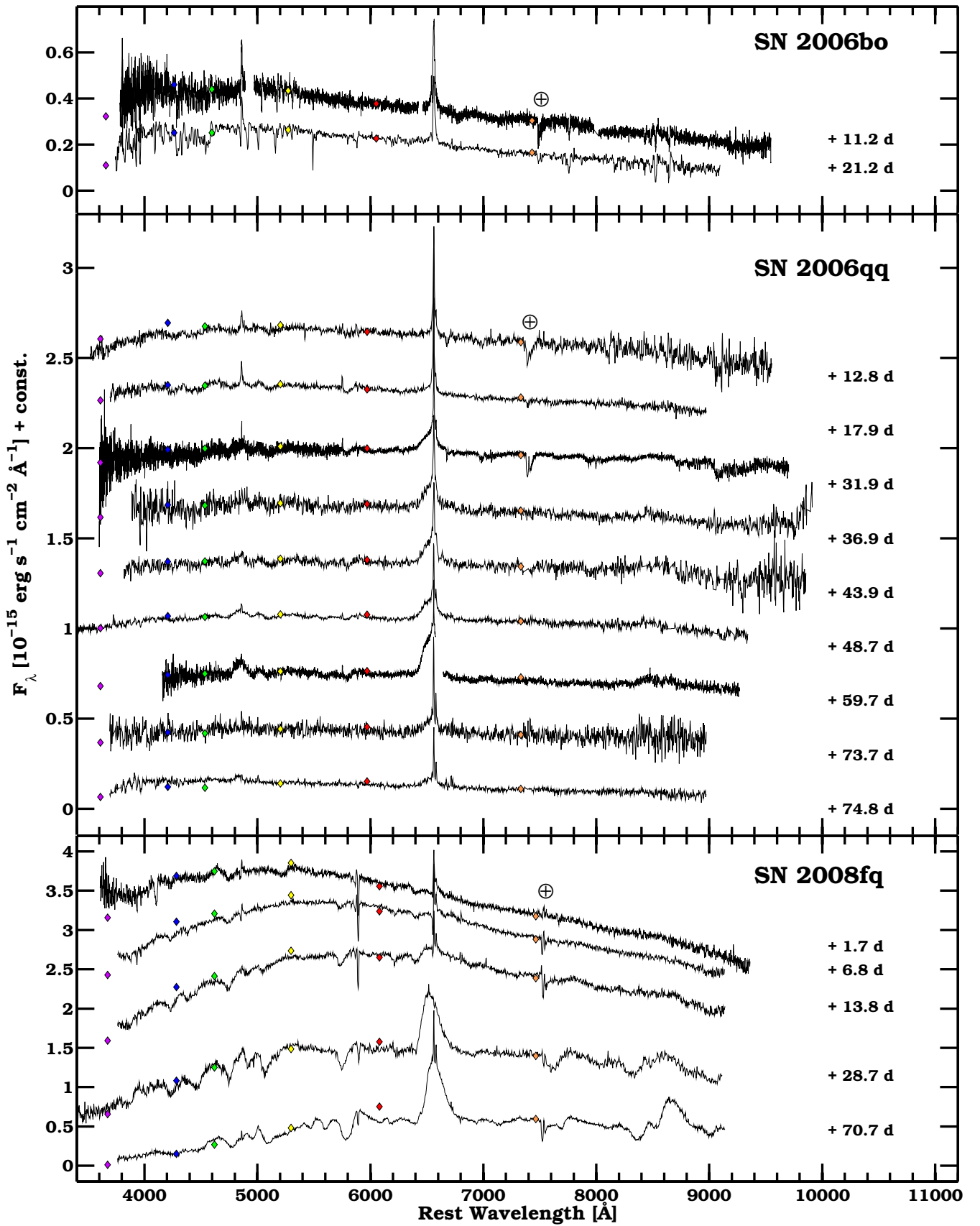


Figure 4: Spectroscopic sequences of SNe 2006bo, 2006qq and 2008fq. Days relative to the discovery epoch are reported next to each spectrum. Fluxes obtained from interpolated magnitudes at the epoch of each spectrum in each optical filter are marked by diamonds.

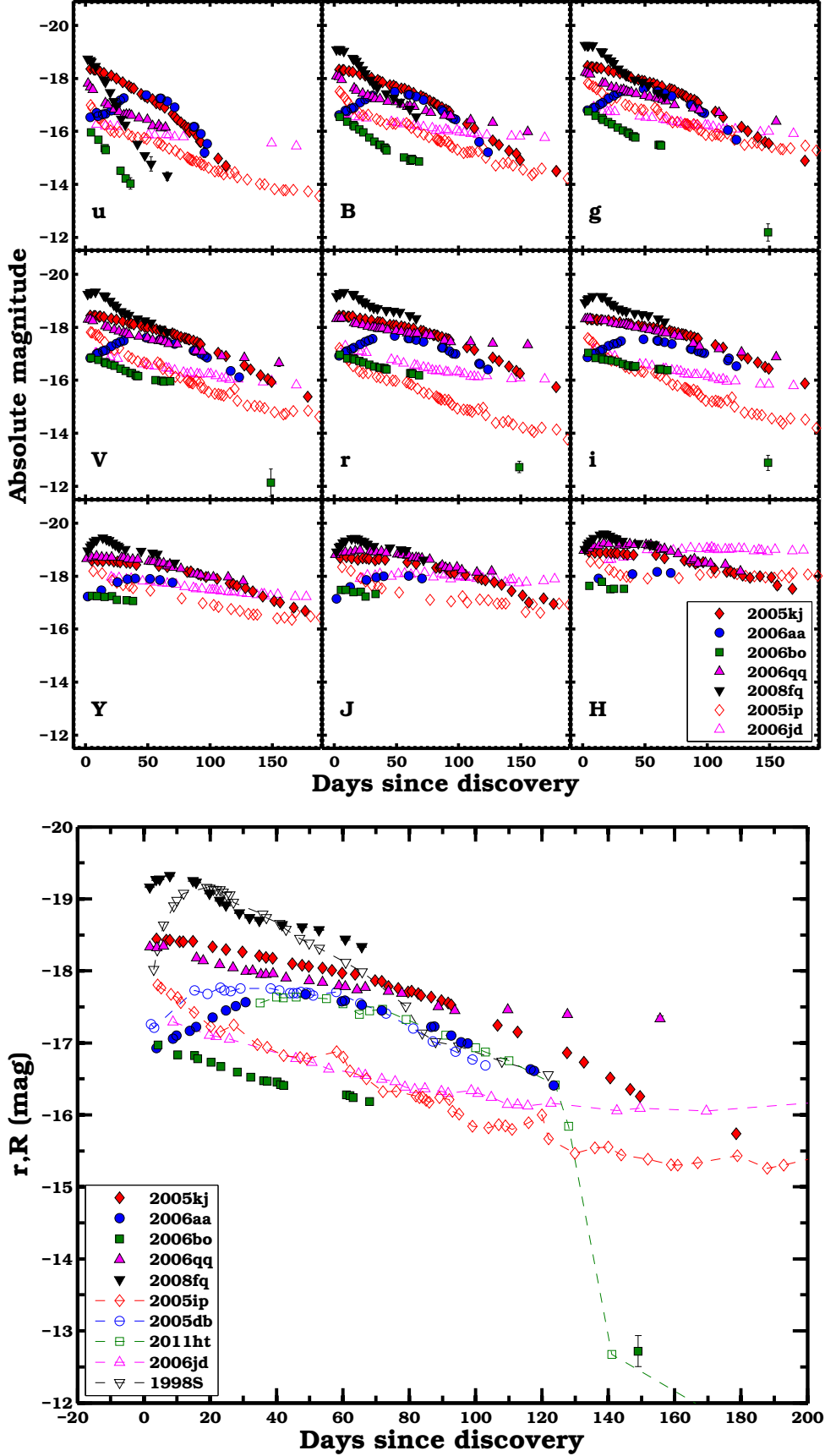


Figure 5: (*Top panel*) Optical and NIR absolute magnitude light curves of the full CSP SN IIIn sample plotted vs. days relative to the epoch of discovery. (*Bottom panel*) The r -band absolute magnitude light curves for the full CSP SN IIIn sample compared to those of other SNe IIIn in the literature. Photometry and values of $E(B - V)_{host}$ of SNe 1998S, 2005db, 2005ip, 2006jd and 2011ht are taken from Liu et al. (2000), Kiewe et al. (2012), S12 and Mauerhan et al. (2012a). To set the absolute flux scale luminosity distances from NED were adopted, using WMAP5 cosmological parameters and correcting for peculiar motions.

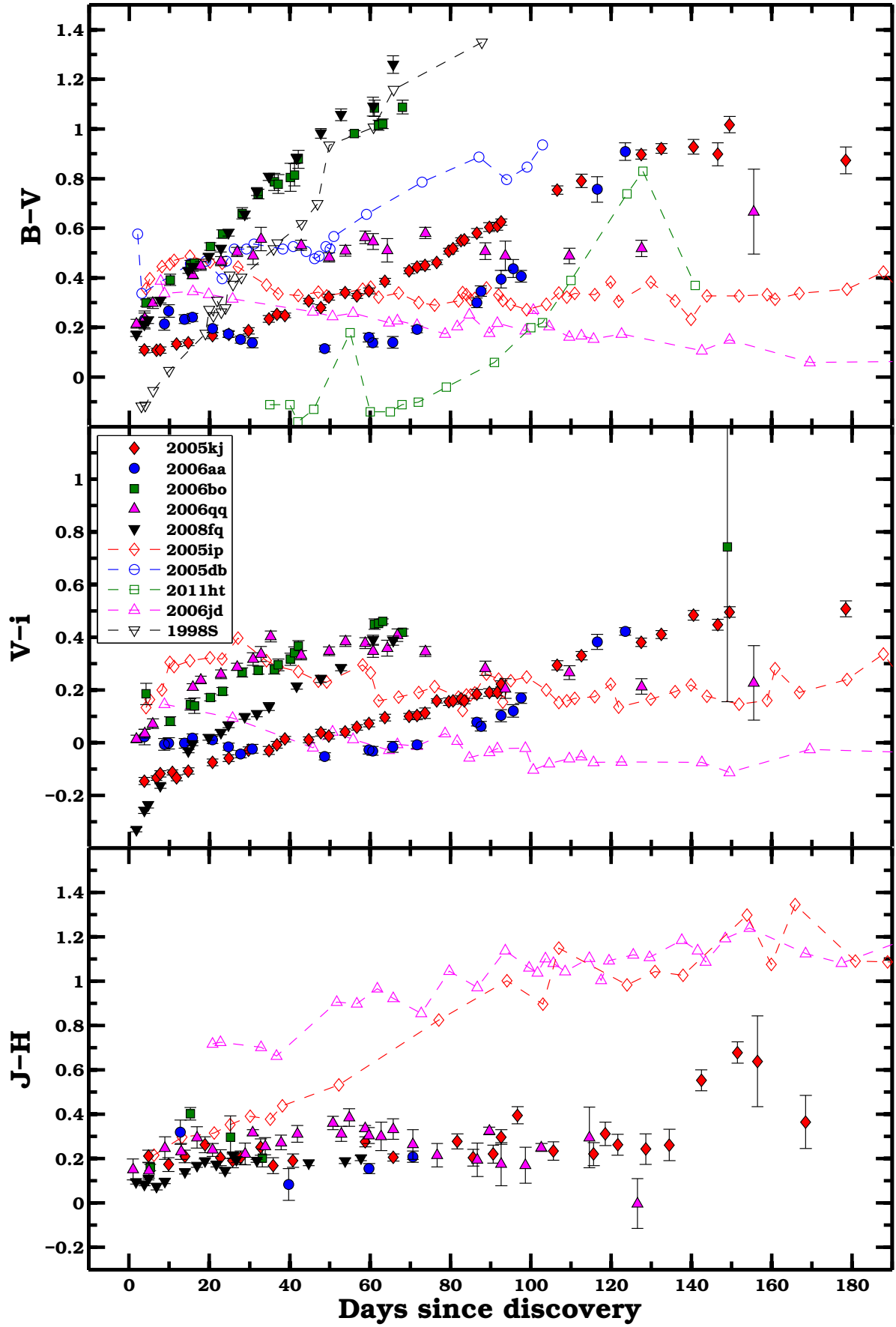


Figure 6: Intrinsic optical and NIR color-curve evolution of the CSP SNe IIIn sample. The top panel ($B - V$) color curves also include several objects from the literature (see caption of Fig. 5 for references).

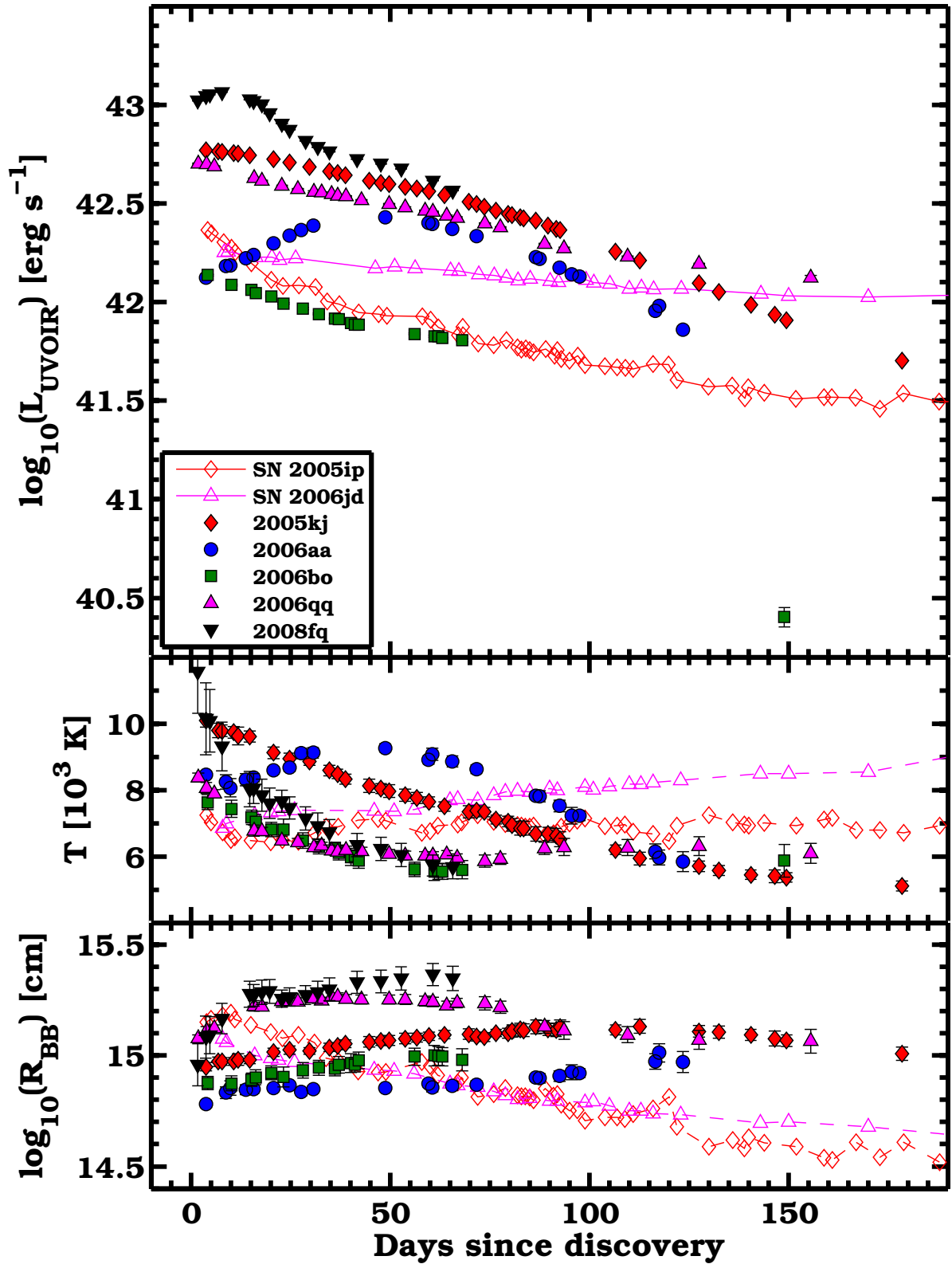


Figure 7: (*Top panel*) UVOIR light curves for the full CSP SN IIIn sample. Theoretical light curve tails powered by radioactive decay for different amounts of ^{56}Ni are included as dashed lines. (*Middle panel*) Temperature evolution derived from BB fits to the time-series of SEDs. For SNe 2005ip and 2006jd we plot the temperature associated with the optical emission (see S12). (*Bottom panel*) Radius evolution computed assuming BB emission. For SNe 2005ip and 2006jd we plot the radius associated with the optical emission (see S12).

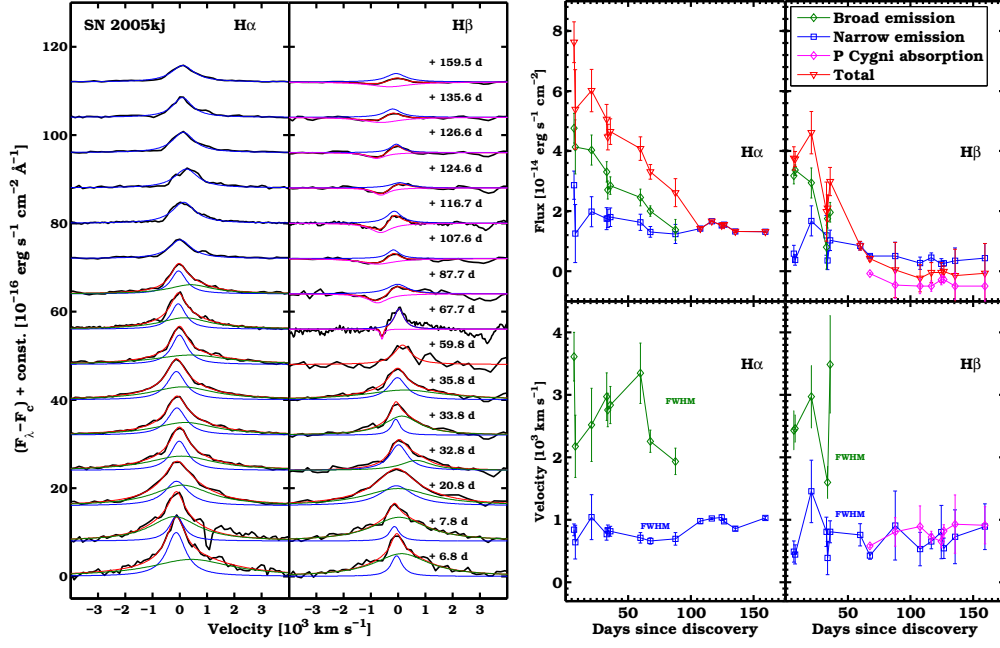


Figure 8: (*Left panel*) H α and H β profiles of SN 2005kj after low-order polynomial continuum subtraction and reddening correction. A combination of Lorentzians has been used to fit the profiles. (*Right panel*) Fluxes and velocities for the different Lorentzian components.

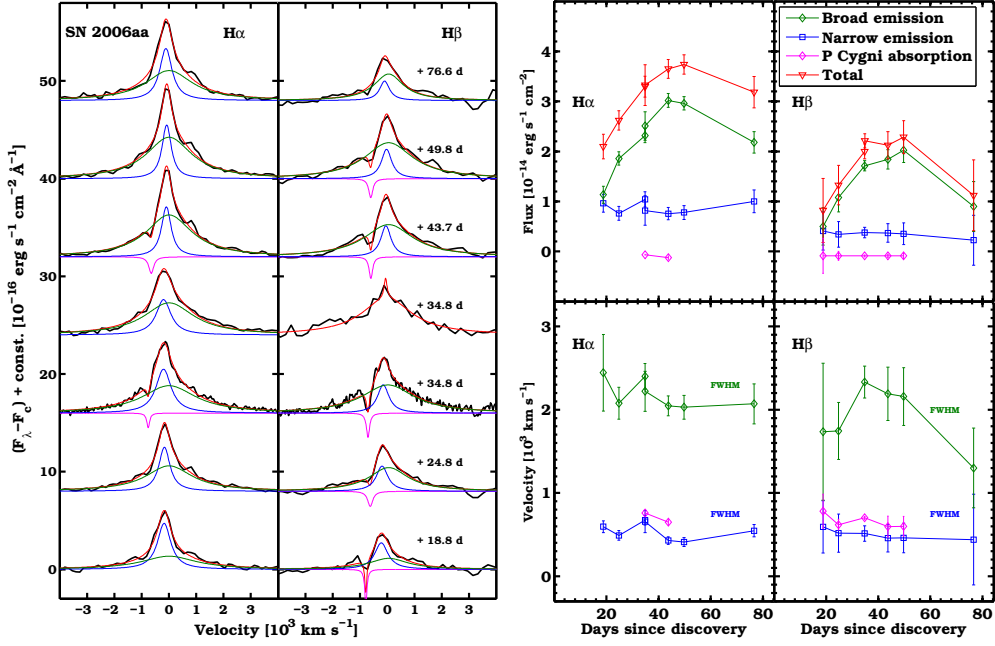


Figure 9: (*Left panel*) H α and H β profiles of SN 2006aa after low-order polynomial continuum subtraction and reddening correction. A combination of Lorentzians has been used to fit the profiles. (*Right panel*) Fluxes and velocities for the different Lorentzian components.

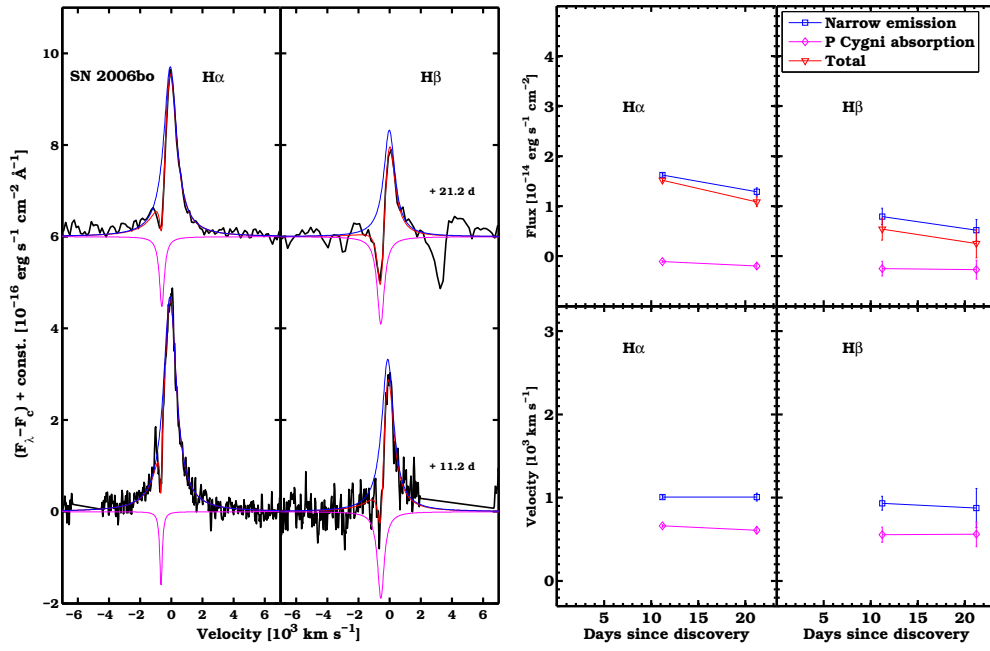


Figure 10: (*Left panel*) $H\alpha$ and $H\beta$ profiles of SN 2006bo after low-order polynomial continuum subtraction and reddening correction. A combination of Lorentzians has been used to fit the profiles. (*Right panel*) Fluxes and velocities for the different Lorentzian components.

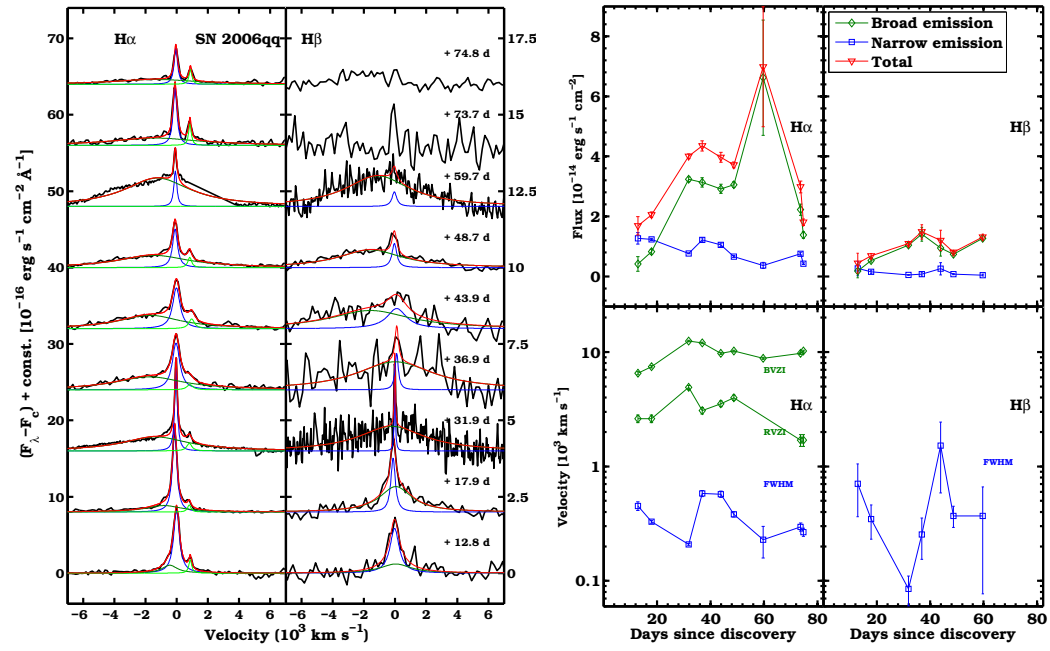


Figure 11: (*Left panel*) $H\alpha$ and $H\beta$ of SN 2006qq profiles after low-order polynomial continuum subtraction and reddening correction. A combination of Lorentzians has been used to fit the profiles. (*Right panel*) Fluxes and velocities for the different Lorentzian components.

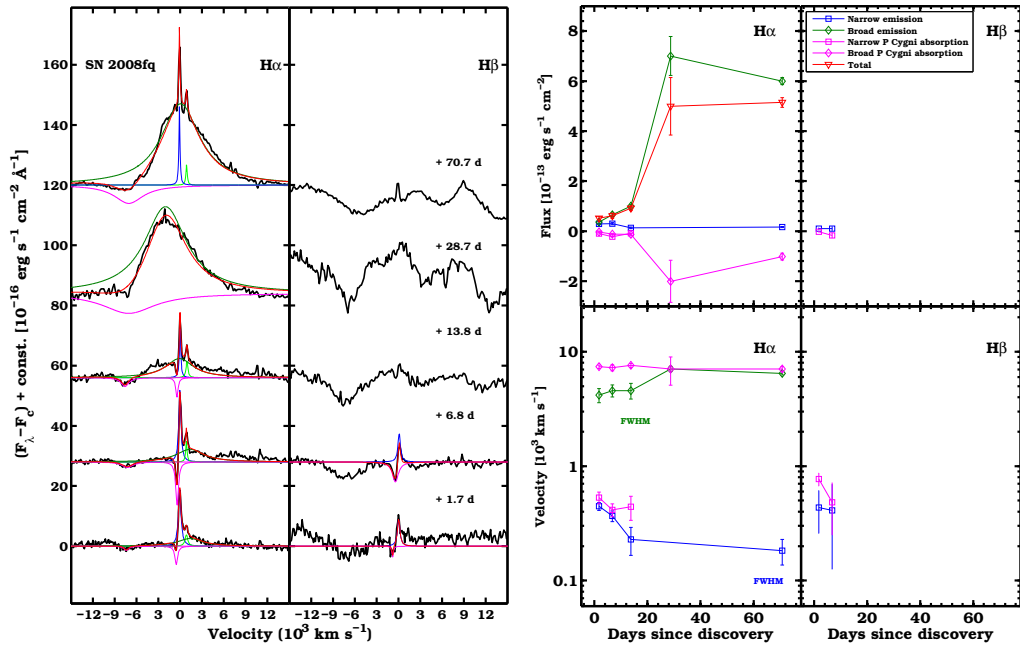


Figure 12: (Left panel) $H\alpha$ and $H\beta$ profiles of SN 2008fq after low-order polynomial continuum subtraction and reddening correction. A combination of Lorentzians has been used to fit the profiles. (Right panel) Fluxes and velocities for the different Lorentzian components.

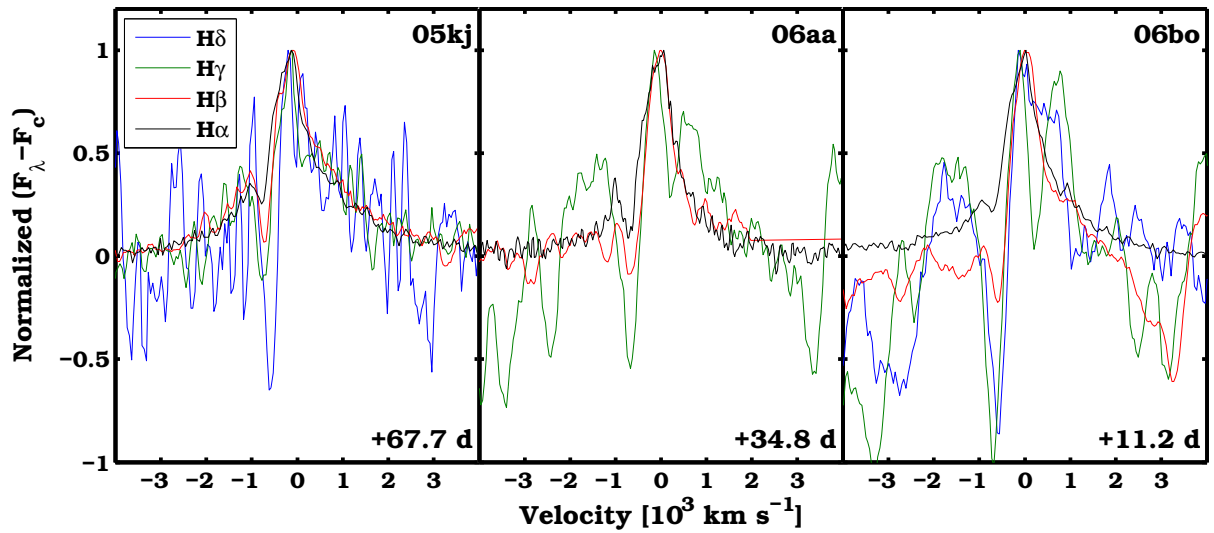


Figure 13: Over-imposed Balmer line profiles after continuum subtraction and peak normalization for SNe 2005kj, 2006aa and 2006bo.

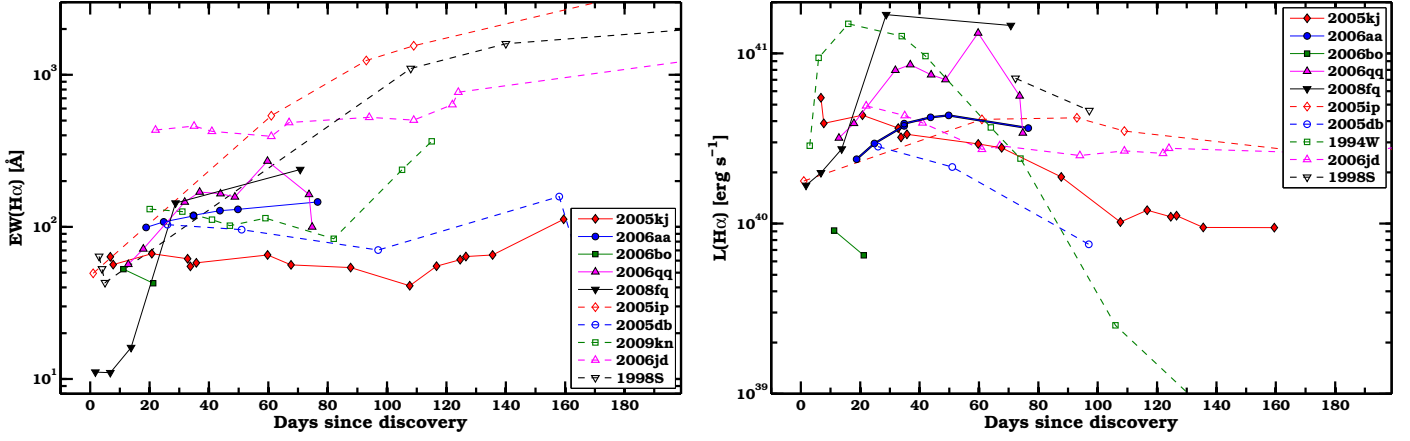


Figure 14: (*Left panel*) $H\alpha$ EW time-evolution for the full CSP SN IIIn sample, and several objects in the literature including: SNe 1998S (Leonard et al. 2000), 2005db (Kiewe et al. 2012), and 2009kn (Kankare et al. 2012). (*Right panel*) $H\alpha$ luminosities for the full CSP SN IIIn sample compared to those of some objects in the literature. Data for SNe 2005db and 1998S are from the spectra published by Kiewe et al. (2012), and Fassia et al. (2001). The $H\alpha$ fluxes of SN 1994W were published by Chugai et al. (2004).

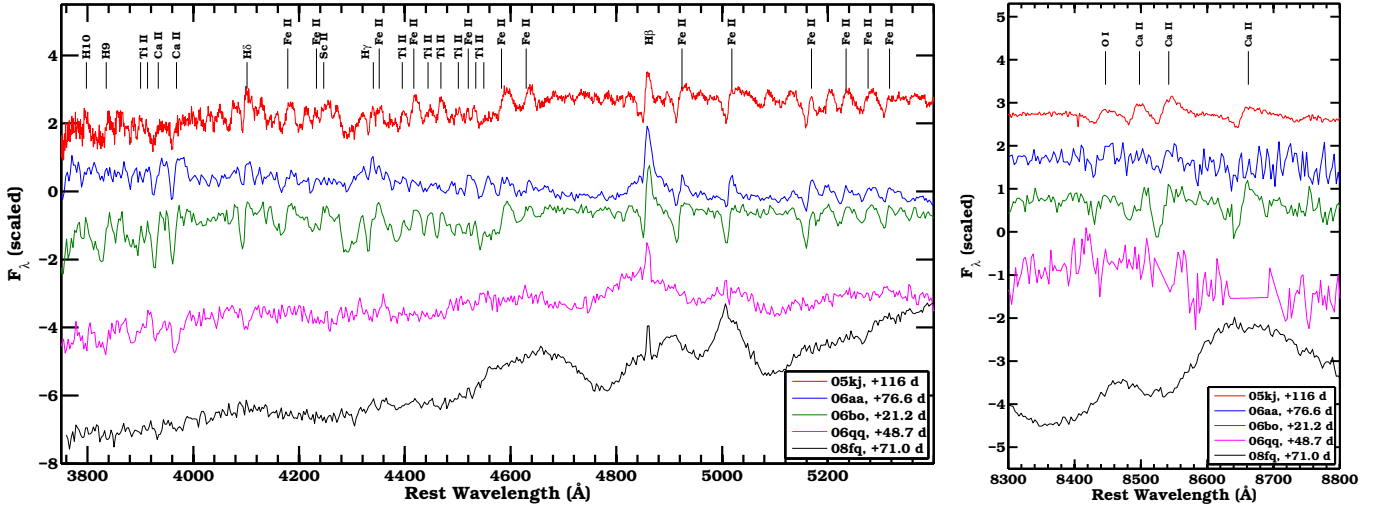


Figure 15: (*Left panel*) Spectral comparison of the five new CSP SNe IIIn between wavelength 3800 and 5300 Å. Line identification is based on Kankare et al. (2012). In addition to Balmer lines, each spectrum is dominated by Fe II and Ti II features. (*Right panel*) Spectral comparison of the same objects in the wavelength region of the Ca II NIR triplet.

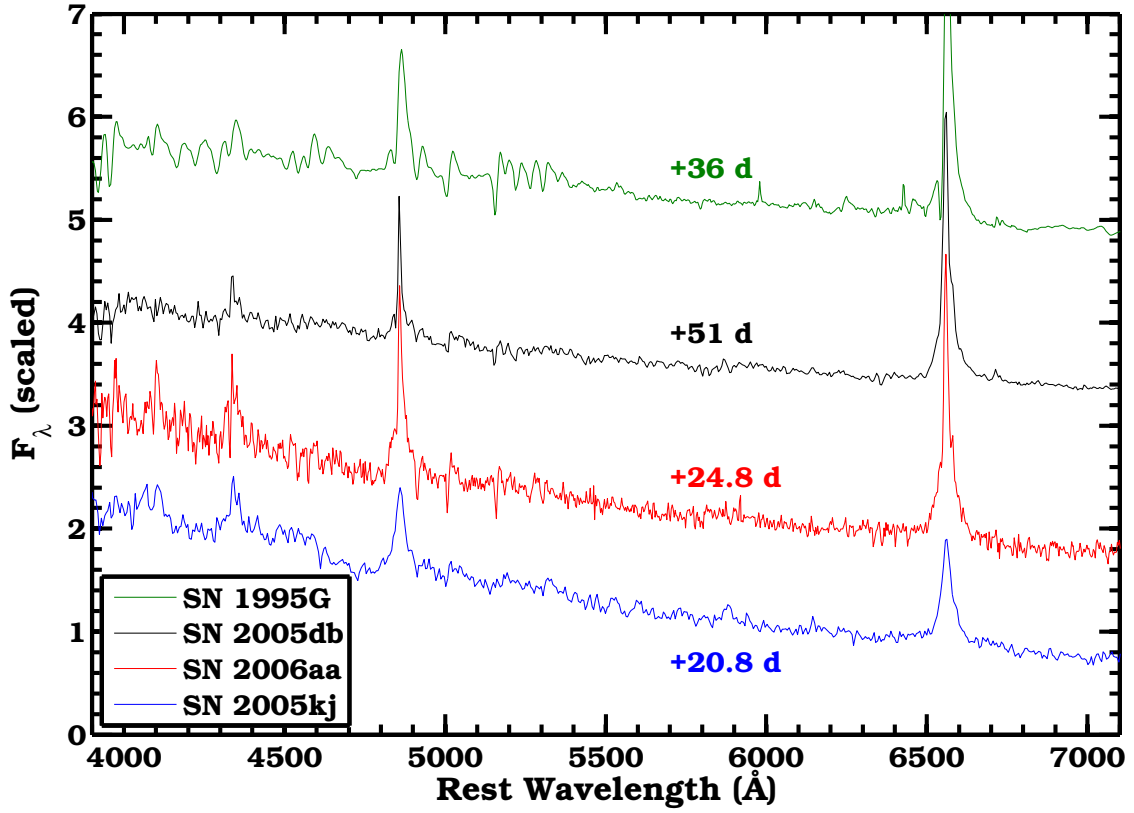


Figure 16: Spectral comparison between SNe 2005kj and 2006aa to SNe 2005db and 1995G.

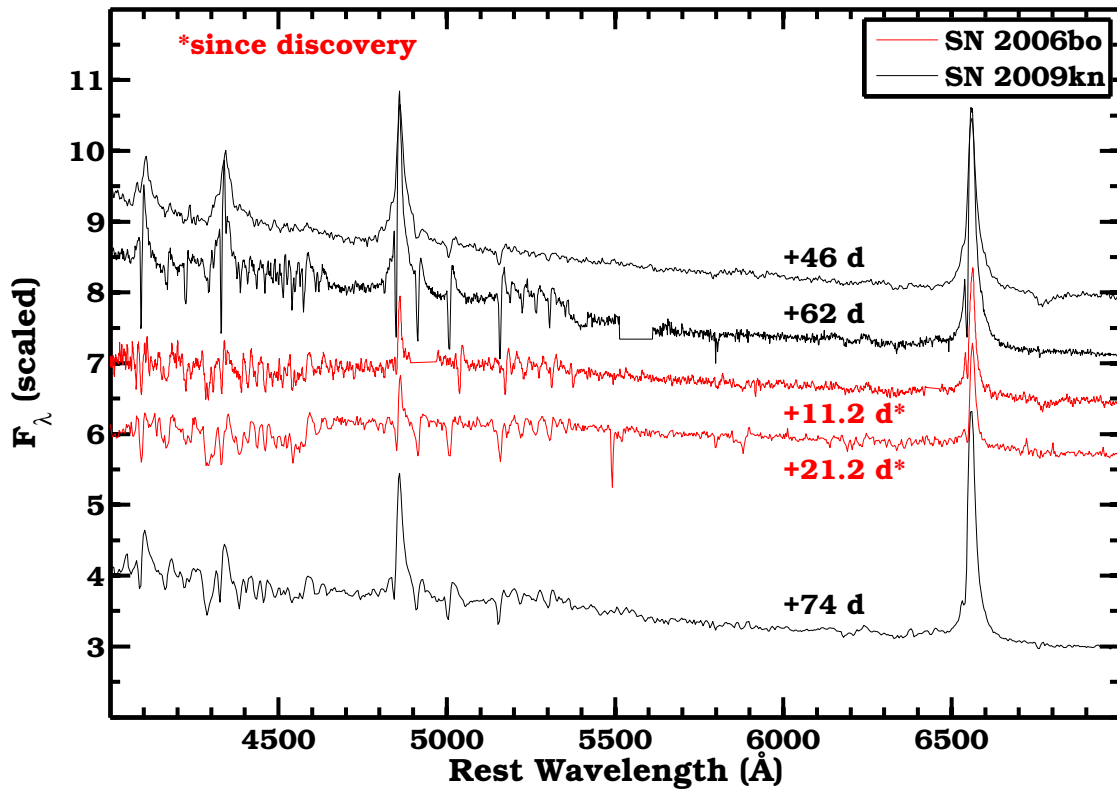


Figure 17: Spectral comparison between SN 2006bo and the 1994W-like SN 2009kn (Kankare et al. 2012).

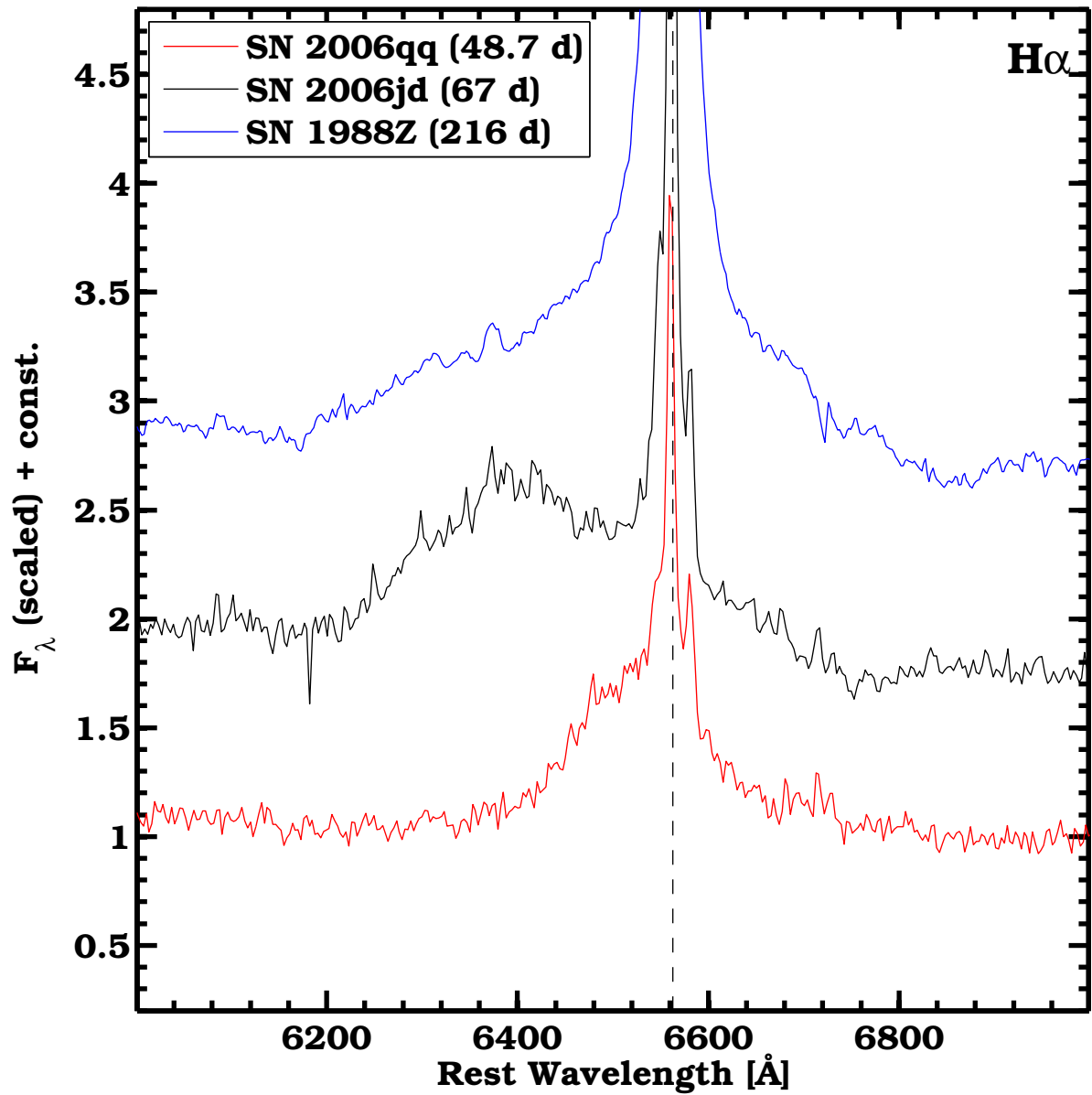


Figure 18: H α comparison between SNe 1988Z, 2006jd and 2006qq. Each object exhibits preferential emission in the blue wing.

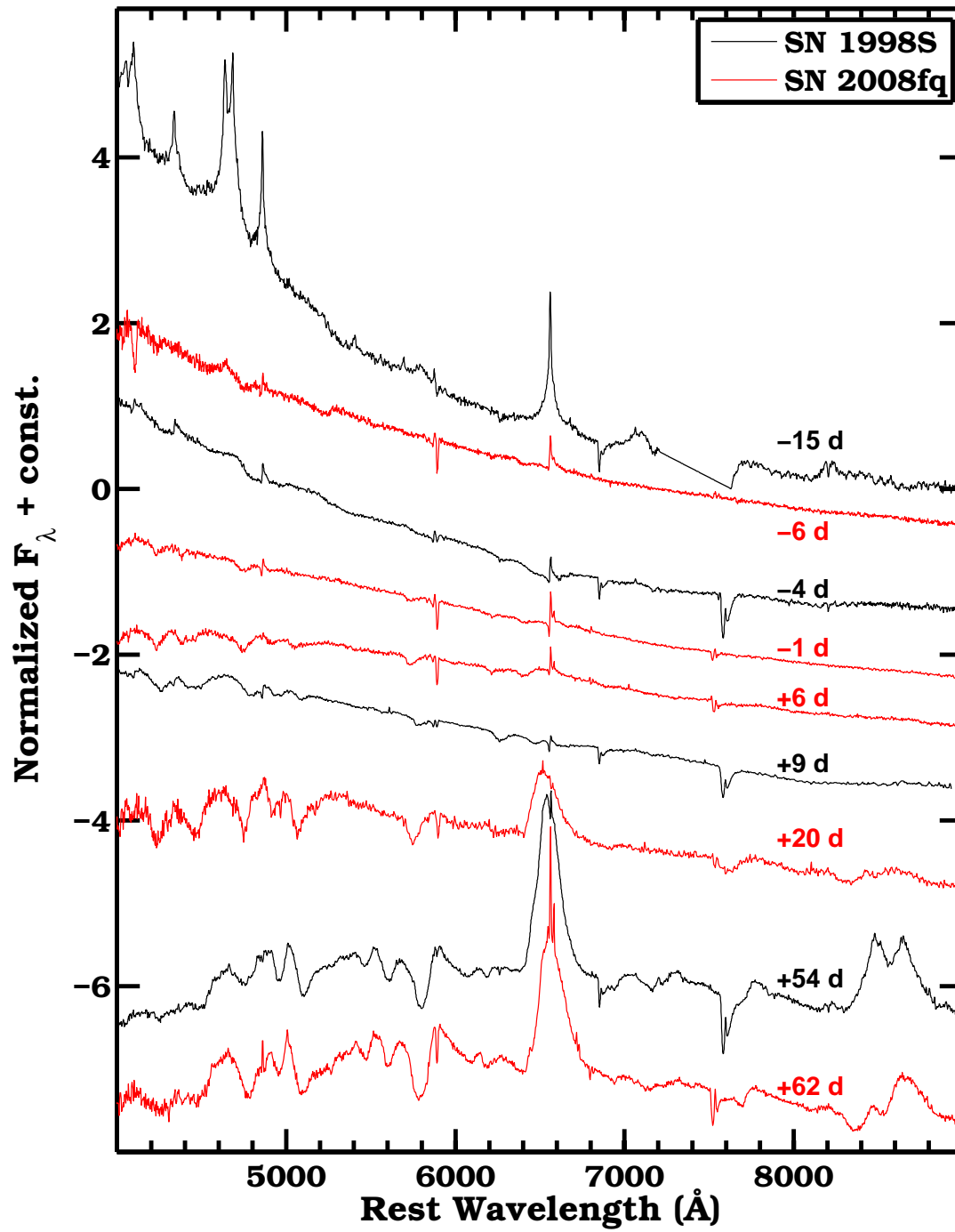


Figure 19: Spectral evolution of SNe 1998S and 2008fq. Temporal phase of each spectrum is given relative to the time of V -band maximum.

Table 3. Optical and near-infrared photometry of the local sequences in the standard system

STAR	$\alpha(2000)$	$\delta(2000)$	u' (mag)	g' (mag)	r' (mag)	i' (mag)	B (mag)	V (mag)	Y (mag)	J (mag)	H (mag)	K_s (mag)
SN 2005kj												
01	08:40:14.48	-05:35:21.98	14.142(016)
02	08:40:06.53	-05:37:07.63
03	08:40:05.50	-05:37:05.35	15.772(015)	14.555(009)	13.753(014)	12.616(005)	12.348(016)	11.932(005)	...
04	08:39:59.04	-05:36:21.37
05	08:40:16.65	-05:37:38.33	15.540(015)	14.434(015)	14.189(015)	14.133(015)	14.710(008)	14.270(008)	13.639(005)	13.457(005)	13.239(005)	...
06	08:39:59.30	-05:33:06.59	16.148(010)	14.931(007)	14.534(007)	14.394(008)	15.282(008)	14.685(007)
07	08:40:09.91	-05:32:33.87	16.671(008)	15.326(007)	14.847(007)	14.673(009)	15.715(008)	15.039(007)	14.047(007)	13.775(007)	13.419(010)	...
08	08:40:18.33	-05:37:23.79	16.433(008)	15.277(007)	14.961(007)	14.875(008)	15.580(008)	15.076(007)	14.328(006)	14.117(005)	13.851(006)	...
09	08:39:58.25	-05:37:37.49	17.131(019)	15.576(007)	15.034(007)	14.814(008)	16.002(008)	15.249(007)
10	08:40:04.83	-05:33:04.74	17.201(017)	16.043(007)	15.682(007)	15.567(009)	16.378(008)	15.820(007)	15.017(007)	14.800(007)	14.507(011)	...
11	08:40:13.98	-05:36:32.59	17.353(013)	16.164(007)	15.739(007)	15.597(010)	16.517(008)	15.899(007)	15.003(005)	14.761(006)	14.424(005)	14.384(015)
12	08:40:14.29	-05:39:07.22	17.907(027)	16.395(007)	15.847(007)	15.647(007)	16.834(008)	16.068(007)	14.967(007)	14.670(010)	14.269(006)	...
13	08:40:06.11	-05:38:50.08	17.897(039)	16.421(007)	15.955(007)	15.813(008)	16.828(008)	16.135(007)	15.217(005)	14.970(005)	14.656(007)	...
14	08:40:01.31	-05:37:38.36	17.851(017)	16.468(007)	15.994(007)	15.827(007)	16.859(008)	16.185(007)
15	08:40:22.60	-05:35:12.62	17.864(019)	16.587(007)	16.148(007)	15.985(010)	16.961(009)	16.312(007)	15.373(005)	15.119(005)	14.770(005)	...
16	08:40:14.45	-05:32:31.58	18.027(022)	16.631(008)	16.160(007)	15.992(008)	17.010(008)	16.341(009)
17	08:40:10.94	-05:34:14.92	18.038(027)	16.664(007)	16.213(007)	16.070(008)	17.052(008)	16.388(007)	15.480(005)	15.227(005)	14.897(007)	...
18	08:40:07.61	-05:38:09.01	19.131(064)	17.137(007)	16.342(007)	16.061(008)	17.660(017)	16.697(007)	15.277(006)	14.934(008)	14.430(006)	...
19	08:40:16.87	-05:35:30.14	18.484(029)	17.218(008)	16.817(007)	16.681(007)	17.565(011)	16.965(007)
20	08:40:15.64	-05:34:50.35	18.768(037)	17.353(013)	16.861(009)	16.698(007)	17.772(008)	17.061(007)
21	08:40:08.45	-05:32:57.14	19.018(048)	17.749(007)	17.300(007)	17.152(011)	18.125(014)	17.480(007)
22	08:40:17.46	-05:34:09.57	18.867(226)	17.845(009)	17.357(009)	17.187(010)	18.235(013)	17.554(013)
23	08:40:05.58	-05:33:42.42	20.211(156)	18.227(010)	17.537(010)	17.288(010)	18.756(030)	17.831(013)
24	08:40:12.45	-05:35:51.28	15.009(005)	14.756(007)	14.418(006)	14.314(017)	...
25	08:40:07.12	-05:36:18.91	16.227(006)	15.792(008)	15.236(007)	15.070(048)	...
26	08:40:07.76	-05:36:34.89	16.071(007)	15.658(007)	15.052(006)	14.900(080)	...
27	08:40:10.34	-05:35:14.26	16.723(008)	16.379(010)	15.862(010)	15.679(066)	...
28	08:40:13.00	-05:35:14.74	16.716(007)	16.300(009)	15.685(010)	15.419(039)	...
29	08:40:07.65	-05:35:03.76	17.548(017)	17.125(014)	16.548(024)	16.224(054)	...
30	08:40:04.51	-05:36:51.69	17.240(016)	16.962(020)	16.514(035)	16.414(056)	...
31	08:40:17.07	-05:36:12.80	15.322(005)	14.834(005)	14.286(005)
32	08:40:16.31	-05:36:01.90	15.957(005)	15.661(006)	15.264(010)
33	08:40:30.21	-05:34:43.65	14.308(005)	13.875(006)	13.243(005)
34	08:40:29.67	-05:37:15.36	12.496(006)	12.279(006)	12.003(005)
35	08:40:31.93	-05:36:53.58	14.960(005)	14.639(006)	14.206(005)
36	08:40:19.26	-05:35:03.61	16.482(009)	16.081(010)	15.521(010)
37	08:40:28.72	-05:33:34.19	13.381(007)	13.149(007)	12.850(007)
38	08:40:16.23	-05:39:02.28	14.383(007)	14.037(007)	13.540(006)
39	08:40:11.59	-05:40:01.15	14.097(007)	13.839(009)	13.487(007)
40	08:40:09.13	-05:32:11.20	14.771(007)	14.324(007)	13.686(008)
41	08:40:25.37	-05:32:31.03	12.312(008)	12.086(008)	11.797(007)
42	08:40:22.35	-05:38:12.10	12.062(007)	11.860(007)	11.612(005)
SN 2006aa												
01	11:53:09.80	+20:46:41.82	15.799(012)	14.810(009)
02	11:53:23.77	+20:45:08.34	18.195(019)	15.559(015)	14.528(015)	14.155(015)	16.114(008)	14.985(014)	13.279(007)	12.920(014)	12.362(020)	...
03	11:53:10.70	+20:42:50.55	16.488(008)	15.332(007)	14.926(007)	14.784(007)	15.658(008)	15.075(007)
04	11:53:19.56	+20:42:36.14	17.433(022)	15.554(007)	14.931(007)	14.740(007)	16.003(008)	15.179(007)	14.050(008)	13.774(014)	13.412(018)	...

Table 3 (cont'd)

STAR	$\alpha(2000)$	$\delta(2000)$	u' (mag)	g' (mag)	r' (mag)	i' (mag)	B (mag)	V (mag)	Y (mag)	J (mag)	H (mag)	K_s (mag)
05	11:53:31.25	+20:41:33.97	17.050(028)	15.781(011)	15.334(011)	15.179(011)	16.134(011)	15.492(010)	14.548(012)	14.305(022)	13.963(020)	...
06	11:53:07.53	+20:47:56.43	17.216(012)	15.814(007)	15.349(007)	15.187(007)	16.188(008)	15.522(007)
07	11:53:38.97	+20:44:05.46	18.856(033)	16.591(007)	15.773(007)	15.487(007)	17.094(012)	16.127(008)	14.693(008)	14.356(022)	13.872(014)	...
08	11:53:09.89	+20:45:07.54	20.229(171)	17.483(013)	16.209(012)	14.898(010)	18.252(010)	16.741(011)
09	11:53:27.89	+20:43:05.29	20.281(128)	17.651(013)	16.293(007)	15.444(007)	18.399(020)	16.888(013)	14.242(008)	13.818(013)	13.252(014)	...
10	11:53:26.04	+20:47:37.05	...	18.175(008)	16.909(007)	16.303(007)	18.842(019)	17.484(010)	15.274(008)	14.854(010)	14.273(022)	...
11	11:53:22.42	+20:49:18.93	18.828(033)	17.488(007)	16.980(007)	16.759(009)	17.847(009)	17.185(007)	16.070(028)	15.800(016)	15.452(047)	...
12	11:53:10.11	+20:44:04.23	20.757(184)	18.767(011)	17.560(007)	17.007(008)	19.364(019)	18.042(048)
13	11:53:29.16	+20:43:56.80	21.003(251)	19.462(013)	18.480(009)	18.082(009)	20.021(032)	18.920(018)
14	11:53:13.91	+20:48:49.24	20.126(110)	18.428(017)	17.687(007)	17.405(007)	18.916(014)	18.033(016)
15	11:53:41.45	+20:45:18.73	20.678(176)	18.111(009)	17.042(009)	16.653(011)	18.699(014)	17.521(019)	15.781(008)	15.409(013)	14.868(021)	...
16	11:53:07.51	+20:43:11.16
17	11:53:38.84	+20:41:15.47	11.953(012)	11.632(020)
18	11:53:42.95	+20:43:05.38	12.450(008)	12.117(017)	11.664(017)	...
19	11:53:46.33	+20:45:15.55	15.001(008)	14.672(014)	14.233(019)	...
20	11:53:35.91	+20:48:38.84	15.445(012)	14.951(018)	14.364(020)	...
21	11:53:36.96	+20:40:28.74	16.118(017)	15.639(012)	15.182(038)	...
22	11:53:25.28	+20:46:31.66	16.686(015)	16.254(011)	15.731(013)	...
23	11:53:27.61	+20:40:09.52	16.673(017)	16.356(020)	16.254(109)	...
24	11:53:42.87	+20:47:35.09	16.839(013)	16.345(016)	15.837(064)	...
25	11:53:32.23	+20:45:47.84	17.146(020)	16.643(033)	16.230(073)	...
26	11:53:17.54	+20:40:25.57	17.162(026)	16.980(066)	16.771(168)	...
27	11:53:34.20	+20:46:19.99	17.400(032)	16.886(024)	16.170(073)	...
28	11:53:44.26	+20:42:40.07	17.384(023)	16.926(042)	16.498(199)	...
29	11:53:15.20	+20:43:37.02	17.490(026)	16.923(024)
30	11:53:34.42	+20:45:32.33	17.492(026)	16.987(024)	16.199(183)	...
31	11:53:18.08	+20:47:57.91	17.572(037)	17.017(032)	16.513(123)	...
32	11:53:27.03	+20:43:31.94	18.006(041)	17.461(071)	17.200(178)	...
33	11:53:24.28	+20:42:39.06	17.911(043)	17.574(041)	16.939(139)	...
34	11:53:27.54	+20:47:08.84	18.101(018)	17.593(023)	17.114(038)	...
35	11:53:30.96	+20:45:17.93	18.138(043)	17.626(057)	17.198(176)	...
36	11:53:29.52	+20:46:49.08	18.175(051)	17.589(057)	16.871(180)	...
37	11:53:41.27	+20:41:12.23	15.283(014)	15.060(027)	14.783(027)	...
38	11:53:32.46	+20:39:54.04	16.488(014)	16.030(044)	15.484(053)	...
SN 2006bo												
01	20:30:29.94	+09:10:16.50	15.722(011)	14.506(015)	14.100(015)	13.972(015)	14.823(011)	14.247(014)
02	20:30:49.83	+09:12:25.20	14.836(015)	13.905(016)	...	12.576(131)	12.173(013)	11.891(014)	...
03	20:30:45.65	+09:09:47.84	15.983(015)	14.592(016)	...	12.391(136)	11.866(010)	11.373(014)	...
04	20:30:44.28	+09:09:05.08	17.494(015)	15.135(015)	14.287(015)	13.960(015)	15.707(008)	14.628(014)
05	20:30:41.33	+09:10:20.32	17.181(010)	15.049(015)	14.276(015)	14.008(015)	15.559(008)	14.592(014)	13.356(078)	12.929(020)	12.521(046)	...
06	20:30:58.03	+09:12:39.96	16.436(009)	14.895(015)	14.235(015)	13.927(015)	15.331(008)	14.493(014)
07	20:30:34.60	+09:08:11.26	16.567(009)	15.254(217)	14.499(015)	14.322(015)	15.442(008)	14.699(010)
08	20:30:49.13	+09:08:51.50	16.443(009)	15.286(110)	14.769(011)	14.625(011)	15.516(008)	14.913(010)
09	20:30:56.30	+09:11:29.26	16.889(009)	15.475(110)	14.812(009)	14.608(009)	15.790(008)	15.025(008)
10	20:30:41.83	+09:13:59.56	16.899(010)	15.590(109)	15.048(125)	14.733(020)	15.901(008)	15.147(007)
11	20:30:31.33	+09:12:27.22	17.523(017)	15.826(110)	15.163(126)	14.799(021)	16.205(008)	15.313(007)
12	20:30:47.98	+09:09:47.74	17.645(015)	15.894(112)	15.267(123)	14.954(018)	16.261(008)	15.402(007)
13	20:30:50.68	+09:11:28.90	18.311(039)	16.143(110)	15.276(122)	14.811(018)	16.622(008)	15.518(007)

Table 3 (cont'd)

STAR	$\alpha(2000)$	$\delta(2000)$	u' (mag)	g' (mag)	r' (mag)	i' (mag)	B (mag)	V (mag)	Y (mag)	J (mag)	H (mag)	K_s (mag)
14	20:30:46.82	+09:12:04.64	18.107(022)	16.219(113)	15.503(124)	15.134(018)	16.612(008)	15.678(007)	14.458(081)	14.036(019)	13.590(018)	...
15	20:30:32.74	+09:12:07.20	18.373(026)	16.330(102)	15.531(127)	15.123(021)	16.753(009)	15.759(007)
16	20:30:29.10	+09:14:24.65	17.872(026)	16.320(141)	15.724(166)	15.378(026)	16.627(019)	15.808(011)
17	20:30:36.54	+09:11:26.12	17.775(016)	16.286(111)	15.720(122)	15.419(020)	16.601(008)	15.827(007)
18	20:30:37.44	+09:08:51.65	18.164(040)	16.438(110)	15.743(121)	15.373(018)	16.802(013)	15.912(007)
19	20:30:55.99	+09:10:16.57	17.641(037)	16.303(107)	15.757(122)	15.423(017)	16.599(008)	15.856(007)	14.892(138)	14.393(016)	14.001(014)	...
20	20:30:51.40	+09:10:00.66	17.418(015)	16.234(111)	15.767(120)	15.481(017)	16.511(008)	15.827(007)
21	20:30:48.27	+09:14:15.14	17.762(032)	16.492(111)	15.930(123)	15.594(022)	16.794(016)	16.040(007)
22	20:30:28.61	+09:11:52.87	18.626(033)	16.804(144)	16.074(167)	15.637(025)	17.165(019)	16.221(009)
23	20:30:50.08	+09:12:57.96	19.369(103)	17.166(114)	16.202(124)	15.678(019)	17.640(009)	16.511(010)
24	20:30:36.13	+09:10:28.31	18.046(027)	16.866(112)	16.379(123)	16.087(020)	17.136(010)	16.448(009)
25	20:30:43.46	+09:08:25.04	19.015(045)	17.258(102)	16.562(122)	16.192(019)	17.635(013)	16.737(008)
26	20:30:36.76	+09:13:04.84	18.750(037)	17.226(103)	16.643(122)	16.337(022)	17.562(009)	16.757(012)
27	20:30:34.09	+09:12:39.60	18.843(048)	17.525(112)	16.992(117)	16.675(022)	17.848(018)	17.090(010)
28	20:30:43.65	+09:13:55.81	18.641(042)	17.713(095)	17.321(108)	17.104(015)	17.928(019)	17.389(014)
29	20:30:55.88	+09:06:47.16	13.905(290)	13.204(014)	12.608(020)	...
30	20:30:49.26	+09:08:38.90	15.158(287)	14.485(019)	13.902(020)	...
31	20:30:48.61	+09:12:23.26	15.371(130)	14.631(014)	14.078(014)	...
32	20:31:01.44	+09:06:47.63	15.995(278)	15.425(014)	14.957(028)	...
33	20:30:38.74	+09:09:52.67	16.093(130)	15.505(012)	14.894(019)	...
34	20:30:51.85	+09:09:29.16	16.204(127)	15.782(017)	15.409(047)	...
35	20:30:39.33	+09:10:26.04	16.230(065)	15.948(026)	15.614(031)	...
36	20:30:43.53	+09:14:13.20	16.468(117)	16.013(055)	15.639(092)	...
37	20:31:05.05	+09:12:47.09	16.421(120)	16.077(016)	15.816(054)	...
38	20:30:57.55	+09:11:16.80	16.716(124)	16.177(018)	15.653(041)	...
39	20:30:44.98	+09:13:12.22	16.675(083)	16.161(018)	15.539(024)	...
40	20:30:56.80	+09:11:49.27	16.631(130)	16.202(032)	15.796(043)	...
41	20:30:39.67	+09:07:41.45	17.050(238)	16.703(049)	16.354(092)	...
42	20:30:39.13	+09:09:24.91	17.143(133)	16.826(031)	16.552(085)	...
43	20:30:43.91	+09:11:55.03	16.285(060)	15.893(021)	15.405(025)	...
44	20:30:42.10	+09:11:05.24	17.017(046)	16.611(020)	15.894(029)	...
45	20:30:43.49	+09:11:07.12	16.857(050)	16.341(025)	15.674(020)	...
46	20:30:39.07	+09:12:20.23	15.848(082)	15.477(017)	15.130(034)	...
47	20:30:38.54	+09:11:07.22	13.610(079)	13.125(020)	12.587(043)	...
48	20:30:45.56	+09:11:02.94	16.444(058)	16.082(011)	15.677(026)	...
49	20:30:38.14	+09:11:27.28	16.096(068)	15.730(025)	15.358(021)	...
50	20:30:54.00	+09:12:15.84	15.803(138)	15.297(022)	14.876(017)	...
51	20:31:00.89	+09:14:24.86	15.965(093)	15.569(014)	15.217(024)	...
52	20:31:01.45	+09:10:23.05	16.901(163)	16.497(039)	16.186(072)	...
53	20:30:53.70	+09:15:47.27	15.112(126)	14.829(026)	14.603(020)	...
SN 2006qq												
01	05:20:05.97	-21:01:36.08	16.333(016)	14.821(016)
02	05:20:01.07	-21:01:54.66	17.296(050)	15.545(009)
03	05:19:59.46	-21:01:55.56
04	05:19:58.41	-21:02:21.05
05	05:19:57.80	-20:59:43.91	12.612(005)	12.341(006)	12.015(005)	...
06	05:19:57.12	-20:57:42.91	16.259(009)	15.173(007)	14.811(011)	14.685(010)	15.494(009)	14.945(010)	14.124(005)	13.895(006)	13.623(005)	...
07	05:20:08.10	-20:58:26.58	14.665(016)	...	12.769(005)	12.478(006)	12.137(005)	...

Table 3 (cont'd)

STAR	$\alpha(2000)$	$\delta(2000)$	u' (mag)	g' (mag)	r' (mag)	i' (mag)	B (mag)	V (mag)	Y (mag)	J (mag)	H (mag)	K_s (mag)
08	05:19:50.53	-20:59:36.53	17.846(027)	15.594(008)	14.758(018)	14.427(012)	16.131(008)	15.113(014)	13.771(125)	13.220(007)	12.742(005)	12.617(028)
09	05:19:43.39	-20:57:45.72	17.697(031)	15.676(007)	14.935(009)	14.642(008)	16.206(009)	15.230(010)	14.018(132)	13.477(008)	12.969(006)	12.854(034)
10	05:19:38.59	-21:00:39.24	18.065(014)	15.860(007)	15.051(007)	14.771(007)	16.381(008)	15.409(008)
11	05:19:43.78	-20:58:24.31	17.550(017)	15.912(007)	15.307(007)	15.085(007)	16.348(008)	15.552(007)	14.468(094)	14.074(008)	13.659(005)	13.586(041)
12	05:19:43.14	-20:56:55.86	20.183(096)	17.426(007)	16.101(007)	15.436(007)	18.117(014)	16.693(008)	14.356(005)	13.930(005)	13.323(005)	...
13	05:19:46.39	-21:01:48.22	...	17.477(013)	16.199(007)	15.466(007)	18.155(011)	16.770(008)
14	05:19:36.25	-20:57:24.62	18.122(031)	16.778(009)	16.294(011)	16.109(017)	17.156(011)	16.484(010)
15	05:19:45.23	-20:58:52.75	19.475(051)	17.385(007)	16.619(007)	16.343(007)	17.856(013)	16.954(007)	15.664(098)	15.225(009)	14.730(007)	14.659(023)
16	05:19:50.87	-21:00:32.51	...	18.199(010)	16.940(007)	16.089(007)	18.943(030)	17.481(009)	14.864(005)	14.411(006)	13.827(005)	...
17	05:19:55.38	-20:54:28.58	18.402(020)	17.360(009)	17.046(013)	16.945(007)	17.645(011)	17.179(007)
18	05:19:51.49	-20:58:54.34	20.810(164)	18.239(009)	17.046(007)	16.550(007)	18.867(020)	17.594(009)	15.761(124)	15.150(008)	14.540(006)	14.360(023)
19	05:20:02.46	-21:00:54.97	18.696(025)	17.517(009)	17.119(007)	16.970(007)	17.865(012)	17.285(009)
20	05:19:50.89	-21:01:41.66	...	18.549(019)	17.172(007)	16.292(007)	19.352(026)	17.775(012)
21	05:19:38.39	-20:57:51.37	19.461(051)	18.184(009)	17.727(007)	17.565(008)	18.590(023)	17.893(011)
22	05:19:41.94	-20:57:07.81	...	18.970(018)	17.658(009)	17.061(007)	19.616(037)	18.268(023)	16.015(007)	15.583(007)	14.969(006)	...
23	05:19:55.77	-20:59:20.18	19.245(059)	18.134(012)	17.754(008)	17.625(014)	18.462(016)	17.919(014)
24	05:19:46.86	-20:55:33.85	19.894(089)	18.416(011)	17.868(007)	17.660(007)	18.814(016)	18.070(013)	16.975(013)	16.671(017)	16.298(036)	...
25	05:19:39.46	-20:59:06.58	...	19.200(022)	17.785(007)	16.502(007)	20.138(051)	18.354(018)
26	05:20:04.72	-20:57:16.16	...	19.372(026)	18.032(009)	17.338(007)	20.164(068)	18.599(020)	16.257(008)	15.796(008)	15.191(008)	...
27	05:20:06.96	-20:59:10.10	19.897(074)	18.558(013)	18.015(012)	17.852(013)	18.913(018)	18.221(014)
28	05:20:06.60	-20:55:02.89	...	19.146(027)	18.251(017)	17.901(010)	19.638(055)	18.729(047)
29	05:19:38.80	-20:55:06.56	20.853(197)	19.202(034)	18.627(022)	18.397(018)	19.592(053)	18.811(023)
30	05:19:36.69	-21:01:01.70	...	19.585(035)	18.307(012)	17.561(009)	20.325(065)	18.895(031)
31	05:20:01.26	-20:58:55.06	...	20.173(077)	18.783(018)	17.885(007)	21.038(158)	19.490(046)	16.669(010)	16.209(012)	15.649(012)	...
32	05:19:52.84	-20:55:34.46	...	19.567(035)	18.702(021)	18.377(011)	20.077(057)	19.137(031)	17.580(020)	17.177(036)	16.705(061)	...
33	05:19:46.68	-20:57:17.64	16.130(006)	15.568(009)	15.006(007)	14.689(045)
34	05:19:40.08	-20:59:40.02	16.166(007)	15.734(008)	15.241(008)	...
35	05:19:42.74	-20:56:39.34	16.416(007)	15.896(008)	15.319(008)	...
36	05:19:48.41	-20:58:47.96	16.579(147)	15.925(010)	15.383(012)	15.133(028)
37	05:19:57.48	-20:55:39.94	17.406(017)	16.952(024)	16.476(029)	...
38	05:19:48.45	-20:56:26.52	17.462(019)	16.928(016)	16.393(021)	...
39	05:19:51.09	-20:56:42.94	18.132(037)	17.727(033)	17.037(045)	...
40	05:19:40.06	-20:59:00.96	18.387(053)	17.958(047)	17.439(054)	...
41	05:19:53.53	-20:57:47.38	16.833(008)	16.248(009)	15.510(009)	14.756(076)
42	05:19:53.42	-20:58:08.65	17.451(186)	16.372(011)	15.604(008)	14.859(103)
43	05:19:48.22	-21:00:11.66	10.998(014)	10.845(012)	10.653(008)	...
44	05:19:53.52	-20:59:49.06	15.962(093)	15.360(008)	14.804(007)	14.559(032)
45	05:19:58.38	-20:58:31.69	16.782(011)	16.331(015)	15.792(015)	...
46	05:19:56.94	-20:58:30.50	17.168(014)	16.680(012)	16.152(015)	...
47	05:20:10.50	-20:57:03.74	15.587(010)	15.275(006)	14.851(006)	...
SN 2008fq												
01	20:24:59.20	-24:50:54.28	16.622(017)	15.381(007)	14.918(007)	14.747(007)	15.741(007)	15.093(006)
02	20:25:01.66	-24:49:28.74	16.991(014)	15.631(007)	15.162(007)	15.010(007)	16.001(007)	15.335(006)	14.398(013)	14.172(013)	13.852(010)	13.806(033)
03	20:25:02.64	-24:48:33.01	18.180(033)	16.178(007)	15.427(007)	15.135(007)	16.682(007)	15.736(006)	14.332(014)	14.001(014)	13.486(012)	13.382(024)
04	20:25:11.83	-24:48:18.40	19.256(041)	16.747(007)	15.815(007)	15.464(007)	17.322(007)	16.221(006)	14.587(014)	14.237(013)	13.714(009)	13.554(024)
05	20:25:22.35	-24:47:18.53	18.011(019)	16.320(007)	15.702(007)	15.487(008)	16.783(007)	15.947(006)	14.781(008)	14.516(012)	14.136(012)	...
06	20:25:09.48	-24:47:48.84	18.629(022)	16.797(007)	16.097(007)	15.830(009)	17.230(056)	16.394(006)
07	20:25:13.39	-24:45:36.22	17.325(015)	16.213(007)	15.769(007)	15.598(008)	16.559(007)	15.936(006)	14.936(012)	14.707(012)	14.377(012)	...

Table 3 (cont'd)

STAR	$\alpha(2000)$	$\delta(2000)$	u' (mag)	g' (mag)	r' (mag)	i' (mag)	B (mag)	V (mag)	Y (mag)	J (mag)	H (mag)	K_s (mag)
08	20:24:53.47	-24:50:40.74	18.604(021)	16.706(007)	15.968(007)	15.666(007)	17.188(007)	16.282(006)
09	20:24:52.25	-24:51:23.00	...	18.797(011)	17.340(013)	15.906(007)	19.664(021)	17.954(012)
10	20:25:14.78	-24:50:12.41	18.362(010)	17.071(007)	16.557(007)	16.353(007)	17.470(007)	16.753(006)	15.654(012)	15.391(009)	15.017(011)	14.896(021)
11	20:25:09.58	-24:45:39.31	18.708(022)	17.211(007)	16.599(007)	16.354(007)	17.648(007)	16.836(006)
12	20:25:19.59	-24:52:10.20	18.778(038)	17.377(007)	16.835(007)	16.628(009)	17.778(007)	17.039(007)
13	20:24:51.55	-24:45:44.17	...	19.383(017)	18.008(009)	16.791(007)	20.209(036)	18.592(012)
14	20:25:02.61	-24:49:21.50	18.973(054)	17.570(007)	17.007(007)	16.786(009)	17.984(008)	17.223(006)	16.095(016)	15.831(015)	15.438(013)	15.395(018)
15	20:25:07.27	-24:44:50.06	18.660(014)	17.482(007)	17.040(007)	16.858(011)	17.864(011)	17.202(006)	16.185(012)	15.899(012)	15.542(016)	...
16	20:25:21.32	-24:47:46.10	...	19.535(016)	18.118(017)	16.796(007)	20.361(054)	18.728(011)
17	20:24:59.43	-24:47:49.96	18.693(019)	17.644(007)	17.110(007)	16.873(008)	18.005(008)	17.323(006)	16.150(010)	15.872(012)	15.473(014)	...
18	20:24:53.45	-24:48:59.08	...	19.386(027)	17.995(016)	17.017(007)	20.118(050)	18.600(012)
19	20:24:52.69	-24:45:49.46	...	18.862(016)	17.646(009)	17.147(008)	19.546(019)	18.190(010)
20	20:25:08.37	-24:46:13.44	20.606(126)	18.423(012)	17.468(023)	17.107(011)	18.957(013)	17.907(007)
21	20:25:07.95	-24:49:29.03	19.298(034)	17.886(007)	17.407(008)	17.227(007)	18.284(009)	17.592(007)
22	20:25:16.50	-24:51:26.24	18.998(029)	17.817(007)	17.364(009)	17.197(007)	18.180(013)	17.525(006)
23	20:25:20.96	-24:51:05.18	19.212(021)	18.010(007)	17.547(007)	17.365(008)	18.361(018)	17.718(006)
24	20:25:11.58	-24:48:35.50	...	19.899(033)	18.470(031)	17.277(007)	20.765(077)	19.100(022)	15.873(016)	15.405(013)	14.793(009)	14.526(028)
25	20:24:53.58	-24:48:19.44	...	19.526(015)	18.151(008)	17.394(007)	20.291(035)	18.768(011)
26	20:24:53.64	-24:48:44.42	...	20.022(033)	18.661(011)	17.482(010)	20.877(090)	19.289(039)
27	20:24:51.86	-24:48:33.98	...	20.132(026)	18.745(017)	17.619(007)	20.774(060)	19.367(020)
28	20:24:58.67	-24:45:36.79	...	19.440(014)	18.147(011)	17.567(007)	20.184(034)	18.765(011)
29	20:24:54.33	-24:48:04.43	19.412(071)	18.255(008)	17.797(008)	17.585(008)	18.634(012)	17.968(008)
30	20:25:00.33	-24:49:34.07	...	20.550(073)	19.116(017)	17.889(008)	21.297(094)	19.699(025)
31	20:24:56.10	-24:45:36.86	19.334(036)	18.423(007)	18.152(014)	18.021(013)	18.713(019)	18.233(011)
32	20:24:54.93	-24:46:00.23	20.170(057)	18.853(012)	18.306(008)	18.079(010)	19.282(016)	18.531(010)
33	20:25:03.17	-24:51:15.26	...	20.207(029)	18.926(018)	18.272(017)	20.979(073)	19.521(029)
34	20:25:22.72	-24:48:47.99	...	20.413(101)	19.204(016)	18.342(023)	21.335(099)	19.716(057)
35	20:25:30.69	-24:51:54.29	12.016(020)	11.662(020)
36	20:25:25.04	-24:51:13.28	12.566(011)	12.293(010)	11.933(008)	...
37	20:25:28.83	-24:46:58.40	12.925(010)	12.549(012)	11.977(012)	...
38	20:25:16.54	-24:43:20.39	13.650(012)	13.426(020)
39	20:25:23.84	-24:45:31.72	13.934(012)	13.709(012)	13.376(012)	...
40	20:25:02.73	-24:47:09.56	13.641(014)	13.377(015)	12.947(012)	12.857(041)
41	20:25:10.38	-24:44:24.14	14.773(012)	14.539(012)	14.189(015)	...
42	20:25:12.28	-24:45:10.48	14.911(012)	14.583(012)	14.095(012)	...
43	20:25:00.82	-24:46:11.64	15.112(009)	14.703(012)	14.062(012)	...
44	20:25:28.76	-24:48:30.85	15.144(008)	15.002(009)	14.817(010)	...
45	20:25:24.20	-24:47:24.47	15.241(009)	14.946(012)	14.520(010)	...
46	20:25:30.47	-24:48:10.48	15.310(008)	14.992(010)	14.518(012)	...
47	20:25:27.11	-24:46:12.47	15.374(009)	15.021(012)	14.491(012)	...
48	20:25:23.48	-24:51:52.42	14.943(020)	...	14.356(015)	...
49	20:25:03.78	-24:46:13.33	15.648(009)	15.390(012)	15.005(012)	...
50	20:25:04.19	-24:49:55.52	15.953(013)	15.658(014)	15.251(020)	15.135(045)
51	20:24:59.93	-24:43:59.84	16.381(012)	16.128(012)	15.812(015)	...
52	20:25:28.99	-24:45:07.27	16.663(021)	16.177(026)	15.658(017)	...
53	20:25:31.46	-24:43:41.05	17.070(020)	16.560(018)

Note. — Uncertainties given in parentheses in thousandths of a magnitude correspond to an rms of the magnitudes obtained on photometric nights.

Table 4. Optical Photometry of five CSP SNe II in the Natural System.

JD-2453000	Phase ^a	<i>u</i> (mag)	<i>g</i> (mag)	<i>r</i> (mag)	<i>i</i> (mag)	<i>B</i> (mag)	<i>V</i> (mag)	Telescope ^b
SN 2005kj								
692.00	+0.00	16.3 ^c
695.83	+3.83	16.196(012)	16.067(007)	16.066(008)	16.192(011)	16.209(009)	16.074(008)	SWO
698.83	+6.83	16.224(011)	16.102(005)	16.084(004)	16.195(007)	16.222(007)	16.089(005)	SWO
699.80	+7.80	16.234(012)	16.103(006)	16.082(008)	16.187(008)	16.231(009)	16.097(009)	SWO
702.79	+10.79	16.284(012)	16.122(005)	16.106(004)	16.201(007)	...	16.116(007)	SWO
703.84	+11.84	16.313(013)	16.134(006)	16.104(008)	16.212(009)	16.264(007)	16.106(007)	SWO
706.79	+14.79	16.356(013)	16.152(007)	16.099(009)	16.217(009)	16.300(008)	16.137(008)	SWO
712.79	+20.79	16.457(012)	16.236(007)	16.177(006)	16.236(009)	16.381(007)	16.189(009)	SWO
716.82	+24.82	16.565(013)	16.286(006)	16.213(008)	16.265(009)	16.431(009)	16.234(008)	SWO
721.77	+29.77	16.703(016)	16.347(008)	16.246(008)	16.306(009)	16.517(008)	16.306(009)	SWO
726.82	+34.82	16.836(016)	16.423(008)	16.301(009)	16.354(012)	16.611(009)	16.352(009)	SWO
728.81	+36.81	16.913(016)	16.449(008)	16.320(008)	16.357(009)	16.654(008)	16.377(009)	SWO
730.84	+38.84	16.945(018)	16.495(005)	16.336(008)	16.371(009)	16.686(008)	16.413(005)	SWO
736.77	+44.77	17.142(017)	16.577(007)	16.410(009)	16.426(008)	16.796(008)	16.465(008)	SWO
739.77	+47.77	17.239(019)	16.617(008)	16.429(009)	16.448(009)	16.818(008)	16.514(009)	SWO
741.75	+49.75	17.284(020)	16.644(004)	16.450(005)	16.468(008)	16.869(009)	16.522(008)	SWO
745.81	+53.81	17.340(017)	16.694(008)	16.469(008)	16.494(009)	16.929(008)	16.563(008)	SWO
748.75	+56.75	17.495(020)	16.724(006)	16.503(006)	16.507(008)	16.945(008)	16.593(007)	SWO
751.75	+59.75	17.554(023)	16.771(007)	16.539(008)	16.530(009)	17.003(009)	16.631(008)	SWO
755.71	+63.71	17.660(018)	16.827(007)	16.558(008)	16.552(010)	17.086(009)	16.675(008)	SWO
761.75	+69.75	17.902(018)	16.932(006)	16.642(007)	16.623(008)	17.204(009)	16.751(008)	SWO
763.69	+71.69	18.002(023)	16.956(010)	16.653(012)	16.661(013)	17.261(009)	16.792(008)	SWO
765.69	+73.69	18.115(025)	16.990(011)	16.724(013)	16.684(015)	17.299(011)	16.824(012)	SWO
768.65	+76.65	18.219(025)	17.077(005)	16.752(005)	16.706(006)	17.380(007)	16.893(006)	SWO
771.68	+79.68	18.327(025)	17.130(010)	16.800(013)	16.745(012)	17.460(009)	16.928(008)	SWO
772.67	+80.67	18.410(022)	17.167(007)	16.790(006)	16.754(009)	17.483(008)	16.940(007)	SWO
774.67	+82.67	18.429(029)	17.215(007)	16.825(009)	16.777(009)	17.545(009)	16.971(008)	SWO
775.54	+83.54	18.590(044)	17.230(007)	16.852(006)	16.799(007)	17.562(011)	16.985(007)	SWO
778.66	+86.66	18.557(047)	17.299(012)	16.876(010)	16.811(012)	17.629(014)	17.024(011)	SWO
781.71	+89.71	18.750(049)	17.352(011)	16.925(009)	16.868(010)	17.716(015)	17.087(010)	SWO
783.68	+91.68	18.939(044)	17.415(008)	16.954(008)	16.921(010)	17.773(013)	17.140(009)	SWO
784.70	+92.70	18.956(043)	17.455(007)	16.982(009)	16.908(009)	17.809(010)	17.159(008)	SWO
798.66	+106.66	19.582(053)	17.791(010)	17.266(012)	17.161(014)	18.262(013)	17.483(011)	SWO
804.68	+112.68	19.859(127)	18.001(013)	17.360(009)	17.257(010)	18.431(024)	17.615(012)	SWO
819.56	+127.56	...	18.365(011)	17.650(011)	17.555(011)	18.886(014)	17.964(012)	SWO
824.60	+132.60	...	18.535(011)	17.780(011)	17.672(011)	19.057(016)	18.111(010)	SWO
832.58	+140.58	...	18.755(016)	17.994(011)	17.817(012)	19.282(026)	18.329(014)	SWO
838.62	+146.62	...	18.935(021)	18.155(013)	17.991(012)	19.390(043)	18.467(017)	SWO
841.57	+149.57	...	18.995(015)	18.255(013)	18.062(013)	19.628(029)	18.586(015)	SWO
870.51	+178.51	...	19.643(026)	18.769(015)	18.607(016)	20.041(048)	19.143(026)	SWO
SN 2006aa								
774.98	+0.00	18.1 ^c	SWO
776.00	+1.02	18.0 ^c	SWO
778.83	+3.85	18.585(054)	18.282(017)	18.116(019)	18.153(019)	18.481(029)	18.215(022)	SWO
783.77	+8.79	18.410(049)	18.184(016)	17.988(013)	18.030(016)	18.314(021)	18.064(016)	SWO
784.87	+9.89	18.540(063)	18.183(016)	17.940(015)	17.998(016)	18.338(020)	18.036(015)	SWO
788.81	+13.83	18.471(031)	18.059(010)	17.875(011)	17.919(015)	18.226(014)	17.957(011)	SWO
790.77	+15.79	18.458(036)	18.001(009)	17.820(009)	17.864(012)	18.198(013)	17.922(010)	SWO
795.76	+20.78	18.338(028)	17.835(008)	17.690(009)	17.724(011)	18.007(011)	17.776(009)	SWO
799.77	+24.79	18.105(023)	17.742(008)	17.592(008)	17.655(010)	17.890(010)	17.680(009)	SWO
802.75	+27.77	17.946(021)	17.637(008)	17.532(009)	17.615(010)	17.799(011)	17.612(009)	SWO
805.70	+30.72	17.856(029)	17.577(011)	17.478(010)	17.544(011)	17.735(016)	17.561(012)	SWO
823.73	+48.75	17.754(016)	17.471(008)	17.372(008)	17.462(010)	17.601(010)	17.450(009)	SWO
834.70	+59.72	17.879(029)	17.565(009)	17.466(009)	17.508(010)	17.716(013)	17.521(011)	SWO
835.63	+60.65	17.873(028)	17.567(010)	17.458(011)	17.535(012)	17.718(013)	17.544(011)	SWO
840.66	+65.68	17.980(039)	17.646(011)	17.519(010)	17.585(014)	17.786(018)	17.610(015)	SWO
846.67	+71.69	18.201(024)	17.748(008)	17.595(008)	17.653(011)	17.912(010)	17.685(009)	SWO
861.60	+86.62	18.944(057)	18.073(009)	17.820(009)	17.827(011)	18.281(016)	17.946(011)	SWO
862.59	+87.61	18.948(053)	18.092(011)	17.816(010)	17.847(012)	18.332(017)	17.950(013)	SWO
867.59	+92.61	19.214(096)	18.239(018)	17.942(016)	17.926(017)	18.499(032)	18.069(016)	SWO
870.61	+95.63	19.914(187)	18.358(016)	18.036(013)	17.972(013)	18.606(030)	18.133(020)	SWO
872.61	+97.63	19.586(079)	18.391(014)	18.049(012)	17.997(014)	18.649(018)	18.207(014)	SWO
891.56	+116.58	...	19.039(022)	18.411(015)	18.282(016)	19.497(046)	18.705(024)	SWO
892.57	+117.59	18.435(025)	18.186(052)	DUP
898.53	+123.55	...	19.393(014)	18.632(009)	18.483(009)	19.890(033)	18.946(012)	DUP
SN 2006bo								
830.65	+0.00	17.6 ^c
832.64	+1.99	17.1 ^c
834.92	+4.27	18.694(035)	17.816(016)	17.506(020)	17.383(040)	18.059(010)	17.671(009)	SWO
840.86	+10.22	18.981(084)	17.981(018)	17.642(013)	17.567(012)	18.233(019)	17.751(012)	SWO
845.92	+15.27	19.292(064)	18.069(013)	17.651(012)	17.579(019)	18.369(015)	17.827(011)	SWO
846.92	+16.27	19.363(045)	18.140(014)	17.695(013)	17.628(028)	18.419(013)	17.871(010)	SWO
850.88	+20.23	...	18.216(012)	17.743(011)	17.645(010)	18.536(012)	17.920(010)	SWO
853.89	+23.24	...	18.298(014)	17.804(014)	17.674(011)	18.639(013)	17.972(010)	SWO
858.83	+28.18	20.147(136)	18.427(016)	17.881(012)	17.716(013)	18.835(019)	18.085(012)	SWO

Table 4 (cont'd)

JD–2453000	Phase ^a	<i>u</i> (mag)	<i>g</i> (mag)	<i>r</i> (mag)	<i>i</i> (mag)	<i>B</i> (mag)	<i>V</i> (mag)	Telescope ^b
862.82	+32.17	20.440(125)	18.542(014)	17.950(011)	17.792(011)	18.998(016)	18.170(010)	SWO
866.82	+36.17	20.627(217)	18.613(021)	18.001(013)	17.861(011)	19.119(031)	18.242(015)	SWO
867.81	+37.16	...	18.661(021)	18.003(013)	17.851(012)	19.117(033)	18.249(018)	SWO
870.83	+40.18	...	18.765(024)	18.016(015)	17.894(011)	19.209(053)	18.314(020)	SWO
871.81	+41.16	...	18.762(026)	18.055(014)	17.907(013)	19.257(041)	18.352(018)	SWO
872.80	+42.15	...	18.804(019)	18.063(015)	17.883(013)	19.321(033)	18.353(015)	SWO
886.79	+56.14	19.590(010)	18.518(006)	DUP
891.76	+61.11	...	19.088(016)	18.199(012)	17.984(011)	19.711(029)	18.537(016)	SWO
892.78	+62.13	...	19.084(013)	18.207(010)	17.990(007)	19.651(020)	18.546(005)	DUP
893.79	+63.14	...	19.105(012)	18.233(009)	18.008(006)	19.682(018)	18.571(007)	DUP
898.75	+68.11	18.290(013)	18.037(009)	19.737(026)	18.559(010)	DUP
979.67	+149.02	...	22.384(328)	21.755(215)	21.534(289)	...	22.380(511)	SWO
SN 2006qq								
1069.87	+0.00	17.0 ^c
1070.88	+1.01	16.9 ^c
1071.73	+1.86	18.418(028)	17.839(010)	17.579(010)	17.486(010)	18.045(013)	17.676(011)	SWO
1073.76	+3.89	18.549(044)	17.877(011)	17.585(009)	17.472(012)	18.073(018)	17.682(012)	SWO
1075.81	+5.94	18.654(044)	17.916(012)	17.565(012)	17.480(012)	18.180(017)	17.728(014)	SWO
1085.73	+15.86	19.155(026)	18.247(010)	17.731(007)	17.545(009)	18.497(012)	17.932(009)	SWO
1087.73	+17.86	19.241(032)	18.266(010)	17.768(010)	17.565(009)	18.581(014)	17.979(011)	SWO
1092.77	+22.90	19.392(036)	18.399(012)	17.821(011)	17.633(012)	18.690(014)	18.069(012)	SWO
1096.75	+26.88	19.491(044)	18.435(010)	17.866(009)	17.664(008)	18.786(015)	18.128(011)	SWO
1100.71	+30.84	19.606(071)	18.512(025)	17.912(016)	17.692(017)	18.828(031)	18.185(017)	SWO
1102.70	+32.83	19.579(133)	18.493(027)	17.910(019)	17.681(014)	18.903(040)	18.193(025)	SWO
1105.17	+35.30	19.576(129)	18.551(024)	17.959(014)	17.680(011)	...	18.259(018)	SWO
1106.73	+36.86	19.618(094)	18.604(017)	17.960(011)	17.740(009)	18.912(025)	...	SWO
1108.80	+38.93	...	18.594(015)	17.946(010)	17.757(011)	SWO
1112.71	+42.84	19.719(038)	18.648(013)	18.008(012)	17.805(011)	18.998(014)	18.313(014)	SWO
1119.69	+49.82	19.773(039)	18.726(013)	18.046(011)	17.855(010)	19.015(013)	18.378(013)	SWO
1123.75	+53.88	20.012(061)	18.772(013)	18.068(010)	17.891(012)	19.116(015)	18.452(016)	SWO
1128.68	+58.81	19.980(095)	18.806(017)	18.118(011)	17.928(011)	19.200(018)	18.482(018)	SWO
1130.60	+60.73	20.103(080)	18.839(020)	18.127(014)	17.946(014)	19.170(026)	18.469(019)	SWO
1134.17	+64.30	20.075(133)	18.875(034)	18.170(018)	17.999(013)	19.199(038)	18.534(027)	SWO
1136.69	+66.82	...	18.926(022)	18.140(012)	18.017(012)	...	18.601(021)	SWO
1143.65	+73.78	...	19.075(017)	18.194(010)	18.096(011)	19.353(017)	18.618(016)	SWO
1147.63	+77.76	18.221(011)	18.149(012)	19.422(017)	...	SWO
1158.62	+88.75	...	19.193(027)	18.406(014)	18.412(016)	19.532(026)	18.870(022)	SWO
1163.61	+93.74	...	19.266(035)	18.459(018)	18.516(016)	19.540(049)	18.897(034)	SWO
1179.54	+109.67	...	19.355(020)	18.451(014)	18.619(015)	19.704(022)	19.061(022)	SWO
1197.50	+127.63	18.513(017)	18.738(018)	19.800(023)	19.127(023)	SWO
1225.47	+155.60	...	19.696(051)	18.574(037)	18.926(040)	20.150(105)	19.329(136)	SWO
SN 2008fq								
1724.79	+0.00	15.4 ^c
1725.71	+0.92	15.5 ^c
1726.57	+1.78	17.224(014)	16.205(006)	15.739(005)	15.625(005)	16.571(007)	15.883(006)	SWO
1728.54	+3.75	17.285(016)	16.224(019)	15.637(006)	15.504(006)	16.563(011)	15.835(009)	SWO
1729.53	+4.74	17.340(014)	16.206(015)	15.628(008)	15.474(008)	16.570(010)	15.826(009)	SWO
1732.59	+7.80	17.513(013)	16.219(014)	15.582(006)	15.384(006)	16.632(007)	15.808(007)	SWO
1739.57	+14.78	18.022(015)	16.442(016)	15.648(006)	15.391(005)	16.891(009)	15.947(004)	SWO
1740.58	+15.79	18.108(017)	16.451(008)	15.671(005)	15.395(005)	16.939(008)	15.978(004)	SWO
1742.59	+17.80	17.003(020)	...	SWO
1744.59	+19.80	18.499(020)	16.678(018)	15.825(007)	15.542(008)	17.151(008)	16.150(007)	SWO
1747.62	+22.83	18.830(029)	16.787(009)	15.925(007)	15.670(006)	17.330(012)	16.297(007)	SWO
1749.57	+24.78	18.992(037)	16.894(009)	15.991(007)	15.727(007)	17.479(012)	16.382(007)	SWO
1753.56	+28.77	19.498(056)	17.095(009)	16.098(005)	15.854(005)	17.711(012)	16.540(007)	SWO
1756.62	+31.83	19.716(054)	17.219(011)	16.161(008)	15.917(007)	17.878(014)	16.615(008)	SWO
1759.59	+34.80	...	17.315(011)	16.199(009)	15.960(012)	18.008(011)	16.685(009)	SWO
1766.53	+41.74	20.442(075)	17.516(018)	16.259(006)	16.025(006)	18.225(015)	16.828(009)	SWO
1772.55	+47.76	20.878(075)	17.604(010)	16.295(006)	16.063(009)	18.392(016)	16.894(010)	SWO
1777.58	+52.79	21.193(267)	17.729(013)	16.331(006)	16.109(006)	18.554(022)	16.981(009)	SWO
1785.56	+60.77	...	18.003(021)	16.462(010)	16.227(007)	18.812(035)	17.206(016)	SWO
1790.54	+65.75	21.648(164)	18.158(014)	16.566(009)	16.351(011)	19.102(033)	17.327(013)	SWO

Note. — Values in parentheses are 1σ measurement uncertainties in millimag. The quoted uncertainties include the error on the zero point as determined from the flux measure of the local sequence stars and the uncertainty on the measured SN flux.

^aDays since discovery.

^bDUP and SWO correspond to the du Pont and Swope telescopes, respectively.

^cUnfiltered magnitudes from discovery and confirmation images (see Table 2 for CBET references).

Table 5. NIR Photometry of five CSP SNe II_n.

JD-2453000	Phase ^a	Y (mag)	J (mag)	H (mag)	K _s (mag)	Telescope ^b
SN 2005kj						
696.83	+4.83	15.875(014)	15.764(019)	15.545(019)	...	SWO
701.82	+9.82	15.890(020)	15.748(020)	15.567(023)	...	SWO
705.86	+13.86	15.898(020)	15.782(023)	15.564(017)	...	SWO
710.86	+18.86	15.871(015)	15.837(026)	15.566(025)	...	SWO
714.79	+22.79	15.918(019)	15.791(026)	15.579(024)	...	SWO
717.81	+25.81	15.913(015)	15.779(023)	15.581(020)	...	SWO
719.78	+27.78	15.948(020)	15.808(025)	15.596(018)	...	SWO
724.80	+32.80	15.956(020)	15.872(030)	15.612(021)	...	SWO
727.86	+35.86	15.973(022)	15.815(028)	15.639(023)	...	SWO
732.83	+40.83	16.049(021)	15.846(022)	15.647(020)	...	SWO
750.82	+58.82	16.090(007)	15.936(007)	15.652(021)	...	DUP
753.69	+61.69	15.476(016)	BAA
755.68	+63.68	15.470(015)	BAA
757.82	+65.82	16.130(007)	15.993(007)	15.780(015)	15.583(014)	DUP
773.75	+81.75	16.309(007)	16.140(011)	15.854(032)	15.572(027)	DUP
776.72	+84.72	16.298(016)	16.148(024)	SWO
777.71	+85.71	...	16.124(026)	15.912(028)	...	SWO
782.68	+90.68	16.384(018)	16.208(027)	15.980(030)	...	SWO
784.69	+92.69	16.436(008)	16.239(008)	15.934(032)	15.663(016)	DUP
785.73	+93.73	...	16.343(020)	...	15.617(027)	DUP
788.73	+96.73	16.497(009)	16.339(014)	15.936(036)	...	DUP
797.67	+105.67	16.573(020)	16.408(026)	16.166(033)	...	SWO
806.51	+114.51	16.004(019)	BAA
807.69	+115.69	16.735(020)	16.520(034)	16.292(040)	...	SWO
810.64	+118.64	16.761(021)	16.580(035)	16.261(040)	...	SWO
813.67	+121.67	16.833(026)	16.613(033)	16.343(033)	...	SWO
820.65	+128.65	16.926(026)	16.687(040)	16.436(056)	...	SWO
826.55	+134.55	17.052(023)	16.790(047)	16.521(053)	...	SWO
834.55	+142.55	17.243(014)	17.020(019)	16.460(043)	16.413(048)	DUP
843.57	+151.57	17.404(017)	17.189(026)	16.503(041)	16.202(058)	DUP
848.51	+156.51	17.470(048)	17.456(135)	16.810(153)	...	SWO
859.48	+167.48	17.659(158)	SWO
860.50	+168.50	...	17.299(083)	16.926(086)	...	SWO
868.48	+176.48	17.779(042)	17.512(068)	SWO
1073.85	+381.85	19.680(060)	19.064(056)	DUP
SN 2006aa						
776.82	+1.84	17.752(033)	17.831(080)	SWO
787.78	+12.80	17.522(010)	17.390(021)	17.060(050)	...	DUP
800.81	+25.83	17.214(015)	17.126(025)	SWO
808.78	+33.80	17.102(018)	17.020(024)	SWO
814.76	+39.78	17.069(019)	16.978(024)	16.883(068)	...	SWO
826.75	+51.77	17.087(017)	SWO
834.73	+59.75	17.134(008)	16.971(009)	16.804(021)	...	DUP
844.70	+69.72	17.224(011)	DUP
845.66	+70.68	...	17.058(009)	16.838(024)	...	DUP
SN 2006bo						
835.90	+5.25	17.075(020)	16.832(008)	16.644(012)	...	DUP
839.90	+9.25	17.089(026)	16.829(025)	SWO
845.90	+15.25	17.119(024)	16.915(012)	16.485(026)	...	DUP
851.92	+21.27	17.087(022)	16.902(027)	SWO
852.89	+22.24	16.763(057)	...	SWO
855.87	+25.22	17.236(039)	17.076(054)	16.751(079)	...	SWO
863.87	+33.22	17.248(021)	16.980(023)	16.749(033)	...	SWO
868.90	+38.25	17.275(024)	SWO
SN 2006qq						
1070.82	+0.95	17.004(016)	16.800(024)	16.600(041)	...	SWO
1074.79	+4.92	16.944(016)	16.715(019)	16.520(029)	...	SWO
1078.79	+8.92	16.903(017)	16.712(038)	16.416(034)	...	SWO
1082.79	+12.92	16.952(018)	16.702(022)	16.421(028)	...	SWO
1086.77	+16.90	16.971(017)	16.666(023)	16.322(042)	...	SWO
1090.70	+20.83	16.950(018)	16.642(018)	16.354(023)	...	SWO
1098.76	+28.89	16.963(016)	16.668(020)	16.398(045)	...	SWO
1100.68	+30.81	16.968(009)	16.694(008)	16.328(009)	...	DUP
1103.76	+33.89	17.015(019)	16.711(026)	16.407(029)	...	SWO
1107.71	+37.84	17.028(017)	16.679(021)	16.358(026)	...	SWO
1111.77	+41.90	17.035(023)	16.740(024)	16.380(028)	...	SWO
1120.65	+50.78	17.104(017)	16.794(020)	16.385(022)	...	SWO
1122.70	+52.83	17.122(018)	16.782(019)	16.422(028)	...	SWO
1124.68	+54.81	17.111(019)	16.813(025)	16.380(031)	...	SWO
1128.65	+58.78	17.128(008)	16.840(009)	16.455(010)	...	DUP
1129.58	+59.71	17.169(019)	16.823(022)	16.470(028)	...	SWO
1132.65	+62.78	17.179(024)	16.930(036)	16.582(053)	...	SWO
1135.60	+65.73	17.279(026)	16.917(031)	16.536(034)	...	SWO
1137.71	+67.84	17.218(009)	16.931(009)	DUP
1140.55	+70.68	17.340(029)	16.948(045)	16.636(049)	...	SWO

Table 5 (cont'd)

JD–2453000	Phase ^a	Y (mag)	J (mag)	H (mag)	K _s (mag)	Telescope ^b
1146.58	+76.71	17.378(023)	16.987(032)	16.723(042)	...	SWO
1156.61	+86.74	17.594(026)	17.216(029)	16.973(069)	...	SWO
1159.57	+89.70	17.595(010)	17.295(011)	16.921(013)	...	SWO
1162.56	+92.69	17.636(038)	17.310(054)	17.086(081)	...	SWO
1168.58	+98.71	17.707(039)	17.280(053)	17.062(061)	...	SWO
1172.56	+102.69	17.709(011)	17.391(011)	17.093(014)	...	DUP
1184.50	+114.63	17.696(071)	17.473(099)	17.129(094)	...	SWO
1196.49	+126.62	17.855(052)	17.430(062)	17.384(093)	...	SWO
1802.73	+732.86	19.838(112)	...	DUP
1839.57	+769.70	20.348(151)	...	DUP
SN 2008fq						
1726.53	+1.74	15.150(006)	15.025(006)	14.769(006)	14.467(011)	DUP
1728.64	+3.85	14.985(005)	14.845(004)	14.600(004)	14.323(009)	DUP
1729.64	+4.85	14.916(004)	14.799(005)	14.527(004)	14.290(010)	DUP
1731.65	+6.86	14.795(010)	14.677(009)	14.442(010)	...	SWO
1733.65	+8.86	14.735(009)	14.611(007)	14.352(008)	...	SWO
1738.70	+13.91	14.661(005)	14.523(006)	14.221(007)	...	SWO
1741.67	+16.88	14.715(009)	14.511(007)	14.180(006)	...	SWO
1743.68	+18.89	14.751(007)	14.543(006)	14.192(007)	...	SWO
1746.53	+21.74	14.854(006)	14.605(010)	14.269(005)	13.890(011)	DUP
1748.68	+23.89	14.927(009)	14.639(007)	14.331(009)	...	SWO
1750.65	+25.86	14.967(008)	14.735(008)	14.358(009)	...	SWO
1751.55	+26.76	15.012(008)	14.727(007)	14.371(011)	13.938(016)	DUP
1756.59	+31.80	15.082(005)	14.811(005)	14.459(004)	14.065(011)	DUP
1769.53	+44.74	15.157(008)	14.879(009)	14.537(007)	...	SWO
1778.57	+53.78	15.229(009)	14.948(008)	14.597(009)	...	SWO
1782.53	+57.74	15.274(007)	14.969(008)	14.605(007)	...	SWO
1796.53	+71.74	15.610(010)	15.336(012)	SWO

Note. — Values in parentheses are 1σ measurement uncertainties in millimag. The quoted uncertainties include the error on the zero point as determined from the flux measure of the local sequence stars and the uncertainty on the measured SN flux.

^aDays since discovery.

^bDUP, SWO and BAA correspond to the du Pont, Swope and Baade telescopes, respectively.

Table 6. UT dates of optical and NIR template observations.

SN/filter	u	B	g	V	r	i	Y	J	H	K _s
2005kj	2008-03-06	2008-03-14	2008-03-06	2008-03-06	2008-03-14	2008-03-06	2011-12-20	2011-12-20	2011-12-20	2013-02-02
2005ip
2006aa	2008-03-14	2008-03-14	2008-03-14	2008-03-14	2008-03-14	2008-03-14	2007-06-28	2007-06-28	2011-02-21	...
2006bo	2007-09-16	2007-09-16	2007-09-16	2007-09-16	2007-09-16	2007-09-16	2007-06-29	2007-06-29	2007-06-29	...
2006jd
2006qq	2008-03-14	2008-03-14	2008-03-14	2008-03-14	2008-03-14	2008-03-14	2009-04-16	2009-04-16	2009-05-03	...
2008fq	2012-04-22	2012-11-07	2012-09-15	2012-09-15	2012-09-15	2012-09-15	2010-04-29	2010-04-29	2011-07-21	2010-09-25

Note. — SNe 2005ip and 2006jd are still visible given their extraordinary long-lasting CSM-interaction, therefore templates are not available yet.

Table 7. Spectroscopic Observations of five CSP SNe II_n.

Date (UT)	Julian Date JD−2453000	Epoch ^a (days)	Telescope	Instrument	Spectral Range (Å)	Resolution (FWHM Å)	Integration (s)
SN 2005kj							
2005 Nov. 24	698.77	+6.8	Du Pont	MS	3780 – 7289	5	600x3
2005 Nov. 25	699.76	+7.8	Du Pont	MS	3780 – 7289	5	600x3
2005 Dec. 08	712.76	+20.8		T60	3200 – 9606	14	900x3
2005 Dec. 20	724.81	+32.8	Du Pont	WFCCD	3800 – 9235	8	400x3
2005 Dec. 21	725.76	+33.8	Du Pont	WFCCD	3800 – 9235	8	400x3
2005 Dec. 23	727.76	+35.8	Du Pont	WFCCD	3800 – 9235	8	400x3
2006 Jan. 16	751.76	+59.8	NTT	EMMI	3200 – 10200	6–9	200x3
2006 Jan. 24	759.66	+67.7	Clay	LDSS	3788 – 9980	2–4	200x3
2006 Feb. 13	779.72	+87.7	NTT	EMMI	4000 – 10200	8	300x3
2006 Mar. 05	799.64	+107.6	Du Pont	WFCCD	3800 – 9235	8	600x3
2006 Mar. 14	808.66	+116.7	Clay	LDSS	3785 – 9972	2–4	400x3
2006 Mar. 22	816.63	+124.6	Du Pont	WFCCD	3800 – 9235	8	600x3
2006 Mar. 24	818.57	+126.6	Du Pont	WFCCD	3800 – 9235	8	900x3
2006 Apr. 02	827.56	+135.6	Du Pont	WFCCD	3800 – 9235	8	600x3
2006 Apr. 26	851.49	+159.5	Du Pont	WFCCD	3800 – 9235	8	900x3
SN 2006aa							
2006 Feb. 27	793.80	+18.8	Du Pont	WFCCD	3800 – 9235	8	600x3
2006 Mar. 05	799.75	+24.8	Du Pont	WFCCD	3800 – 9235	8	600x3
2006 Mar. 15	809.76	+34.8	Clay	LDSS	3785 – 9969	2–4	600x3–400x3
2006 Mar. 15	809.80	+34.8	NTT	EMMI	3200 – 10200	6–9	300x3
2006 Mar. 24	818.69	+43.7	Du Pont	WFCCD	3800 – 9235	8	600x3
2006 Mar. 30	824.73	+49.8	Du Pont	WFCCD	3800 – 9235	8	600x3
2006 Apr. 26	851.60	+76.6	Du Pont	WFCCD	3800 – 9235	8	600x3
SN 2006bo							
2006 Apr. 16	841.86	+11.2	Baade	IMACS	3842 – 9692	4	600x3
2006 Apr. 26	851.88	+21.2	Du Pont	WFCCD	3800 – 9235	8	1200x3
SN 2006qq							
2006 Dec. 13	1082.71	+12.8	Du Pont	B&C	3622 – 9833	8	600x3
2006 Dec. 18	1087.77	+17.9	Du Pont	WFCCD	3800 – 9235	8	600x3
2007 Jan. 01	1101.73	+31.9	Clay	LDSS	3705 – 9985	2–4	600x3
2007 Jan. 06	1106.75	+36.9	NTT	EMMI	4000 – 10200	6–9	450x3
2007 Jan. 13	1113.78	+43.9	Du Pont	B&C	3931 – 10140	8	900x3
2007 Jan. 18	1118.59	+48.7	Du Pont	B&C	3402 – 9615	8	1800x3
2007 Jan. 29	1129.58	+59.7	Baade	IMACS	4279 – 9538	4	900x4
2007 Feb. 12	1143.59	+73.7	Du Pont	WFCCD	3800 – 9235	8	900x4
2007 Feb. 13	1144.64	+74.8	Du Pont	WFCCD	3800 – 9235	8	900x3
SN 2008fq							
2008 Sep. 17	1726.54	+1.7	Clay	LDSS	3646 – 9459	7	500x1
2008 Sep. 22	1731.56	+6.8	Du Pont	WFCCD	3800 – 9235	8	900x3
2008 Sep. 29	1738.57	+13.8	Du Pont	WFCCD	3800 – 9235	8	900x3
2008 Oct. 14	1753.53	+28.7	NTT	EFOSC	3401 – 9210	27–39	600x3
2008 Nov. 25	1795.53	+70.7	Du Pont	WFCCD	3800 – 9235	8	900x3

^aDays since discovery.Table 10. Balmer line fluxes in units of 10^{-14} erg s⁻¹ cm⁻² for SN 2005kj.

Days since discovery	F(H α _b)	F(H α _n)	F(H α _{tot})	F(H β _b)	F(H β _n)	F(H β _{P-Cyg})	F(H β _{tot})
+6.77	4.76(0.50)	2.86(0.47)	7.63(0.68)	3.18(0.27)	0.58(0.28)	...	3.76(0.39)
+7.76	4.14(0.90)	1.25(0.97)	5.39(1.32)	3.37(0.18)	0.37(0.17)	...	3.74(0.25)
+20.76	4.03(0.50)	1.98(0.50)	6.02(0.71)	2.94(0.50)	1.67(0.50)	...	4.61(0.71)
+32.81	3.31(0.34)	1.75(0.36)	5.06(0.50)	0.80(0.73)	1.19(0.66)	...	1.99(0.98)
+33.76	2.70(0.30)	1.76(0.30)	4.46(0.43)	1.75(0.31)	0.35(0.31)	...	2.10(0.44)
+35.76	2.85(0.29)	1.80(0.31)	4.65(0.43)	1.96(0.33)	1.03(0.34)	...	2.98(0.47)
+59.76	2.45(0.28)	1.63(0.27)	4.08(0.39)	...	0.85(0.14)	...	0.85(0.14)
+67.66	2.00(0.17)	1.31(0.18)	3.31(0.25)	...	0.50(0.05)	-0.08(0.03)	0.42(0.08)
+87.72	1.38(0.34)	1.24(0.32)	2.61(0.47)	...	0.50(0.46)	-0.46(0.46)	0.04(0.92)
+107.64	...	1.42(0.04)	1.42(0.04)	...	0.26(0.20)	-0.50(0.25)	-0.24(0.45)
+116.66	...	1.66(0.02)	1.66(0.02)	...	0.45(0.16)	-0.50(0.17)	-0.05(0.33)
+124.63	...	1.52(0.05)	1.52(0.05)	...	0.24(0.17)	-0.29(0.16)	-0.05(0.33)
+126.57	...	1.55(0.03)	1.55(0.03)	...	0.26(0.09)	-0.28(0.10)	-0.01(0.19)
+135.56	...	1.32(0.03)	1.32(0.03)	...	0.35(0.43)	-0.50(0.45)	-0.15(0.88)
+159.49	...	1.32(0.02)	1.32(0.02)	...	0.43(0.49)	-0.50(0.49)	-0.07(0.99)

Note. — Values in parentheses are 1σ uncertainties.

Table 11. Balmer line velocities for SN 2005kj.

Phase (days)	FWHM(H α _b) km s ⁻¹	FWHM(H α _n) km s ⁻¹	FWHM(H β _b) km s ⁻¹	FWHM(H β _n) km s ⁻¹	v_{\min} (H β _{P-Cyg}) km s ⁻¹
+6.77	3610(391)	839(96)	2432(313)	490(170)	...
+7.76	2175(499)	641(269)	2460(219)	443(153)	...
+20.76	2518(584)	1041(360)	2969(500)	1455(500)	...
+32.81	2972(381)	770(95)	1385(515)	808(234)	...
+33.76	2758(267)	833(81)	1597(254)	387(264)	...
+35.76	2837(297)	815(80)	3487(780)	805(176)	...
+59.76	3345(485)	710(85)	...	758(177)	...
+67.66	2256(179)	661(51)	...	425(56)	-582(21)
+87.72	1933(211)	694(100)	...	907(554)	-805(228)
+107.64	...	978(41)	...	531(268)	-892(331)
+116.66	...	1020(15)	...	653(118)	-722(94)
+124.63	...	1036(49)	...	802(429)	-652(103)
+126.57	...	975(28)	...	542(163)	-819(103)
+135.56	...	858(33)	...	726(430)	-929(467)
+159.49	...	1028(24)	...	889(368)	-911(296)

Note. — Values in parentheses are 1σ uncertainties.

Table 12. Balmer line fluxes in units of 10^{-14} erg s⁻¹ cm⁻² for SN 2006aa.

Days since discovery	F(H α _b)	F(H α _n)	F(H α _{P-Cyg})	F(H α _{tot})	F(H β _b)	F(H β _n)	F(H β _{P-Cyg})	F(H β _{tot})
+18.82	1.13(0.17)	0.96(0.18)	...	2.10(0.24)	0.50(0.37)	0.41(0.38)	-0.09(0.35)	0.82(0.64)
+24.77	1.86(0.13)	0.76(0.14)	...	2.62(0.19)	1.08(0.29)	0.34(0.26)	-0.09(0.09)	1.33(0.39)
+34.78	2.32(0.14)	1.04(0.15)	-0.06(0.01)	3.29(0.21)	1.71(0.10)	0.38(0.10)	-0.09(0.02)	2.00(0.15)
+34.82	2.51(0.28)	0.82(0.29)	...	3.33(0.41)	2.14(0.12)	0.07(0.08)	...	2.21(0.14)
+43.71	3.02(0.14)	0.76(0.12)	-0.13(0.04)	3.65(0.19)	1.84(0.19)	0.37(0.19)	-0.09(0.03)	2.12(0.27)
+49.75	2.96(0.13)	0.78(0.14)	...	3.74(0.19)	2.02(0.24)	0.35(0.21)	-0.09(0.05)	2.29(0.33)
+76.62	2.18(0.21)	1.00(0.23)	...	3.18(0.31)	0.90(0.50)	0.22(0.50)	...	1.12(0.71)

Note. — Values in parentheses are 1σ uncertainties.

Table 13. Balmer line velocities for SN 2006aa.

Phase (days)	FWHM(H α _b) km s ⁻¹	FWHM(H α _n) km s ⁻¹	v_{\min} (H α _{P-Cyg}) km s ⁻¹	FWHM(H β _b) km s ⁻¹	FWHM(H β _n) km s ⁻¹	v_{\min} (H β _{P-Cyg}) km s ⁻¹
+18.82	2444(460)	595(70)	...	1735(823)	593(313)	-780(204)
+24.77	2077(191)	490(58)	...	1744(342)	518(229)	-619(65)
+34.78	2401(154)	674(58)	-759(17)	2332(192)	513(94)	-702(17)
+34.82	2221(240)	657(133)
+43.71	2046(120)	429(45)	-648(37)	2190(319)	457(164)	-596(125)
+49.75	2029(143)	410(53)	...	2158(347)	461(177)	-600(120)
+76.62	2070(240)	547(74)	...	1301(479)	441(544)	...

Note. — Values in parentheses are 1σ uncertainties.

Table 14. Balmer line fluxes in units of 10^{-14} erg s⁻¹ cm⁻² for SN 2006bo.

Days since discovery	F(H α _n)	F(H α _{P-Cyg})	F(H α _{total})	F(H β _n)	F(H β _{P-Cyg})	F(H β _{tot})
+11.21	1.62(0.03)	-0.11(0.01)	1.51(0.03)	0.79(0.16)	-0.25(0.15)	0.54(0.22)
+21.23	1.28(0.08)	-0.20(0.05)	1.08(0.10)	0.52(0.21)	-0.27(0.19)	0.25(0.28)

Note. — Values in parentheses are 1σ uncertainties.

Table 15. Balmer line velocities for SN 2006bo.

Phase (days)	FWHM(H α_n) km s ⁻¹	v _{min} (H α_{P-Cyg}) km s ⁻¹	FWHM(H β_n) km s ⁻¹	v _{min} (H β_{P-Cyg}) km s ⁻¹
+11.21	1007(20)	-661(14)	933(82)	-555(90)
+21.23	1008(47)	-607(39)	876(233)	-561(149)

Note. — Values in parentheses are 1 σ uncertainties.

Table 16. Balmer line fluxes in units of 10⁻¹⁴ erg s⁻¹ cm⁻² for SN 2006qq.

Days since discovery	F(H α_b)	F(H α_n)	F(H α_{tot})	F(H β_b)	F(H β_n)	F(H β_{tot})
+12.84	0.42(0.24)	1.27(0.19)	1.69(0.31)	0.18(0.22)	0.26(0.24)	0.44(0.33)
+17.90	0.82(0.08)	1.24(0.04)	2.06(0.09)	0.53(0.06)	0.15(0.05)	0.69(0.07)
+31.86	3.24(0.08)	0.77(0.02)	4.00(0.08)	1.05(0.07)	0.05(0.01)	1.10(0.07)
+36.88	3.13(0.16)	1.22(0.07)	4.35(0.17)	1.41(0.23)	0.08(0.07)	1.48(0.24)
+43.91	2.92(0.15)	1.05(0.06)	3.97(0.16)	0.94(0.27)	0.25(0.21)	1.20(0.34)
+48.72	3.06(0.09)	0.66(0.03)	3.72(0.10)	0.73(0.04)	0.07(0.01)	0.81(0.05)
+59.71	6.62(1.92)	0.36(0.10)	6.99(2.00)	1.27(0.08)	0.04(0.03)	1.32(0.09)
+73.72	2.22(0.19)	0.76(0.05)	2.98(0.20)
+74.77	1.38(0.11)	0.43(0.03)	1.81(0.11)

Note. — Values in parentheses are 1 σ uncertainties.

Table 17. Balmer line velocities for SN 2006qq.

Phase (days)	BVZI(H α_b) km s ⁻¹	RVZI(H α_b) km s ⁻¹	FWHM(H α_n) km s ⁻¹	FWHM(H β_n) km s ⁻¹
+12.84	6523(200)	2613(200)	450(39)	706(343)
+17.90	7437(200)	2613(200)	328(9)	346(115)
+31.86	12462(200)	4897(200)	208(5)	85(25)
+36.88	12005(200)	3070(200)	579(34)	254(100)
+43.91	9721(200)	3526(200)	572(36)	1516(929)
+48.72	10178(200)	3983(200)	381(20)	370(78)
+59.71	8807(200)	...	228(70)	370(293)
+73.72	9721(200)	1699(200)	296(24)	...
+74.77	10178(200)	1699(200)	267(22)	...

Note. — Values in parentheses are 1 σ uncertainties.

Table 18. Balmer line fluxes in units of 10⁻¹⁴ erg s⁻¹ cm⁻² for SN 2008fq.

Days since discovery	F(H α_b)	F(H α_n)	F(H α_{P-Cygb})	F(H $\alpha_{P-Cygni^n}$)	F(H α_{tot})	F(H β_n)	F(H α_{P-Cygn})
+1.75	3.65(0.51)	2.85(0.25)	-0.37(0.12)	-0.96(0.26)	5.17(0.63)	1.00(0.30)	-0.22(0.23)
+6.77	6.58(0.73)	3.00(0.41)	-1.19(0.32)	-2.25(0.48)	6.13(1.01)	1.00(0.84)	-1.69(1.04)
+13.78	10.00(0.74)	1.30(0.30)	-1.31(0.34)	-0.87(0.42)	9.12(0.97)
+28.75	70.00(7.80)	...	-20.11(8.40)	...	49.89(11.47)
+70.74	60.00(1.41)	1.64(0.18)	-10.19(1.31)	...	51.44(1.94)

Note. — Values in parentheses are 1 σ uncertainties.

Table 19. Balmer line velocities for SN 2008fq.

Phase (days)	FWHM(H α _b) km s ⁻¹	FWHM(H α _n) km s ⁻¹	v _{min} (H α _{P-Cyg^b}) km s ⁻¹	v _{min} (H α _{P-Cygⁿ}) km s ⁻¹	FWHM(H β _n) km s ⁻¹	v _{min} (H β _{P-Cygⁿ}) km s ⁻¹
+1.75	4166(581)	446(36)	-7387(239)	-531(63)	435(177)	770(100)
+6.77	4568(545)	366(38)	-7236(450)	-414(52)	410(284)	482(232)
+13.78	4568(711)	229(63)	-7581(307)	-441(104)
+28.75	7063(371)	...	-7049(1947)
+70.74	6463(216)	183(46)	-7049(364)

Note. — Values in parentheses are 1 σ uncertainties.

Table 20. H α EWs for 5 CSP SNe II_n.

Phase (days since discovery)	EW(H α) (Å)	$\Delta_{EW(H\alpha)}$ (Å)
SN 2005kj		
+6.77	64	7
+7.76	56	15
+20.76	67	26
+32.81	62	6
+33.76	55	6
+35.76	58	5
+59.76	65	6
+67.66	56	4
+87.72	54	10
+107.64	41	1
+116.66	55	1
+124.63	61	2
+126.57	64	1
+135.56	65	2
+159.49	112	2
SN 2006aa		
+18.82	99	8
+24.77	108	5
+34.78	118	5
+34.82	119	11
+43.71	128	4
+49.75	130	5
+76.62	146	9
SN 2006bo		
+11.21	53	10
+21.23	43	10
SN 2006qq		
+12.84	57	10
+17.90	72	3
+31.86	146	3
+36.88	169	8
+43.91	165	6
+48.72	157	4
+59.71	271	50
+73.72	163	9
+74.77	100	6
SN 2008fq		
+1.75	11	1
+6.77	11	2
+13.78	16	2
+28.75	143	30
+70.74	238	9

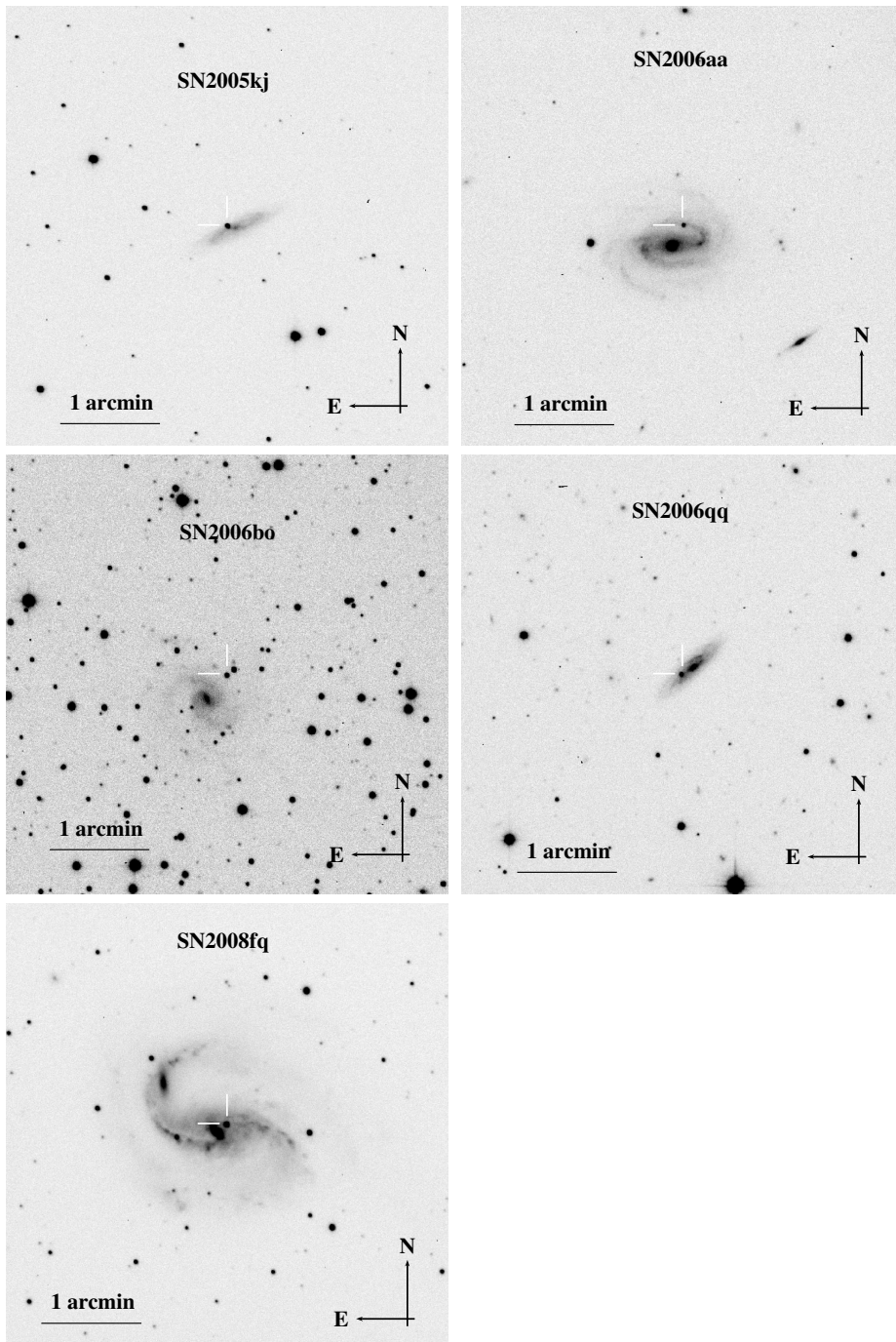


Figure 1: Swope V-band images of 5 CSP SNe II_n.